On the performance of spatial modulation and full duplex radio architectures

Yanni Zhou

N° d'ordre NNT : 2021LYSEI094

THESE DE DOCTORAT DE L'UNIVERSITE DE LYON

OPÉRÉE AU SEIN DE

L'INSTITUT NATIONAL DES SCIENCES APPLIQUÉES DE LYON

ECOLE DOCTORALE N° ED160 EEA

ÉLECTRONIQUE, ÉLECTROTECHNIQUE, AUTOMATIQUE

SPÉCIALITÉ/DISCIPLINE DE DOCTORAT :

Électronique, micro et nanoélectronique, optique et laser

Soutenue publiquement le 10/12/2021, par :

Yanni Zhou

On the Performance of Spatial Modulation and Full Duplex Radio Architectures

Devant le jury composé de :

Marco DI RENZO	Directeur de recherche, CNRS	Rapporteur
Matthieu CRUSSIERE	Professeur, INSA-Rennes	Rapporteur
Christelle AUPETIT-BERTHELEMOT	Professeure, Université de Limoges	Examinatrice
Taneli RIIHONEN	Maître de Conférences, Tampere University	Examinateur
Jean-Marie GORCE	Professeur, INSA-Lyon	Examinateur
Dinh-Thuy PHAN-HUY	Docteur, Orange Lab	Examinatrice
Guillaume VILLEMAUD	Maître de Conférences, HDR, INSA-Lyon	Directeur de thèse
Florin-Doru HUTU	Maître de Conférences, INSA-Lyon	Co-directeur de thèse

Département FEDORA – INSA Lyon - Ecoles Doctorales

SIGLE	ECOLE DOCTORALE	NOM ET COORDONNEES DU RESPONSABLE
CHIMIE	**CHIMIE DE LYON** **https://www.edchimie-lyon.fr** Sec. : Renée EL MELHEM Bât. Blaise PASCAL, 3e étage secretariat@edchimie-lyon.fr	**M. Stéphane DANIELE** C2P2-CPE LYON-UMR 5265 Bâtiment F308, BP 2077 43 Boulevard du 11 novembre 1918 69616 Villeurbanne **directeur@edchimie-lyon.fr**
E.E.A.	**ÉLECTRONIQUE, ÉLECTROTECHNIQUE, AUTOMATIQUE** **https://edeea.universite-lyon.fr** Sec. : Stéphanie CAUVIN Bâtiment Direction INSA Lyon Tél : 04.72.43.71.70 secretariat.edeea@insa-lyon.fr	**M. Philippe DELACHARTRE** INSA LYON Laboratoire CREATIS Bâtiment Blaise Pascal, 7 avenue Jean Capelle 69621 Villeurbanne CEDEX Tél : 04.72.43.88.63 **philippe.delachartre@insa-lyon.fr**
E2M2	**ÉVOLUTION, ÉCOSYSTÈME, MICROBIOLOGIE, MODÉLISATION** **http://e2m2.universite-lyon.fr** Sec. : Sylvie ROBERJOT Bât. Atrium, UCB Lyon 1 Tél : 04.72.44.83.62 secretariat.e2m2@univ-lyon1.fr	**M. Philippe NORMAND** Université Claude Bernard Lyon 1 UMR 5557 Lab. d'Ecologie Microbienne Bâtiment Mendel 43, boulevard du 11 Novembre 1918 69 622 Villeurbanne CEDEX **philippe.normand@univ-lyon1.fr**
EDISS	**INTERDISCIPLINAIRE SCIENCES-SANTÉ** **http://ediss.universite-lyon.fr** Sec. : Sylvie ROBERJOT Bât. Atrium, UCB Lyon 1 Tél : 04.72.44.83.62 secretariat.ediss@univ-lyon1.fr	**Mme Sylvie RICARD-BLUM** Institut de Chimie et Biochimie Moléculaires et Supramoléculaires (ICBMS) - UMR 5246 CNRS - Université Lyon 1 Bâtiment Raulin - 2ème étage Nord 43 Boulevard du 11 novembre 1918 69622 Villeurbanne Cedex Tél : +33(0)4 72 44 82 32 **sylvie.ricard-blum@univ-lyon1.fr**
INFOMATHS	**INFORMATIQUE ET MATHÉMATIQUES** **http://edinfomaths.universite-lyon.fr** Sec. : Renée EL MELHEM Bât. Blaise PASCAL, 3e étage Tél : 04.72.43.80.46 infomaths@univ-lyon1.fr	**M. Hamamache KHEDDOUCI** Université Claude Bernard Lyon 1 Bât. Nautibus 43, Boulevard du 11 novembre 1918 69 622 Villeurbanne Cedex France Tél : 04.72.44.83.69 **hamamache.kheddouci@univ-lyon1.fr**
Matériaux	**MATÉRIAUX DE LYON** **http://ed34.universite-lyon.fr** Sec. : Yann DE ORDENANA Tél : 04.72.18.62.44 yann.de-ordenana@ec-lyon.fr	**M. Stéphane BENAYOUN** Ecole Centrale de Lyon Laboratoire LTDS 36 avenue Guy de Collongue 69134 Ecully CEDEX Tél : 04.72.18.64.37 **stephane.benayoun@ec-lyon.fr**
MEGA	**MÉCANIQUE, ÉNERGÉTIQUE, GÉNIE CIVIL, ACOUSTIQUE** **http://edmega.universite-lyon.fr** Sec. : Stéphanie CAUVIN Tél : 04.72.43.71.70 Bâtiment Direction INSA Lyon mega@insa-lyon.fr	**M. Jocelyn BONJOUR** INSA Lyon Laboratoire CETHIL Bâtiment Sadi-Carnot 9, rue de la Physique 69621 Villeurbanne CEDEX **jocelyn.bonjour@insa-lyon.fr**
ScSo	**ScSo*** **https://edsciencessociales.universite-lyon.fr** Sec. : Mélina FAVETON INSA : J.Y. TOUSSAINT Tél : 04.78.69.77.79 melina.faveton@univ-lyon2.fr	**M. Christian MONTES** Université Lumière Lyon 2 86 Rue Pasteur 69365 Lyon CEDEX 07 **christian.montes@univ-lyon2.fr**

*ScSo : Histoire, Géographie, Aménagement, Urbanisme, Archéologie, Science politique, Sociologie, Anthropologie

Abstract

Index modulation techniques have exhibited great potential in the scenarios foreseen in next-generation wireless networks. Applying in the spatial domain, spatial modulation (SM) as a single radio-frequency (RF) multiple-input–multiple-output (MIMO) solution has attracted wide attention. The SM system has only one transmitting antenna activated for each time slot which results in low system complexity and cost. It exploits the index of the transmitting antennas to convey additional information bits.

To analyze the SM performance, a simulated framework over the time-varying Rician fading channel is built with ADS and Matlab software and a channel state information (CSI) detector is highlighted. The simulation results are verified by the experimental implementation based on the National Instruments (NI) PXI chassis hardware and LabVIEW programming environment. In the practical analysis, two models of the propagation environments are considered, where a channel sounding method is employed in order to extract the channel coefficients.

Despite issues on system complexity and cost, a shortage of spectrum resources can also restrict the development of mobile communications technology. Full duplex (FD) communications have been developed to double the radio link data rate and spectral efficiency through simultaneous and bidirectional communication. The main challenge of FD systems is self-interference (SI), which is caused by the coupling of the transmitting antenna with the receiving one. The combination of FD and SM will not only maintain spectral efficiency but also decrease the complexity of the self-interference cancellation (SIC) because of the single RF chain.

Based on these, a full duplex spatial modulation (FDSM) system is proposed as well as the SIC method. Moreover, the impact of SIC accuracy on the system performance is studied. We focus on the FDSM system imperfections including IQ imbalance, phase noise, power amplifier (PA) nonlinearities and RF switch nonidealities. The bit error rate (BER) performance under different scenarios with these imperfections is analyzed, along with the estimation and cancellation method.

RÉSUMÉ

Les techniques de modulation d'indice ont montré un grand potentiel dans les réseaux de communication sans fil de prochaine génération. Dans le domaine de l'indice spatial, la modulation spatiale (SM) en tant que solution à chaine de radio fréquence (RF) unique et à entrées multiples et sorties multiples (MIMO) a attiré une large attention. Le système SM n'a qu'une seule antenne d'émission activée pour chaque intervalle de temps, ce qui diminue la complexité et le coût du système. Il exploite l'indice des antennes émettrices pour véhiculer des bits d'information supplémentaires.

Pour analyser les performances de la SM, un environnement simulé avec le canal d'évanouissement de Rice variable dans le temps est construit avec les logiciels ADS et Matlab et un détecteur d'informations sur l'état du canal (CSI) est mis en évidence. Les résultats sont vérifiés par l'implémentation expérimentale basée sur le matériel du type PXI et l'environnement de programmation LabVIEW de National Instruments (NI). L'analyse pratique prend en compte deux modèles d'environnements de propagation, où une méthode de sondage de canal est utilisée afin d'extraire les coefficients du canal.

Malgré les problèmes de complexité et de coût du système, le manque de ressources spectrales peut également restreindre le développement de la technologie des communications mobiles. Les communications en full duplex (FD) ont été développées pour doubler le débit de données de la liaison radio et l'efficacité spectrale grâce à une communication simultanée et bidirectionnelle. Le principal challenge des systèmes FD est l'auto-interférence (SI), qui est causée par le couplage de l'antenne d'émission avec celle de réception. La combinaison de FD et SM non seulement maintiendra l'efficacité spectrale mais aussi réduira la complexité de l'annulation d'auto-interférence (SIC) grâce à la chaîne RF unique.

Par conséquent, un système de modulation spatiale en full duplex (FDSM) est proposé ainsi que la méthode SIC. De plus, l'impact de la précision du SIC sur les performances du système est étudié. Nous nous concentrons sur les imperfections du système FDSM, notamment les déséquilibres IQ, le bruit de phase, les non-linéarités d'amplificateur (PA) et les non-idéalités de switch RF. Les performances de taux d'erreur binaire (BER) dans différents scénarios sont analysées, ainsi que la méthode d'estimation et le SIC.

TABLE OF CONTENTS

LIST OF FIGURES

List of Tables

List of Acronyms

1G	First Generation mobile networks.
2G	Second Generation mobile networks.
3D	Three-Dimension.
3G	Third Generation mobile networks.
4G	Fourth Generation mobile networks.
5G	Fifth Generation mobile networks.
6G	Sixth Generation mobile networks.
ADC	Analog-to-Digital Converter.
AI	Artificial Intelligence.
ASM	Augmented Spatial Modulation.
AWGN	Additive White Gaussian Noise.
BB	Baseband.
BER	Bit Error Rate.
CRN	Cognitive Radio Networks.
CSI	Channel State Information.
CSMA/CA	Carrier Sense Multiple Access with Collision Avoidance.
DL	Downlink.
DQSM	Differential Quadrature Spatial Modulation.
FD	Full-Duplex.
FDD	Frequency Division Duplex.
FDSM	Full Duplex Spatial Modulation.
GPRS	General Packet Radio Service.
GPSM	Generalized Precoding aided Spatial Modulation.
GSM	Generalized Spatial Modulation.
GSSK	Generalised Space Shift Keying.
HD	Half-duplex.
ICI	Inter-Channel Interference.
INR	Self-Interference-to-Noise Ratio.
IQ	In-phase and Quadrature.
IQSM	Improved Quadrature Spatial Modulation.
IoE	Internet of Everything.
IoT	Internet of Things.

IRR	Image Rejection Ratio.
LO	Local Oscillator.
LOS	Line-of-Sight.
LOS/NLOS	line-of-sight/non-line-of-sight
LNA	Low Noise Amplifier.
LS	Least Square.
LTE	Long-Term Evolution.
MASM	Multiple Active Spatial Modulation.
MEMS	Micro Electro Mechanical Systems.
MIMO	Multiple-Input Multiple-Output.
mmWave	Millimeter-Wave.
MTC	Machine-Type Communication.
NLOS	Non-Line-of-Sight.
NI	National Instruments.
OFDMA	Orthogonal Frequency-Division Multiple Access.
PA	Power Amplifier.
PDF	Probability Density Function.
PLL	Phase-Locked Loop.
QAM	Quadrature Amplitude Modulation.
QPSK	Quadrature phase-shift keying.
QSM	Quadrature Spatial Modulation.
RF	Radio Frequency.
SI	Self-Interference.
SIC	Self-Interference Cancellation.
SISO	Single-Input Single-Output.
SM	Spatial Modulation.
SRC	Sample Reference Clock.
SSK	Space Shift Keying.
STBC	Space-Time Block Code.
TDD	Time Division Duplex.
TDMA	Time Division Multiple Access.
THz	Terahertz.
UL	Uplink.
UMTS	Universal Mobile Telecommunications System.
VLC	Visible Light Communications.
VR	Virtual Reality.
VSA	Vector Signal Analyzer.
VSG	Vector Signal Generator.
VST	Vector Signal Transceivers.
WAP	Wireless Application Protocol.

0.1 Introduction

Ces dernières années, les communications sans fil ont servi tous les aspects de la production et de la vie sociale et est devenue une infrastructure soutenant le fonctionnement fondamental de la société. Le système de communication sans fil continue d'évoluer en fonction de l'évolution de la demande, et est passé de la première génération (1G) à la cinquième génération (5G) [42] en 40 ans. Les services qu'il prend en charge ont également évolué, passant de la communication vocale initiale à de multiples services tels que le multimédia à large bande passante et les objets connectés. En outre, les objets de service du système ont également changé, passant de la communication entre personnes à l'interconnexion orientée machines [10, 126]. Chaque évolution de la technique de communication sans fil reflète les changements révolutionnaires de la productivité et du mode de vie. Avec l'augmentation de la demande, la couche physique du futur système de communication sans fil doit non seulement fournir une bande passante plus large, une latence plus faible, un taux de transmission des données plus élevé et une fiabilité plus grande, mais elle doit également prêter attention à la consommation d'énergie, à la complexité du système, à la cybersécurité et à la prise en charge de services multiples [24, 97].

Pour répondre à ces exigences, la modulation d'indice est un nouveau type de technique de modulation qui a fait son apparition ces dernières années [119]. Dans les systèmes de communication sans fil traditionnels, le processus de modulation consiste à faire correspondre tous les bits d'information qui doivent être transmis à des symboles de modulation d'amplitude/de phase, tandis que la modulation d'indice peut utiliser l'indice des ressources spatiales pour transmettre l'information. La modulation spatiale (SM) est un représentant typique de la modulation d'indice. La SM est une nouvelle technique de transmission MIMO (Multi-Input-Multi-Output) qui a été développée ces dernières années. Elle transporte des informations en activant l'indice d'antenne et les symboles

de constellation de modulation numérique. Elle peut fournir un schéma de conception MIMO basé sur la radio clairsemée, simplifiant ainsi l'architecture MIMO traditionnelle. Cette structure réduit le coût de mise en œuvre du MIMO et devrait permettre de fournir une solution MIMO massive efficace. L'idée de base de la SM est qu'une seule antenne est activée pour chaque intervalle de temps afin de transmettre les symboles traditionnels de modulation amplitude/phase ; les informations binaires sont transmises conjointement par l'indice de l'antenne activée et les symboles de constellation.

Par rapport aux techniques MIMO traditionnelles, la SM présente les avantages suivants : **(1) Taux de transmission élevé** : La SM utilise l'indice d'antenne comme support d'information pour transmettre des données supplémentaires. Par rapport à la technique à antenne unique basée sur la transmission par modulation d'amplitude/de phase et à la technique multi-antennes basée sur la diversité d'espace, un taux de transmission plus élevé peut être obtenu. **(2) Éviter les interférences inter-antennes (ICI) et la synchronisation des canaux** : Puisqu'une seule antenne transmet des données pour chaque intervalle de temps, les problèmes d'ICI et de synchronisation des canaux causés par le multiplexage spatial peuvent être évités efficacement. **(3) Détection à faible complexité** : L'extrémité de réception peut utiliser des méthodes de détection étape par étape pour réduire efficacement la complexité de la détection. Plus précisément, l'indice de l'antenne est d'abord détecté, puis l'indice détecté est utilisé pour détecter le symbole. **(4) Configuration d'antenne flexible** : Puisqu'une seule antenne est activée pour chaque intervalle de temps, l'extrémité de réception n'a besoin que de très peu d'antennes pour estimer avec précision le flux binaire de données transmis. Par conséquent, comparé au système V-BLAST, la SM est plus adaptée aux canaux MIMO asymétriques où le nombre d'antennes de réception est beaucoup plus petit que celui d'émission. **(5) Performances de transmission fiables** : La littérature [61] a prouvé qu'avec le même taux de transmission, la SM peut atteindre de meilleures performances en termes de taux d'erreur binaire (BER) que les systèmes traditionnels V-BLAST. **(6) Faible consommation d'énergie et coût de mise en œuvre** : Une seule chaîne de radiofréquence (RF) est nécessaire de coté émission de la SM, ce qui simplifie la structure MIMO traditionnelle et réduit efficacement le coût de mise en œuvre de la technique de transmission MIMO, notamment coté RF.

Comme les exigences augmentent sans cesse en matière de vitesse de communication, cela pose de nouveaux défis pour une utilisation plus efficace des ressources limitées du spectre existant. Par conséquent, le full duplex (FD) a fait l'objet d'une grande attention car il peut théoriquement doubler l'efficacité spectrale existante et la capacité du système.

Afin de réaliser une communication bidirectionnelle dans les systèmes de communication sans fil antérieurs, il était nécessaire de diviser le canal entre l'émetteur et le récepteur dans le domaine temporel ou dans le domaine fréquentiel pour éviter l'interférence entre les émetteurs-récepteurs. Ces deux divisions correspondent aux deux techniques de duplexage, respectivement le duplexage par répartition dans le temps (TDD) et le duplexage par répartition en fréquence (FDD). Dans ces deux techniques, la même ressource spectrale est soit partagée dans le temps par le canal émetteur-récepteur, soit ne peut être utilisée exclusivement que par l'un des canaux. L'utilisation d'une même fréquence pour émettre et recevoir des signaux en même temps était considérée comme presque impossible dans le passé [49]. Cependant, ces dernières années, grâce aux recherches notamment de l'université Rice [12, 15, 39–41] et de l'université Stanford [22, 23, 31, 56, 58], les chercheurs ont vu la faisabilité de sa réalisation. L'annulation de l'auto-interférence (SIC) est le principal défi pour réaliser le FD. Étant donné que le signal d'émission local et le signal d'émission de l'extrémité distante utilisent les mêmes ressources en fréquences, et que l'antenne d'émission locale est beaucoup plus proche de celle de réception, le signal d'émission local causera une forte auto-interférence (SI) au signal d'intérêt. En outre, certains facteurs RF non idéaux limitent les performances du SIC, notamment sur le bruit de phase, le déséquilibre I/Q, la non-linéarité de l'amplificateur de puissance, etc. Diverses techniques SIC ont été développées et peuvent être divisées en trois catégories en fonction de l'emplacement du SIC : **(1) SIC passif** : En étudiant les caractéristiques et la propagation des antennes pour augumenter le découplage. **(2) SIC analogique** : Le signal SI est reconstruit dans le domaine analogique, puis le SI reconstruit est soustrait à l'extrémité de réception pour supprimer le SI. **(3) SIC numérique** : Le SIC numérique fait référence à la réalisation du SIC dans le domaine numérique, y compris la reconstruction du SI dans le domaine numérique et sa soustraction de l'extrémité de réception. De plus, les composantes RF non idéales peuvent être incluses dans la modélisation à l'intérieur de l'annulateur numérique [76].

La combinaison du FD et de la SM peut être intéressante car lorsqu'une seule chaîne RF est mise en œuvre, la complexité du SIC n'augmente pas par rapport aux systèmes à entrée unique et sortie unique (SISO), mais l'efficacité spectrale est doublée. De plus, les systèmes de modulation spatiale en full duplex (FDSM) offrent les avantages du MIMO, comme la diversité et les gains de multiplexage, mais avec une faible consommation d'énergie. La supériorité du système FDSM est discutée dans [99, 138].

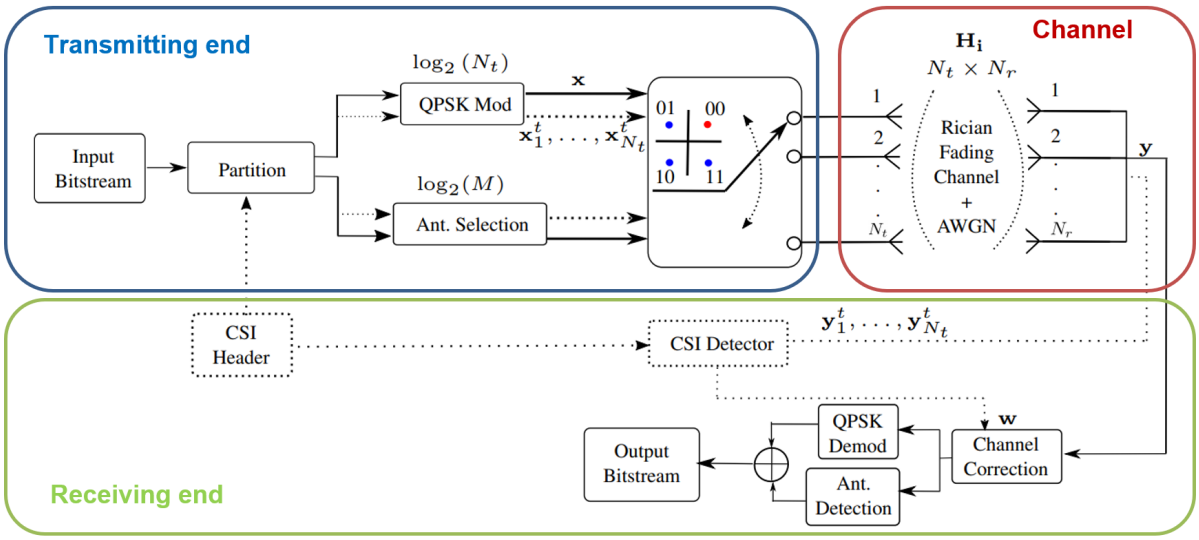

Figure 0.1: Modèle de système SM $N_t \times N_r$ avec un détecteur CSI

0.2 Résultats principaux

0.2.1 Système SM simulé

Nous proposons tout d'abord un système SM avec un détecteur CSI. On ne suppose plus qu'un CSI parfait puisse être obtenu à l'extrémité de réception. On considère que le CSI est dégradé par le bruit de type AWGN et par le canal de propagation. Afin d'étudier les performances du système proposé, des co-simulations avec ADS (Advanced Design System) - Matlab seront réalisées. Plus précisément, la performance de la SM sur le canal d'évanouissement de Rice variant dans le temps sera analysée. Un modèle de système SM sur le canal à évanouissement de Rice variable dans le temps avec un détecteur CSI est présenté sur la Figure 0.1. Ici, N_t est le nombre d'antennes émettrices et N_r est le nombre d'antennes réceptrices. L'architecture de la SM peut être divisée en trois parties principales:

1. **Partie émettrice:** Ici, le flux binaire d'entrée est divisé en deux parties. Une partie est utilisée pour la sélection de l'antenne et l'autre est utilisée pour former les symboles. Les autres N_t ensembles de données sont envoyés pour l'estimation CSI comme en-tête.

2. **Canal:** Un modèle de canal $N_t \times N_r$ est construit. L'antenne activée transmet les symboles modulés à travers un canal d'évanouissement de Rice variant dans le temps. En outre, un bruit AWGN est également considéré.

3. **Partie réceptrice:** Ici, le CSI du détecteur est utilisé pour la détection d'antenne. De plus, chaque symbole reçu est démodulé. Les bits résultant de la détection d'antenne sont concaténés avec ceux de l'étape de démodulation, formant ainsi le flux binaire de sortie.

Le principe du détecteur CSI est basé sur l'algorithme des moindres carrés (LS) [46]. Le détecteur calcule les éléments de la matrice du canal sur la base de la matrice de covariance d'échantillonnage estimée. Ensuite, l'algorithme de détection optimale à maximum de vraisemblance (ML) est appliqué pour la démodulation de l'indice de l'antenne émettrice et des symboles modulés par QPSK [91], où un détecteur ML à faible complexité est considéré.

Un simulateur du schéma SM (Figure 0.1) est construit afin d'évaluer la performance en termes de variation du BER par rapport à Eb/No, qui est l'énergie par bit sur la densité spectrale de puissance du bruit. Nous simulons les extrémités de transmission et de réception sur ADS et implémentons le traitement du signal numérique et une partie de l'algorithme de détection sur Matlab.

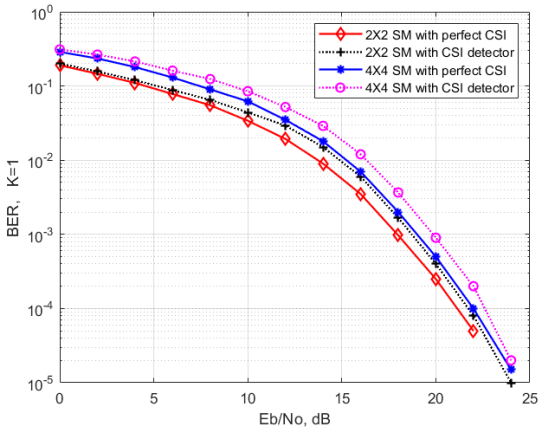

Figure 0.2: Performance en termes de BER des systèmes SM 2×2 et 4×4 avec le détecteur CSI parfait et réaliste sur un canal à d'évanouissement de Rice variant dans le temps

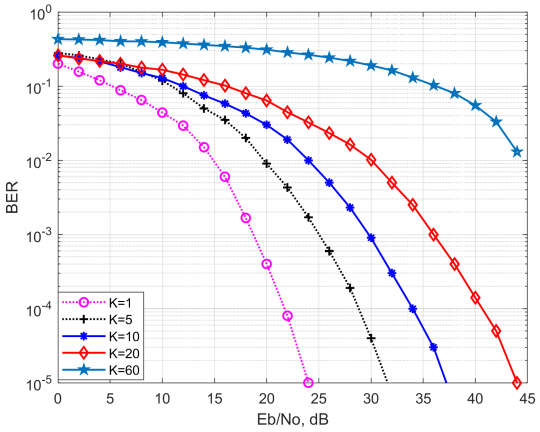

Figure 0.3: Performance en BER du système SM 2×2 avec le détecteur CSI réaliste et avec différents facteurs K de Rice

La performance BER avec le détecteur parfait et réaliste et sous différents facteurs K de Rice est montrée dans les Figure 0.2 et Figure 0.3. Les résultats de la simulation du système indiquent que l'erreur du détecteur est acceptable avec le détecteur CSI proposé et la méthode ML considérée, en particulier lorsque le facteur K de Rice est petit.

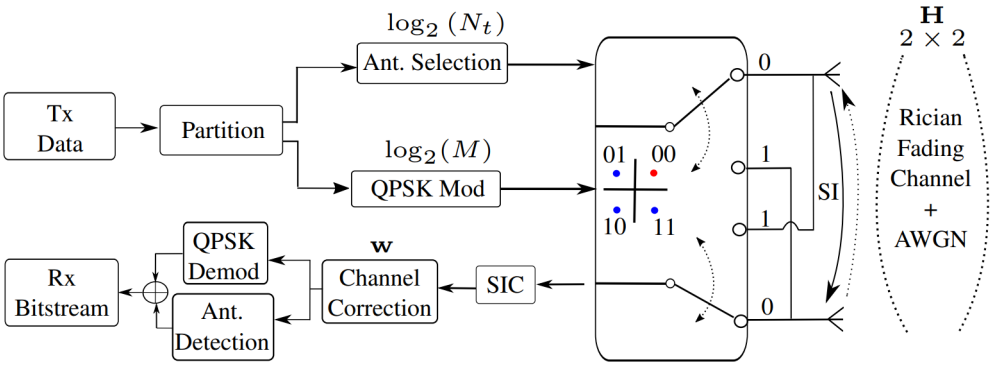

Figure 0.4: Schéma fonctionnel d'un système FDSM 2 × 2: nœud A

0.2.2 Système FDSM simulé

Nous décrivons un système FDSM 2 × 2 sur un canal à évanouissement de Rice, notamment avec un module de correction de canal et un module SIC. On considère deux nœuds (à savoir le nœud A et le nœud B) ayant les mêmes fonctions. En raison des caractéristiques du système de communication FD, les deux extrémités du système ont les mêmes fonctions d'émission et de réception simultanées. Par conséquent, nous ne présentons que les caractéristiques structurelles d'une seule extrémité. Le choix pour l'émission ou pour la réception de l'antenne est déterminé par le mappage SM du flux binaire d'entrée. Le schéma fonctionnel de ce système au nœud A est présenté à la Figure 0.4.

Comme nous pouvons remarquer, une antenne au nœud A est utilisée pour transmettre et l'autre est utilisée pour recevoir simultanément pour chaque période de symbole. Le système peut être divisé en trois parties principales: partie modulation et démodulation, partie modèle de canal et module de correction de canal, partie module d'auto-interférence et d'annulation. Dans cette thèse, le modèle de canal SI est supposé être un canal à une voie. En outre, le rapport auto-interférence/bruit (INR) est introduit comme le rapport de puissance du signal SI reçu sur le bruit thermique du récepteur, afin d'évaluer la puissance du SI. Dans un sens pratique, nous pouvons comprendre l'influence des changements de l'INR comme celle des changements de la distance entre les deux nœuds sur les performances du système. De plus, pour effectuer l'estimation du canal SI par la méthode LS, nous supposons une connaissance parfaite du canal de propagation. Une fois que le CSI (l'amplitude et la phase) du signal SI est estimé, un signal ayant la même amplitude mais la phase inversée est généré comme le signal SI de régénération, pour

effectuer l'annulation analogique active.

Un simulateur FDSM est réalisé afin d'étudier la performance BER. Le système FD est également simulé pour comparer au système FDSM. Le système FD est une communication FD-SISO utilisant une modulation QPSK et les mêmes paramètres système que le système FDSM proposé. Trois scénarios différents sont considérés. Premièrement, nous analysons l'effet du SI sur les performances du système sans SIC. Ensuite, nous étudions l'impact de la précision du SIC dans le cas d'une estimation imparfaite du SI. Enfin, un système FDSM complet est construit en introduisant un SI estimé. Un environnement de canal à évanouissement variant dans le temps avec $K = 1$ est considéré dans la simulation.

Nous discutons des résultats de la performance avec différentes précisions d'estimation. Deux facteurs sont définis pour évaluer les erreurs qui se produisent dans l'estimation du SI. Le facteur σ représente la différence d'amplitude entre le SIC réel et le SIC parfait, exprimée en dB. Le facteur θ représente la différence de phase entre le SIC réel et le SIC parfait, exprimée en degrés d'angle. La Figure 0.5 donne un exemple typique qui montre la différence de la valeur BER entre le système FDSM et le système FD pour INR=40 dB sous Eb/No=10 dB. La zone avec une valeur supérieure à zéro (zone jaune) représente que le BER du système FDSM est inférieur au BER du système FD. Nous remarquons que bien que le système FD est plus performant que le système FDSM lorsqu'il n'y a pas d'erreur. Lorsque σ et θ augmentent, la performance BER du système FDSM peut atteindre le même niveau que le système FD, voir même, avoir des meilleures performances. .

0.2.3 Système FDSM en présence de non-idéalités

La problématique principale du système FDSM est d'atténuer à la fois le signal SI et les composantes de bruit associées. Cependant, plusieurs contraintes limitent les performances de l'atténuation du SI. Les raisons de ces limitations représentent un certain nombre de facteurs, notamment le déséquilibre IQ, le bruit de phase, la non-linéarité de l'amplificateur de puissance et le délai de réponse du commutateur qui effectue le sélection de l'antenne.

En pratique, si l'on souhaite obtenir des performances élevées du système, il faut tenir compte des imperfections générées dans l'émetteur et dans le récepteur. En raison de la différence de puissance élevée entre le signal SI et le signal d'intérêt, par rapport à ce dernier, même une légère distorsion dans le premier peut sérieusement affecter les performances du système, tandis que le second sera affaibli en raison d'une distance de

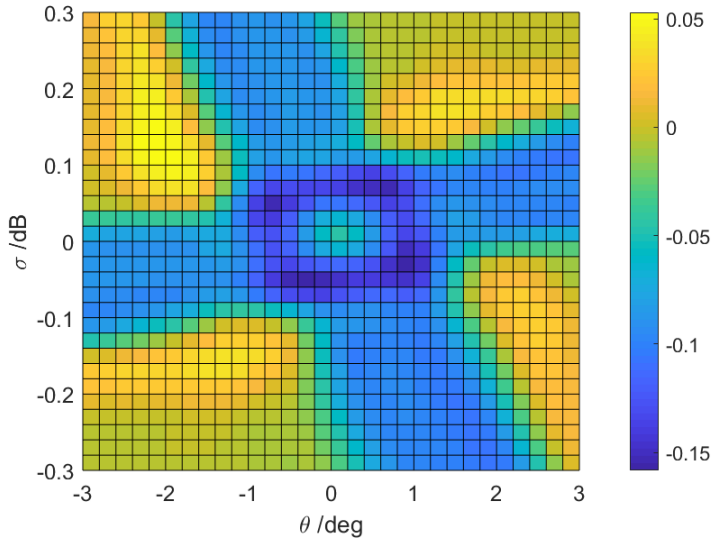

Figure 0.5: Différence de BER entre les systèmes FDSM et FD pour INR=40 dB sous Eb/No=10 dB

propagation beaucoup plus longue. En outre, le commutateur d'antenne est commuté juste avant la génération de chaque symbole et reste dans la même position pendant tout le processus de génération des symboles. En effet, il peut avoir un délai entre l'instruction et l'exécution effective de la commutation. De plus, la mauvaise isolation entre les sorties du switch peut également avoir un impact sur les performances du système FDSM. Les performances du système FDSM ont été analysées en présence du déséquilibre IQ, de l'amplificateur de puissance (PA) non linéaire, du bruit de phase et des imperfections du commutateur.

0.2.3.1 Effet des non-idéalités du récepteur

Les deux nœuds du système FDSM (c'est-à-dire le nœud A et le nœud B) ont des capacités d'émission et de réception. Nous supposons que le nœud A et le nœud B émettent simultanément sur le même canal de communication. Au niveau du nœud A, pendant l'émission du signal modulé avec une antenne, la deuxième antenne reçoit le signal du nœud B en même temps que le signal SI. Par conséquent, le signal provenant noeud B subit une forte interférence. Le signal entrant et le signal SI sont transposés en bande de base (BB) par un frontal radio analogique et ils sont supposé être affecté par un déséquilibre IQ et un bruit de phase.

L'architecture simplifiée du frontal radio analogique du récepteur est illustrée sur la Figure 0.6. Dans la pratique, le gain total sur les voies I en phase et Q en quadra-

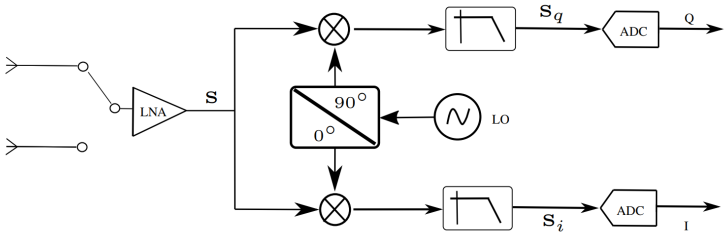

Figure 0.6: Système de modulation spatiale Full Duplex 2 × 2: frontal radio du récepteur

ture du frontal radio RF n'est pas exactement égal. De même, le déphasage de 90° du signal provenant de l'oscillateur local pour le chemin Q peut également être inexact. Lorsque la partie analogique du frontal radio ne respecte pas l'équilibre de puissance et l'orthogonalité entre les branches I et Q, un déséquilibre IQ se produit.

Un estimateur LS est proposé pour supprimer le signal SI reçu par le récepteur RF imparfait. Nous avons observé que le système est plus sensible au déséquilibre IQ lorsque le rapport signal/bruit est faible. Les résultats numériques montrent que l'estimateur proposé peut atteindre un BER acceptable. Le bruit de phase de l'instrument prévu pour les campagnes de mesure n'influence que légèrement les performances du BER du système et peut être négligé.

0.2.3.2 Effet de distorsion non linéaire introduite par le PA

Malgré les non-idéalités du récepteur, la distorsion non linéaire à l'émission est aussi inévitablement introduite puisque le matériel réel n'est pas aussi idéal que les hypothèses théoriques, ce qui entraîne un écart entre le signal SI récupéré par l'estimation de canal traditionnelle et le signal SI réel. Cependant, les effets non linéaires sur le système FDSM ont été peu étudiés du point de vue du PA. C'est pourquoi nous analysons en particulier les effets non linéaires du PA et une annulation numérique est utiliséé pour supprimer le signal SI.

Afin d'étudier cet impact, nous choisissons le PA à faible coût de type CC2595 de Texas Instruments [9] et appliquons son modèle dans la simulation au niveau système du FDSM. La distorsion non linéaire du signal produite par le PA a des effets significatifs sur le signal SI. Ici, le modèle non linéaire est supposé être un modèle polynomial sans mémoire. Un annulateur numérique de non-linéarité est utilisé après la conversion analogique-numérique au niveau de la partie réception. L'idée de cet annulateur est de régénérer un signal SI estimé. Cet estimateur est basé sur l'algorithme LS.

Comme nous pouvons conclure de la figure 0.7, le SI est généralement réduit au

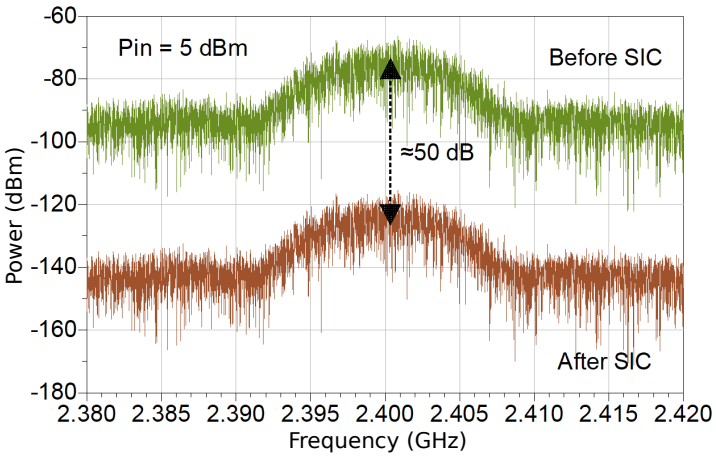

Figure 0.7: Puissance SI avant et après annulateur numérique avec INR = 40 dB et P_{in} =5 dBm

niveau approximatif du bruit thermique, où l'atténuation de la puissance du SI est d'environ 50 dB avec INR = 40 dB et P_{in} = 5 dBm (zone non linéaire).

0.2.3.3 Imperfections du commutateur RF

Au stade actuel de la recherche sur les systèmes SM, l'imperfection du commutateur est le plus souvent ignorée. En effet, le commutateur RF joue un rôle important dans le frontal RF en tant que support pour la sélection de l'antenne des systèmes SM. Le commutateur RF est connu dans l'application des microsystèmes électromécaniques (MEMS) pour contrôler les conditions d'activation et de désactivation des circuits. Cependant, le temps de commutation de la plupart des MEMS est de $2-50\mu s$ [108] et ne peut satisfaire les systèmes actuels à grande vitesse, particulièrement au regard du le débit de symboles de notre système FDSM simulé. Pour garantir les performances du système, le temps de commutation doit être nettement inférieur à la période de symbole. Les différentes valeurs du temps de réponse du commutateur peuvent dégrader les performances du système à différents niveaux. Un autre facteur de contrôle du commutateur RF est sa perte d'insertion qui exprime l'atténuation de la puissance du signal avant et après le commutateur. Par conséquent, l'efficacité, la réponse rapide, la précision et la haute fiabilité sont les exigences spécifiques aux commutateurs dans les systèmes FDSM et autres systèmes de circuits modernes. Dans cette thèse, deux effets d'imperfection de commutateur sont considérés. Nous introduisons le temps de réponse du commutateur et l'impact de la perte d'insertion du commutateur ainsi que celle de l'isolation entre les deux voies. Les performances BER avec les imperfections de commutation sont analysées.

De plus, une solution est proposée pour améliorer la performance du système dans le cas du retard du temps de réponse du commutateur, ce qui entraîne une diminution du BER.

0.2.4 Analyse expérimentale du système SM

Bien que l'analyse théorique et l'étude de simulation de la SM soient globales et approfondies, les expériences réelles sur la SM sont très limitées. La performance du système SM en utilisant des canaux réalistes mesurés est discutée pour la première fois dans [131]. Dans cette thèse, les performances des systèmes SM sont étudiées à l'aide d'un banc d'essai expérimental dans les environnements mixtes line-of-sight/non-line-of-sight (LOS/NLOS). La proportion des composantes LOS et NLOS est évaluée par le facteur K de Rice. Deux méthodes sont employées pour réaliser cette étude. La première consiste à combiner les sorties de deux sources SM qui émulent les chemins directs et complémentaires. Le signal résultant est acheminé au récepteur par câble afin d'obtenir un accord précis des voies de communication LOS/NLOS. La deuxième méthode consiste à mettre en œuvre un scénario de transmission par voie hertzienne dans un environnement intérieur ("indoor"). Afin de faire varier les caractéristiques du canal de propagation, des absorbants électromagnétiques sont insérés entre les antennes émettrices et réceptrices pour contrôler le niveau de puissance du signal LOS. Une méthode de sondage du canal est également appliquée pour évaluer les caractéristiques du canal de propagation. Les performances du système SM dans la mise en œuvre pratique sont comparées aux résultats de la simulation.

La configuration de cette expérimentation peut être simplement divisée en parties matérielles et logicielles, respectivement au niveau physique et au niveau de la simulation. La fonction de bloc et la chaîne de transmission sont données dans la Figure 0.8. Le système SM est mis en œuvre en utilisant quatre modules VST PXIe-5646 de National Instruments (NI) [3] qui sont programmés à l'aide de l'environnement de programmation LabVIEW. Le VST est un émetteur-récepteur de signaux vectoriels capable d'émettre et de recevoir en même temps. Ici, pour réaliser un système SM de 2×2, deux modules VST sont censés travailler pour l'émission et les deux autres modules sont employés pour la réception. Les quatre modules VST sont intégrés dans un châssis PXIe qui peut garantir la synchronisation des symboles.

Les performances du BER dans un environnement à propagation contrôlée et dans un environnement hertzien sont présentées respectivement sur la Figure 0.9 et la Figure 0.10. Par conséquent, les performances du BER de la mise en œuvre pratique pour les deux environnements de propagation proposés ont été analysées et les deux ont bien

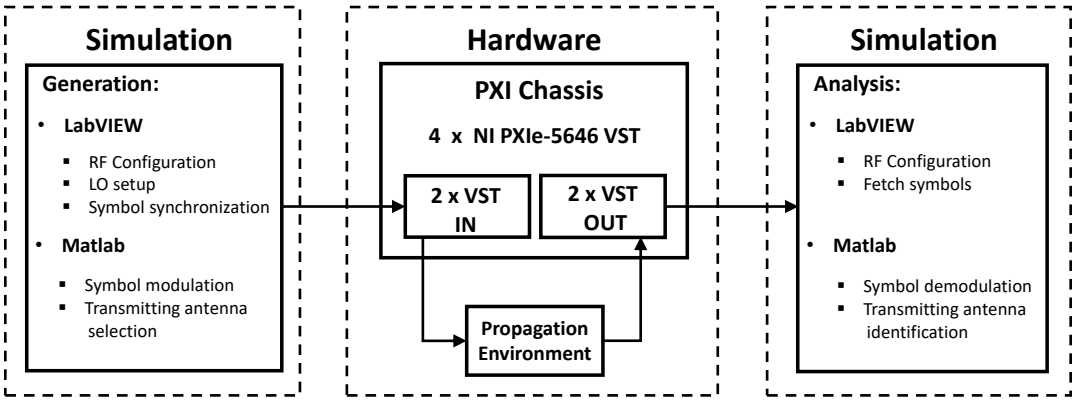

Figure 0.8: Principales parties du montage expérimental

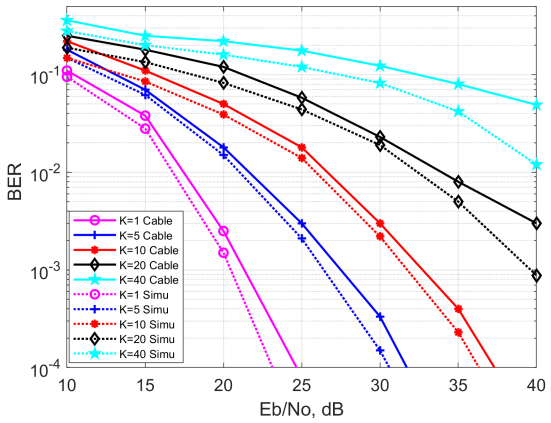

Figure 0.9: Simulation et résultats expérimentaux avec un environnement de propagation contrôlé pour la performance BER du système SM dans des scénarios mixtes LOS/NLOS

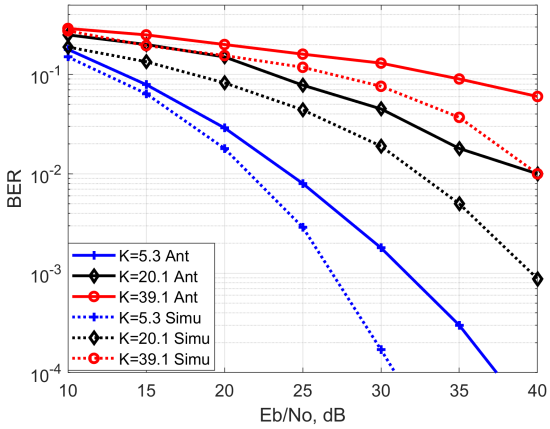

Figure 0.10: Simulation et résultats expérimentaux avec environnement de propagation réel pour les performances BER du système SM avec $N_t = 2$ sous trois scénarios mixtes LOS/NLOS

suivi les résultats de la simulation. Plus précisément, les performances en termes de BER pourraient être meilleures en présence de trajets multiples et de conditions de propagation NLOS.

0.3 Conclusion

Nous pouvons conclure cette thèse par deux contributions principales : la recherche sur le système SM et la recherche sur le système FDSM.

- **Système SM** : Le cadre de simulation et l'expérimentation pratique du système

SM sont étudiés respectivement au chapitre 3 et au chapitre 6. Le chapitre 3 traite un système SM sur un canal à évanouissement de Rice variant dans le temps. En particulier, un détecteur CSI variant dans le temps basé sur LS pour l'estimation du canal est conçu au lieu de supposer un CSI parfait au niveau du récepteur. En outre, l'indice d'antenne et le symbole sont détectés séparément en utilisant une méthode de détection ML à faible complexité, où la détection de l'indice d'antenne est simplifiée comme l'optimisation de l'amplitude, et la détection du symbole est simplifiée comme l'optimisation de la phase. Les performances du système SM proposé sur un canal à évanouissement de Rice variant dans le temps sont analysées au niveau de la simulation à l'aide des logiciels Keysight ADS et Matlab. Les résultats de la co-simulation montrent que le BER peut être maintenu à un niveau acceptable en utilisant le détecteur CSI proposé et le système a des meilleures performances avec un facteur de Rice faible, ce qui indique que nous pouvons mieux détecter l'antenne émettrice en présence de plus de trajets multiples. Le chapitre 6 analyse les performances du système SM dans des conditions LOS/NLOS à l'aide d'un cadre expérimental basé sur le matériel du châssis NI PXI et le module VST. La configuration expérimentale est analysée en détail et deux stratégies sont envisagées afin de configurer les canaux de propagation. La première stratégie consiste à construire un environnement de propagation contrôlé. La deuxième approche consiste à transmettre par voie aérienne sur un canal de propagation réaliste et non contrôlé. En outre, une méthode de détection de canal utilisant la bonne propriété de corrélation des séquences PN est appliquée afin d'extraire les coefficients de canal. En conséquence, la performance BER de l'implémentation expérimentale dans les deux environnements de propagation est analysée, les deux suivent bien les résultats de la simulation avec une légère dégradation.

- **Système FDSM** : La recherche sur le système FDSM est abordée au chapitre 4 et au chapitre 5. Dans le chapitre 4, un environnement de simulation d'un système FDSM 2×2 est présenté. Nous avons introduit différents modules (sélection d'antenne, module de modulation et de démodulation, module de correction de canal, estimation SI, module SIC, etc.) pour compléter ce cadre de simulation. En particulier, l'algorithme de l'étape de démodulation est décrit en détail. Pour analyser la performance du système FDSM proposé, l'impact de la précision SIC sur la performance BER pour différents INRs est mis en évidence. Nous pouvons conclure qu'une performance BER acceptable nécessite de maintenir l'erreur d'estimation du SI dans une petite plage. Le système FDSM est moins performant que le système

FD lorsqu'il n'y a pas d'erreurs ou lorsqu'il y a de légères erreurs de l'estimation de SI. Cependant, la sensibilité plus faible permet au système FDSM de maintenir une performance BER proche de celle du système FD, voire meilleure en présence d'erreurs importantes.

De plus, nous analysons la relation entre la performance BER et le nombre de symboles pour la détection, où INR est introduit comme le rapport du signal d'auto-interférence au bruit. On peut remarquer le fait que le nombre de symboles pour la détection a moins d'impact sur les performances lorsque l'INR est grand. Dans le chapitre 5, la performance du système FDSM avec des non-idéalités du récepteur, un PA non-linéaire et des imperfections de commutation est analysée. En ce qui concerne les non-idéalités du récepteur, le déséquilibre IQ et le bruit de phase sont les deux principaux problèmes. Nous observons le fait que le système est plus sensible au déséquilibre IQ avec un SNR faible. Les résultats numériques montrent que l'estimateur proposé peut atteindre un BER acceptable en présence d'un déséquilibre IQ, ce qui est en accord avec la théorie. Parallèlement, le bruit de phase de NI PXI VST influence légèrement les performances du système en termes de BER et peut être négligeable. De plus, les effets non linéaires du PA à faible coût sont rigoureusement modélisés et un annulateur numérique est considéré pour supprimer le signal SI impacté par les non-linéarités du PA. Enfin, l'effet d'imperfection du commutateur RF a également été étudié, ce qui inclut le temps de réponse du commutateur et la perte d'insertion du commutateur. En particulier, une solution pour atténuer l'effet du temps de commutation a été proposée.

CHAPTER 1

GENERAL INTRODUCTION

1.1 Introduction

In recent years, wireless communication has served all aspects of social activity and life, and has become an infrastructure supporting the normal operation of society. The wireless communication systems continues to evolve with changes in demand, and has evolved from the first generation (1G) to the fifth generation (5G) [42]. The services that it supports have also evolved from the initial voice communication to multiple services such as broadband multimedia and connected objects. In addition, the service objects of the system have also changed, from communication between people to machine-oriented interconnection [10, 126]. Every evolution of wireless communication technique reflects revolutionary changes in productivity and lifestyle. With the further increase in demand, the physical layer of the future wireless communication system not only needs to provide higher bandwidth, lower latency, higher data transmission rate and reliability, but also needs to pay attention to energy consumption, system complexity, cybersecurity and support for multiple services [24, 97].

To respond to these requirements, the index modulation is a new type of modulation technique that has emerged in recent years [119]. In traditional wireless communication systems, the modulation process is to map all the information bits that need to be transmitted into amplitude/phase modulation symbols, while index modulation can use the index of spatial resources to transmit information. Spatial modulation (SM) is a typical representative of index modulation [19]. SM as a new Multiple-Input Multiple-

Output (MIMO) transmission technique has been developed in recent years. It carries information by activating the one individual antenna corresponding to a certain index and by digital modulation constellation symbols. It can provide a sparse radio-based MIMO design scheme, thereby simplifying the traditional MIMO architecture. The structure reduces the implementation cost of MIMO, and is expected to further provide an efficient massive MIMO solution. The basic idea of SM is that only one antenna is activated for each time slot to transmit traditional amplitude/phase modulation symbols; bit information is jointly transmitted by the activated antenna index and constellation symbols. Compared to the traditional MIMO techniques, SM has the following advantages: **(1) High transmission rate**: SM uses the antenna index as an information carrier to transmit additional data. Compared with the single antenna technique based on amplitude/phase modulation transmission and the multi-antenna technique based on space diversity, a higher transmission rate can be obtained. **(2) Avoid inter-antenna interference (ICI) and channel synchronization**: Since only one antenna transmits data for each time slot, and other antennas do not transmit data, the problems of ICI and channel synchronization caused by spatial multiplexing can be effectively avoided. **(3) Low-complexity detection**: The receiving end can use step-by-step detection methods to effectively reduce the detection complexity. More precisely, the antenna index is first detected, and then the detected index is used to further detect the symbol. **(4) Flexible antenna configuration**: Since a single antenna is activated for each time slot, the receiving end only needs very few antennas to accurately estimate the transmitted data bit stream. Therefore, compared with V-BLAST system, SM is more suitable for asymmetric MIMO channels where the number of receiving antennas is much smaller than the number of transmitting antennas. **(5) Reliable transmission performance**: The literature [61] proved that with the same transmission rate, SM can achieve better bit error rate (BER) performance than traditional V-BLAST and space-time block code (STBC) systems. **(6) Low energy consumption and implementation cost**: Only one radio frequency (RF) chain is required in the transmitting end of SM, which simplifies the traditional MIMO structure and effectively reduces the implementation cost of MIMO transmission technique.

Meanwhile, the ever-increasing requirements for communication demands bring new challenges to be more efficient on the use of the limited existing spectrum resources. Therefore, full duplex (FD) has received extensive attention because it can theoretically double the existing spectral efficiency and system capacity. In the classical wireless communication systems, in order to achieve two-way communication, it is necessary to

divide the wireless communication channel in time or in frequency (one part for the transmission in one way and another part for the transmission in the opposite way), in order to achieve two-way communication in the past wireless communication system, it is necessary to divide the transceiver channel from the time domain or the frequency domain to avoid interference conflicts between emission and reception parts. These two divisions correspond to the two duplex techniques i.e. time division duplex (TDD) and frequency division duplex (FDD) respectively. In these two techniques, the same spectrum resource is either time-shared by the transceiver channel, or can only be used exclusively by one of the channels. Using the same frequency to transmit and receive signals at the same time was considered to be almost impossible in the past [49]. However, in recent years, with the research of Rice University [12, 15, 39–41] and Stanford University [22, 23, 31, 56, 58], people have seen the feasibility of its realization. Self-interference cancellation (SIC) is the main challenge to realize FD. Since the local transmit signal and the signal received from the remote end (i.e. the signal of interest) use the same frequency resources, and the local transmit antenna is much closer to the receiving antenna, the local transmit signal will cause strong self-interference (SI) to the signal of interest. In addition, there are some nonideal RF factors that limit the performance of SIC, including: phase noise, I/Q imbalance, power amplifier nonlinearity, etc [71]. Various SIC techniques have been developed which can be divided into three categories according to the location of SIC: **(1) Passive SIC**: By varying the distance between the antennas in order to increase their decoupling. **(2) Analog SIC**: Because the SI and the corresponding propagation channels are known by the FD node, it is subtracted from the receiver end in order to bring it below the noise level. **(3) Digital SIC**: Digital SIC refers to the realization of SIC in the digital domain (after ADC), including reconstruction of SI in the digital domain and subtracting it from the receiving end. Moreover, the nonideal RF components can be included in the modeling within the digital canceller [76].

The combination of FD and SM can be interesting because when a single RF chain is implemented, the complexity of SIC will not increase compared with single-input single-output (SISO) systems, but the spectral efficiency is doubled. Moreover, full duplex spatial modulation (FDSM) systems offer the benefits of MIMO like diversity and multiplexing gains but with low energy consumption. The superiority of the FDSM system is discussed in [99, 138].

1.2 Contributions

Different contributions have been made in this PhD thesis preparation in order to evaluate the performance of the SM system and the FDSM one.

- **Simulation framework of the SM system**: A SM system over the time-varying Rician fading channel is introduced. In particular, a time-varying channel state information (CSI) detector for the channel estimation is designed instead of assuming the availability of the perfect CSI at the receiver. Moreover, the index of transmitting antenna and symbol are detected respectively by employing a low complexity ML detection method. The ADS-Matlab co-simulation results demonstrate that the BER can be maintained at an acceptable level with a realistic CSI detector, and in this case the system offers better performance with a small Rician factor.

- **Simulation framework of the FDSM system**: In this FDSM framework, different modules (antenna selection module, modulation, and demodulation, channel correction module, SI estimation, SIC module, etc.) are introduced. The results demonstrate that the requirement of estimation accuracy is higher as the self-interference-to-noise ratio (INR) increases. The FDSM system is less sensitive than the FD system in presence of high estimated error value. Furthermore, an SI detector is presented to resolve the influence of the number of detect symbols.

- **Nonideal effects on the FDSM system**: The performance of the FDSM system has been analyzed in presence of the IQ imbalance, of the nonlinear power amplifier (PA), of the phase noise and of the switch imperfections. A least-square (LS) estimator is proposed to suppress the SI signal received by the imperfect RF receiver. We observed that the system is more sensitive to IQ imbalance under low signal-to-noise ratios. The numerical results show that the proposed estimator can reach an acceptable BER. The phase noise of the instrument planned for the measurement campaigns slightly influences the system BER performance. Moreover, the nonlinear effects of a low-cost PA are modeled rigorously and a digital canceller is considered to suppress the SI signal taking into account PA nonlinearities. Lastly, the imperfection effects of the RF switch are also considered, which includes the switch response time and the switch insertion loss.

- **Experimental implementation of SM system**: The performance of a SM system has been analyzed, for the first time, under mixed line-of-sight/non-line-of-sight

(LOS/NLOS) conditions with the help of an experimental framework based on NI VST modules. An extensive analysis of the experimental setup is presented and two models of the propagation environments (controlled one and over-the-air one) are proposed. Moreover, a channel sounding method by using the good correlation property of pseudo-noise (PN) sequences has been employed in order to extract the channel coefficients. As a result, the BER performance of practical implementation for the two proposed propagation environments is analyzed and both followed well the simulation results. Specifically, the performance in terms of BER could be better in presence of multipath and NLOS propagation conditions.

1.3 Thesis outline

The outline of this thesis is as follows:

- **Chapter 2**: This chapter gives the reviews about the state-of-the-art and background of this research. A wireless communication evolution is first presented to introduce the current status of wireless communication systems. MIMO as a wireless communication technique is highlighted. Then SM and FD as our research field of this thesis are introduced, specifically related to their realization principles, development status, challenges and applications.

- **Chapter 3**: This chapter discusses a SM system over the time-varying Rician fading channel. The modulation module as well as the channel model are introduced. Also, we introduce a channel state information (CSI) detector for the channel estimation and analyze the performance of the proposed spatial modulation (SM) system over the time-varying Rician fading channel. The BER performance is evaluated under different conditions.

- **Chapter 4**: A FDSM framework is introduced in this chapter. SM increases spectral efficiency and uses only one radio frequency chain. For FD communication systems, SI is always a central problem. Therefore, combining FD and SM can drastically reduce the difficulty of SIC due to the single SI chain. A FDSM system model is proposed and an active analog SIC is highlighted. Moreover, the impact of SIC accuracy on the system performance is studied.

- **Chapter 5**: In this chapter, the performance of a FD system combined with spatial modulation technique in presence of nonidealities is analyzed. IQ imbalance and

phase noise are the two radio front-end mismatch factors that have been considered, as well as the nonlinear power amplifier (PA) effects. The impact of the IQ imbalance on the BER performance of the FDSM system under different noise levels is investigated. An estimator has been proposed for the self-interference cancellation (SIC) after the imperfect receiver. A digital canceller is also adopted to deal with the strong SI in presence of PA nonlinearities. The imperfections of the switch are discussed lastly from the aspect of switching time, path isolation and insertion loss.

- **Chapter 6**: This chapter introduces the experimental implementation. It aims to analyze the SM system transmission under different LOS/NLOS propagation scenarios. The analysis of the SM system performance is based on both simulation and experimental results and the BER is tackled. Concerning the experimental results, two strategies are considered in order to configure the propagation channel. The first one consists in constructing a controlled propagation environment. More precisely, the multipath channel's Rician K-factor is imposed by configuring the power levels of the LOS and of the NLOS components. The second method consists in performing over-the-air transmissions on a realistic propagation channel. A channel sounding method allows us to measure the channel characteristics.

- **Chapter 7**: A summary of this thesis together with the highlight of the main results is provided in this chapter. Some propositions to be provided in future works are also given in this chapter.

1.4 List of publications

JOURNAL :

1. **Y. Zhou**, F. Hutu and G. Villemaud, "Impact of Receiver Non-Idealities on a Full Duplex Spatial Modulation System Performance," in IEEE Wireless Communications Letters, vol. 9, no. 12, pp.2083-2087, Dec. 2020, doi: 10.1109/LWC.2020.3013195.

2. **Y. Zhou**, F. Hutu and G. Villemaud, "Experimental Analysis of Spatial Modulation Systems in Mixed LOS/NLOS Scenarios," Submitted in IEEE Access.

INTERNATIONAL CONFERENCES :

3. **Y. Zhou**, F. Hutu and G. Villemaud, "Analysis of a Spatial Modulation System over Time-varying Rician Fading Channel with a CSI Detector," 2020 IEEE Radio and Wireless Symposium (RWS), San Antonio, TX, USA, 2020, pp. 217-220, doi: 10.1109/RWS45077.2020.9050121

4. **Y. Zhou**, F. Hutu and G. Villemaud, "Full Duplex Spatial Modulation System Performance Depending on Self-interference Cancellation Accuracy," 2020 14th European Conference on Antennas and Propagation (EuCAP), Copenhagen, Denmark, 2020, doi: 10.23919/EuCAP48036.2020.9135954

5. **Y. Zhou**, F. Hutu and G. Villemaud, "Full Duplex Spatial Modulation System in presence of IQ imbalance," 2020 XXXIIIrd General Assembly and Scientific Symposium of the International Union of Radio Science, Rome, Italy, 2020, doi: 10.23919/URSIGASS49373.2020.9231978

6. **Y. Zhou**, F. Hutu, G. Villemaud and T. Riihonen, "Nonlinear Power Amplifier Effects on a Full Duplex Spatial Modulation System," PIMRC 2021 - IEEE 32nd Annual International Symposium on Personal, Indoor and Mobile Radio Communications, Oulu / Virtual, Finland, 2021

CHAPTER 2

BACKGROUND AND STATE OF ART

2.1 Introduction

The wireless communication system has completely changed the way people communicate, combining both information exchange and mobility. Looking back at the development history of wireless communication, great progress has been made in a very short period. In the past few decades, the demand for wireless connections has grown exponentially. Hence, 5G communications have far more functions and capabilities than the fourth-generation (4G), and will soon be deployed globally. At the same time, the rapid development of various emerging applications such as artificial intelligence (AI), virtual reality (VR), three-dimensional (3D) media, and Internet of Everything (IoE) has brought massive amounts of traffic [33]. With the explosive growth of wireless mobile devices and services, it is estimated that by 2030, the demand for data rates will reach 1 Tbit/s, which will be nearly 1000 times the rate provided by 5G networks [139]. Therefore, we should pay attention to the issues such as spectrum resources and high energy consumption. In this case, severals solutions have been proposed to save energy consumption and to improve spectrum efficiency. Among them, two representative ones are spatial modulation (SM) and full duplex (FD). SM solves some drawbacks of MIMO systems such as strong inter-channel interference (ICI), high power consumption and systems complexity due to multiple radiofrequency (RF) chains [93]. FD communications can double the radio link data rate and the spectral efficiency through simultaneous and bidirectional communication.

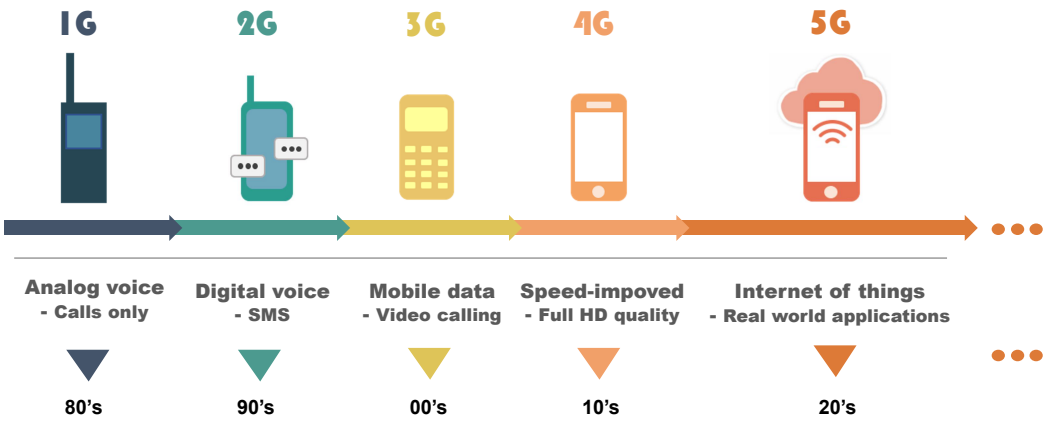

Figure 2.1: Evolution of mobile communication network

2.2 Wireless communication evolution

2.2.1 From 1G to 5G

James Clerk Maxwell presented his famous equation to the Royal Society in 1864, which mathematically described the behavior of electromagnetic fields., which was proved by the Heinrich Hertz's spark discharge experiment in 1887. Since Guglielmo Marconi's wireless communication experiment in 1895, wireless communication technique has emerged. It has gradually involved land, ocean, aviation, aerospace and other fixed and mobile wireless communication fields. Here, we introduce the evolution of wireless communication from 1G to 5G in the past several decades.

Mobile wireless generation (G) generally refers to the changes in system speed, technique, frequency, data capacity, latency, etc. In recent decades, mobile communication has realized the evolution from 1G to 5G. Each generation is different from the previous one due to standard evolution, i.e. capacity increase, and emergence of new technologies and new features. This evolution was made possible by advances in both analog and digital electronics and signal processing, especially in understanding the phenomena occurring on the propagation channel, and by advances in information theory. More details about transformation of mobile communication network from 1G to 5G are presented in [35, 57, 80]. The evolution of the mobile wireless generation is shown in Figure 2.1.

1G communication introduces analog mobile voice services, and establishes seamless wireless connections through authorized spectrum (i.e. installing base stations, providing mobile network access through dedicated radio spectrum) and frequency reuse (i.e.

real-time connection of multiple base stations ensuring that users' voice calls are not disturbed when moving). Although 1G is revolutionary, in terms of spectral efficiency, the capacity of analog transmission is limited, and the scalability of using analog equipment (large, expensive, low-efficiency) is also limited.

Next is the global system for mobile communications standard (GSM, European standard for 2G), which has been evolved from analog transmission to digital transmission. It uses the time division multiple access (TDMA) method to achieve the data capacity increase and to support roaming between different networks. 2G provides a network platform that supports new mobile services (SMS, MMS, picture messages), and improves voice quality and clarity through digital coding. The scalability of digital devices has been improved because they are cost-saving and lighter than analog devices (digital signals consume less battery power). General packet radio service (GPRS) was later introduced to support packet switching technique, which ultimately provides data communication services such as wireless application protocol (WAP), e-mail, and world wide web access at a data rate of 56 Kbit/s-144 Kbit/s.

Shortly after the passage into the new millennium, we saw an increase in demand for mobile data services (games, video conferencing, large emails, videos), and the third generation (3G) network create a high-speed Internet with a transmission speed of 2 Mbit/s where universal mobile telecommunications system (UMTS) is implemented to respond to this request.

As the demand for higher network speed grows continuously, 4G network was launched in 2009 to provide a faster and better mobile broadband experience through higher data capacity. Its advantage is the increase of the bandwidth and the services, while improving efficiency by reducing the cost per bit on the network. It provides a higher data rate (up to 100 Mb/s) by implementing orthogonal frequency-division multiple access (OFDMA) technique, supporting wide channels and using signal coding and multiplexing modes. The key difference between 4G and 3G is the realization of an all-IP network and the decommissioning of the circuit switching infrastructure.

If 4G only changes our daily life in a personal way, the impact of 5G is much greater. 5G is not only coming only with high data rate, reduced latency, energy saving, cost reduction, increased system capacity, and large-scale device connection but also with a multi-service and multi-technique integrated network. The intelligent network of user experience will eventually create a user-centric information ecosystem. 5G applications can be divided into three major areas: the improvement of the existing 4G experience, the application on autonomous driving and VR/AR, and the Internet of Things (IoT) [25].

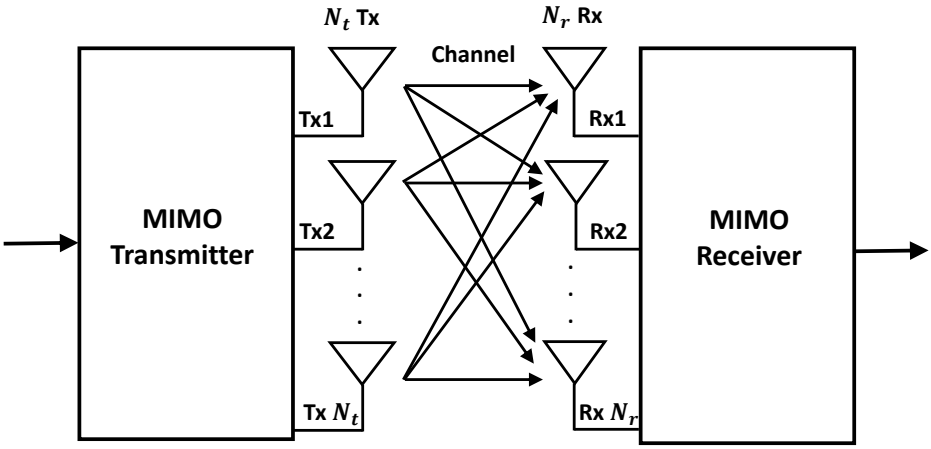

Figure 2.2: Block diagram of MIMO transmission system

Although 5G wireless networks are yet to be fully investigated, the sixth-generation (6G) of mobile networks has already come into the discussion and is expected to burgeon in the coming decade [14, 62]. It is foreseeable that 6G will further improve spectral efficiency and system reliability, reduce energy consumption and at the same time ensure privacy and security, finally aims to achieve an IoE society across the ground, underwater and space, and achieve the breakthrough in tactile communication and tactile applications

2.3 Multiple-antenna wireless communication systems

2.3.1 Overview of MIMO systems

Wireless transmission technique is a core part of wireless communication systems. In order to meet the needs of high data rate and high system capacity, it is important to develop wireless communication technologies with high spectral efficiency and reliable transmission performance. MIMO is a wireless communication technique that can meet the above requirements. It is equipped with multiple antennas at the transmitting and/or receiving ends and is combined with advanced space-time coding and modulation methods. By fully exploiting the spatial degrees of freedom, it can bring additional gains such as diversity, multiplexing and beamforming [47, 49]. A traditional $N_t \times N_r$ MIMO transmission system is shown in Figure 2.2.

MIMO has been thoroughly studied in theory and practice. However, while MIMO technique brings us various gains, it is also accompanied by drawbacks such as complex structure and high implementation cost [37]. This is mainly due to the following problems in the transmission design of MIMO:

- **Inter-antenna channel interference**: The signal processing complexity will increase due to the electromagnetic coupling of multiple symbols introduced in time and space.
- **Synchronization between the emitters associated to the transmitting antennas**:

  When multiple transmitting antennas emit signals to a receiving antenna at the same time, the different transmitters associated to the antennas are required to be synchronous (RF and symbol synchronization) to ensure the accuracy of the MIMO implementation.
- **Multiple RF chains**:

  All signals need to be transmitted at the same time, and each transceiver antenna needs to be equipped with a corresponding RF chain, which increases the cost and the consumption.

In addition, traditional space division multiplexing systems often require a higher number of receiving antennas than the transmitting ones [114]. However, with the constraints on the cost and size of mobile terminals, this requirement is difficult to meet.

2.3.2 MIMO Channel modelling

Propagation channel as the medium for wireless communication contains multipaths, which will introduce attenuation and delay when different signal versions arrive at the receiver. It results in chromatic dispersion and fading (rapid fluctuations in power level) effects [121], chromatic dispersion is the term given to the phenomenon by which different spectral components of a pulse travel at different velocities. The path from the transmitter to the receiver is not flat, and the transmitted signal may experience various attenuations, including path loss, multipath fading, etc. The signal attenuation through the path depends on various factors (e.g. time, RF, and path or position of transmitter/receiver). In general, it's crucial to predict expected mean received signal power in determining cell size, frequency reuse, and other system design issues. The power of the received signal is impacted by three factors:

- **Propagation pathloss**:

  The propagation pathloss is caused by the distance effect. One can simply use physical laws to derive theoretical formula to describe propagation pathloss, but more often in complex environment, empirical models like Hata model are sought.

- **Slow (large-scale) fading**:

  Large-scale fading (i.e. shadowing) refers to the shadow variations that are caused by large terrain features, such as small hills and tall buildings, between base station and mobile station. Power variation statistics due to large-scale fading can be well quantified, as the process is “slow”.

- **Fast (small-scale) fading**:

  Small-scale fading concerns rapid fluctuations of received signal strength in a very short distance and within a short time period. Based on multipath delay spread there are two types of small-scale fading (i.e. flat fading and frequency selective fading). These multipath fading types depend on the propagation environment. It is difficult to model small-scale fading accurately, because the factors that influence fast fading characteristics are highly complex.

For the small-scale fading, if the fading characteristics of the received power is studied over a short distance of about 20 wavelengths, the in-phase (I) component and quadrature (Q) component models of the superimposed signal (i.e. the impulse response) can be considered as independent zero-mean Gaussian processes. This model assumes that the number of scattered components is large and independent of each other. Therefore, the energy or envelope of the channel response corresponds to a Rayleigh distribution and its probability density function (PDF) is

$$\mathrm{PDF}_{\mathrm{Rayleigh}}(x) = \frac{x}{\sigma^2} \exp\left(-\frac{x^2}{2\sigma^2}\right) \tag{2.1}$$

where x is a random variable, which is the amplitude of the received voltage, and σ is the standard deviation. For a static user, due to the relative movement of the scatterers in the vicinity of him, there are also responses of channel on time. The Rayleigh fading model is suitable to describe wireless channels in dense urban areas, where there is no direct path, and where signals are attenuated, reflected, refracted and diffracted.

If there is a direct path between the transmitter and the receiver, the signal envelope is no longer a Rayleigh distribution, and the statistical characteristics of the signal amplitude will be a Rice distribution. Rice fading is formed by the sum of Rayleigh

distributed signals and direct or line-of-sight (LOS) signals. The Rice fading environment has a strong direct path, and its time delay to the receiver is roughly the same as the multipath arrival delay from the local scatterer. The voltage amplitude envelope of the Rice distribution has the following PDF:

$$\mathrm{PDF}_{\mathrm{Rice}}(x) = \frac{x}{\sigma^2}\exp\left(-\frac{x^2}{2\sigma^2} - K\right) I_0\left(\frac{x}{\sigma}\sqrt{2K}\right) \tag{2.2}$$

where K is the Rician K-factor corresponding to the ratio of LOS power to total power of all indirect paths, $I_0(\cdot)$ is the modified 0^{th} order Bessel-function of 1^{st} kind. x is a random variable and σ is standard deviation.

For MIMO wireless systems, the spatial channel model required for the communication link needs to have both transmit and receive diversity. the key to the simulation of MIMO communication channels is the modeling of the spatial channel impulse response. The MIMO channel can be characterized based on the propagation environment or the MIMO system circuitry (antenna configuration, antenna type, antenna orientation map, filter mechanism, etc.). Characterizing the MIMO channel according to the former case is termed the bidirectional channel impulse response, while the latter is termed the MIMO channel matrix [122, 123].

The MIMO channel impulse response is the sum of several multipath components, each with its own amplitude, phase, delay, angle of arrival and angle of departure. The distribution of these parameters depends on the type of propagation environment being modeled.

The channel state matrix can provide the required information to characterize whether spatial multiplexing is possible for multilayer data transmission. Assume a MIMO system with N_t transmitting antennas and N_r receiving antennas. The time-varying channel impulse response between the j^{th} ($j = 1,2,...,N_t$) transmitting antenna and the i^{th} ($j = 1,2,...,N_t$) receiving antenna is supposed as $h_{ij}(\tau,t)$. Hence, the $N_t \times N_r$ MIMO channel matrix $\mathbf{H}(\tau,t)$ can be given by

$$\mathbf{H}(\tau,t) = \begin{bmatrix} h_{1,1}(\tau,t) & h_{1,2}(\tau,t) & \dots & h_{1,N_t}(\tau,t) \\ h_{2,1}(\tau,t) & h_{2,2}(\tau,t) & \dots & h_{2,N_t}(\tau,t) \\ \vdots & \vdots & \ddots & \vdots \\ h_{N_r,1}(\tau,t) & h_{N_r,2}(\tau,t) & \cdots & h_{N_r,N_t}(\tau,t) \end{bmatrix} \tag{2.3}$$

where the matrix elements are complex numbers corresponding to the attenuation and phase shift of the signal introduced into the wireless channel to reach the receiver with delay τ .

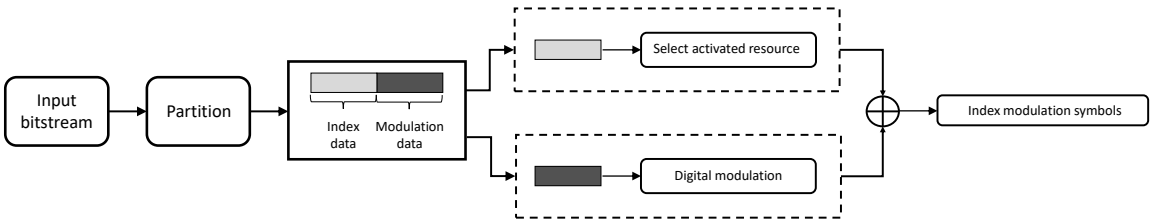

Figure 2.3: Block diagram of index modulation

2.3.3 Index modulation techniques

Index modulation technique is a new type of modulation technique in MIMO systems that has emerged in recent years [19, 119]. In the traditional wireless communication systems, the modulation process is to map all the information bits that need to be transmitted into amplitude/phase modulation symbols [104]. The case of index modulation mapping is different which is shown in Figure 2.3. It can be seen from the figure that index modulation divides the information bits that need to be transmitted into two parts: one part is used to select activated resource; the other part is mapped to amplitude/phase modulation symbols which will be transmitted by the activated resources. According to different index resource domains, index modulation can be further divided into spatial index modulation system, frequency domain index modulation system, and other domain index modulation systems.

This unique modulation method gives the index modulation system the following advantages: firstly, the transmission of the bit information carried by the index does not require additional transmission power, which makes the index modulation system more energy efficient than traditional wireless communication systems. Secondly, because only part of the resources is activated, the transmitted signal of the index modulation system demonstrates a certain sparse characteristic, which is conducive to the realization of low-complexity detection algorithms. Finally, the sparse signal reduces adjacent channel interference, making index modulation have strong anti-interference ability. In general, index modulation technique has the advantages of low power consumption, low complexity and high energy efficiency. It is a solution suitable for future mobile communications in terms of physical layer modulation technique [17].

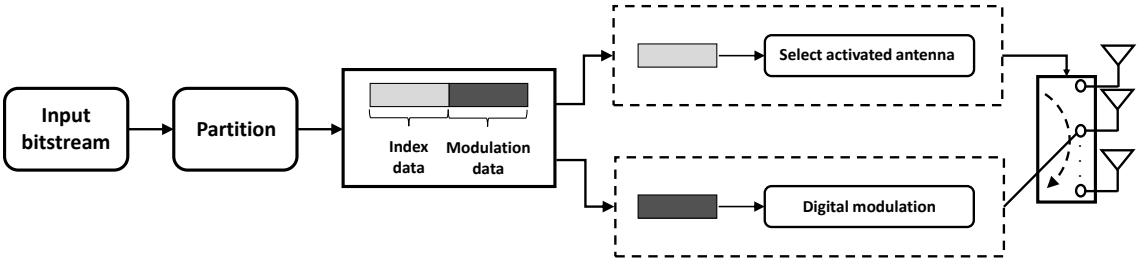

Figure 2.4: Block diagram of spatial modulation

2.4 Transmit spatial modulation

Index modulation was first applied in the spatial domain, resulting in a spatial index modulation technique, also known as SM technique [37, 94, 109, 128]. At the transmitting end of the SM system, the information bits are divided into two parts: one part is mapped to traditional amplitude modulation/phase modulation symbols; the other part is used to activate a specific antenna from all transmitting antennas for symbol transmission. The receiving end can recover the information bits carried by the two parts at the same time by detecting the index of the symbol and the activated antenna. We discuss the background and the state of art of SM from two aspects: transmitter design and prospects of application.

2.4.1 Transmitter design

2.4.1.1 Principle

SM uses the spatial dimension and the transmitter selects only one antenna (could be more for generalized spatial modulation) to transmit the data in each time slot. The transmitted information bits are mapped to the traditional digital modulation constellation. On the other hand, the remaining bits are mapped to the spatial dimension generated by the antenna number. The principle of SM is shown in Figure 2.4. Hence, SM effectively avoids symbol interference and antenna synchronization, while ensuring the spectral efficiency of the system by using the active state of antennas as a support for information transmission.

In order to give an example of SM system, it is assumed that the number of transmitting antennas in the system is N_t, the number of receive antennas is N_r, the modulation method is M-QAM (i.e. the modulation order is M), N is the bits of information transmitted in each time slot which is equal to $\log_2(N_t)+\log_2(M)$ bits. With SM mapping method,

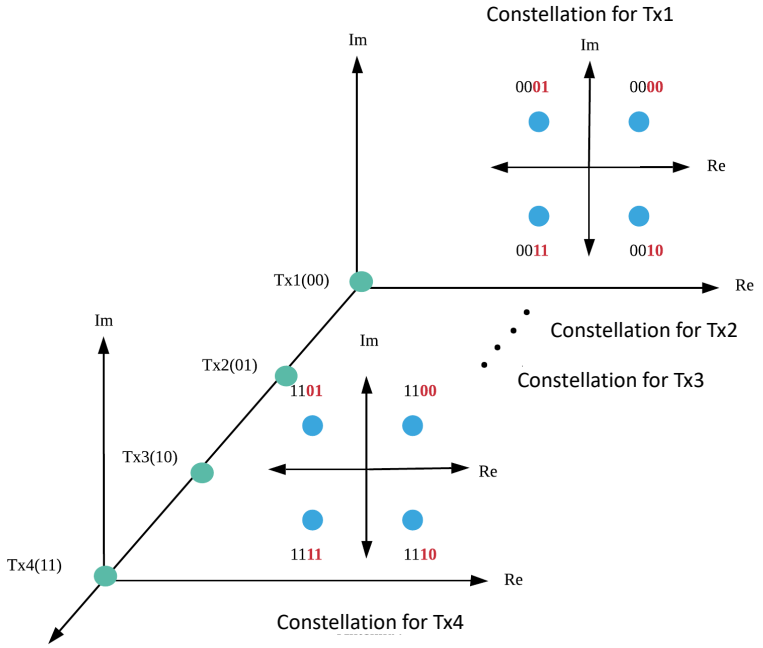

Figure 2.5: 3D constellation diagram of SM with QPSK modulation

$\log_2(M)$ bits are mapped to a certain point in the traditional modulation constellation, and $\log_2(N_t)$ bits are mapped to the antenna numbers performing in the system to form a spatially modulated 3D constellation.

The 3D constellation diagram of the modulation type QPSK ($M = 4$) for four transmitting antennas ($N_t = 4$) is demonstrated in Figure 2.5. One can remark that each 4-bit information is divided into two groups: the first two bits are used to select the number of antenna, and the last two bits are used as traditional QPSK modulation. It can be concluded that the number of transmission bits per slot is determined by the modulation method and the number of the transmitting antennas.

With SM 3D mapping, $\mathbf{x}$ is assumed as the transmission matrix, where $\mathbf{x} \in \mathbb{C}^{N_t \times 1}$ and has the form:

$$\mathbf{x} = \boldsymbol{e}_i \cdot s_m \tag{2.4}$$

where

$$\mathbf{e_i} = \begin{pmatrix} 0 & 0 & \dots & 1 & \dots & 0 & 0 \end{pmatrix} \tag{2.5}$$

Only the j^{th} column that corresponds to the index of the transmitting antenna j has the

value 1 and the value in the remaining columns is 0. The amplitude/phase modulation symbol is denoted by s_m, $m \in [1,2,\ldots,M]$. Hence, the received signal of the SM system can be expressed as

$$\mathbf{y} = \mathbf{H} \cdot \mathbf{x} + \eta \tag{2.6}$$

where $\mathbf{H} \in \mathbb{C}^{N_r \times N_t}$ represents a flat fading channel matrix. $\eta \in \mathbb{C}^{N_r \times N_1}$ denotes the thermal noise at the receiving end which corresponds to a Gaussian distribution $\mathbb{CN}\left(0,\sigma^2\right)$. Due to the special structure of the transmitted signal $\mathbf{x}$, the SM system can also be regarded as the selection of the channel matrix, and the corresponding received signal y can be expressed as

$$y = \mathbf{h}_i \cdot s_m + \eta \tag{2.7}$$

where $\mathbf{h}_i$ represents the i^{th} column of the channel fading matrix H.

2.4.1.2 Derivative techniques

Once the basic system model of SM was proposed in [94, 96], a series of derivative designs of transmitters based on the idea of SM emerged. From the perspective of reducing system complexity, space shift keying (SSK) technique was proposed in [61]. In SSK systems, it is the antenna index used during transmission that relays information, rather than the transmitted symbols themselves. The simplicity involved in modulation reduces the detection complexity compared to that of SM while achieving almost identical performance gains. However, only one antenna is activated for each transmission which leads to a limited spectral efficiency.

In order to improve the spectral efficiency, a generalized space shift keying (GSSK) method was described in [59]. As SSK systems, GSSK systems also use only the antenna index in order to transmit information. However, it can activate multiple transmitting antennas at the same time in one transmission, which keeps the system complexity low and improves spectral efficiency.

Also, based on the idea of generalization, the authors in [130] improved the SM system that uses index and amplitude/phase modulation signals to transmit information at the same time, and extended the number of activated transmitting antennas from one to multiple. This method is called generalized spatial modulation (GSM) and has been further studied in [45, 125, 129]. Among them, the literature [125] introduced the multiplexing concept of the MIMO system into SM, and proposed multiple active spatial modulation (MASM), which further improves the system's spectral efficiency.

Moreover, in terms of improving BER performance, Basar et al. combined space-time block code (STBC) technique with SM and proposed a space time block coded spatial modulation (STBC-SM) [21]. STBC-SM systems can improve the transmit diversity gain of the system by performing STBC encoding at the transmitting end, thereby improving the BER performance. Meanwhile, in order to improve the diversity gain, quadrature spatial modulation (QSM) has been proposed in [95]. QSM systems utilize the orthogonal characteristics of the real part and the imaginary part of the signal and improve the diversity gain by independently selecting the antenna to transmit the real part and the imaginary part. In other words, it exploits the in-phase and quadrature antenna dimensions to increase the number of spatial constellation points.

In recent years, an improved version of QSM called improved quadrature spatial modulation (IQSM) was proposed [124]. The main feature of the proposed scheme is to send a second constellation symbol over the in-phase and quadrature antenna dimensions. Significant performance advantage of the proposed scheme is realized at the cost of a slight increase in the number of radio-frequency (RF) chains.

All the above-mentioned SM systems use coherent detection methods, and the receiver needs to have the knowledge of CSI. For the research of non-coherent detection without CSI, a differential QSM (DQSM) method was proposed to alleviate the requirement of channel knowledge at the receiver side [92]. Time dimension and orthogonal in-phase and quadrature spatial dimensions of QSM are exploited to facilitate differential modulation and demodulation while maintaining single RF-chain transmitters. The complexity of the receiver is reduced, but the BER performance is lower than that of the coherent detection system. In addition, CSI can be used not only to detect at the receiving end but also to precode at the transmitting end. When the CSI is known by the transmitter, the authors in [82] proposed the generalized precoding aided spatial modulation (GPSM), which can effectively eliminate interference between antennas at the receiver and reduce the complexity of signal detection. It can be seen that the above-mentioned various transmission modes based on SM are all designed by considering trade-offs between system capacity, BER performance, and detection complexity.

2.4.2 Application and prospect

SM has shown promising potential and compatibility in emerging research fields. Nowadays, as millimeter-wave (mmWave) and terahertz (THz) communications have triggered widespread interest both in the academic and industrial fields, SM can also guarantee its energy-efficiency characteristic even with a higher free space path loss [84, 90, 111].

Among them, [84] proposed novel TX and RX hardware architectures, both of which use only a single RF chain, for the implementation of SM/GSM (Generalized spatial modulation) at mmWave frequencies. It has demonstrated that both simplicity and good performance are exhibited thus making SM very attractive techniques for short-range indoor mmWave communications at 60GHz. Meanwhile, SM caters to the core issue of cost-saving and energy consumption reduction for smart society, which is considered to be particularly appropriate for application to Internet of Things (IoT) and Internet of Everything (IoE) [100, 102, 127]. Relying on the ON/OFF state of transmitting antennas for embedding information, SM can be an energy-efficient and cost-effective technique for the IoT to connect a massive number of machine-type communication (MTC) devices. Since MTC devices usually have low data rate requirements, periodic data traffic arrivals, limited signal processing capability and strict energy constraints, the specific design and integration of SM to the IoT is also a promising research direction. Moreover, an augmented spatial modulation (ASM) solution has been proposed in [67] to overcome the channel uniqueness requirement for visible light communications (VLC) systems. It adopts massive-ASM for IoT applications with a focus on investigating ASM's complexity and introducing different machine learning based receiver designs, including support vector machine, logistic regression, and neural network.

2.5 Full duplex radios

As will be discussed more in details in Chapter 5, a A radio transceiver includes a base-band (BB) system and a RF front end. It is the core part of the wireless communication system which aims to transmit and receive digital data on the form of complex symbols through its RF front end. Among them, the RF front end should be able to process different RF signals, and the BB system should have the ability to separate and recover different data symbols. FD is a radio communication mode that provides the ability to transmit and receive information on the same frequency band and at the same time. In this section, we first give an introduction to the background, principle and research status of FD and HD radio communication, and then introduce the main problem of realizing FD, i.e. self-interference (SI), and discuss the solutions that can be employed to solve this SI problem. Finally, we introduce the interest of combining SM and FD.

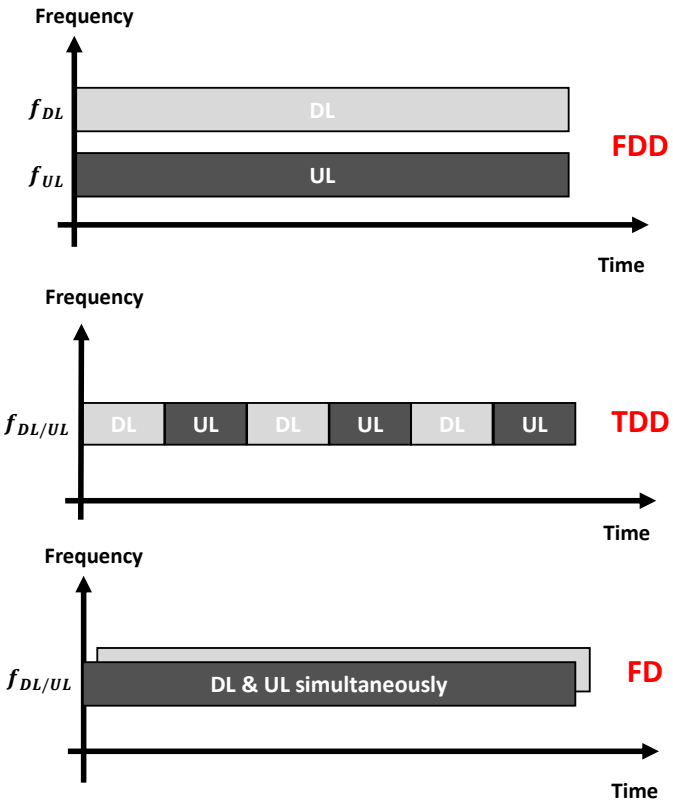

Figure 2.6: Difference between FDD, TDD and FD

2.5.1 Overview of duplex communication systems

Current radio communication systems usually apply HD mode which use separate time or frequency resources to transmit and to receive information. There are two HD methods that ensure bidirectional communication: FDD and TDD. The difference between FDD, TDD and FD system is shown in Figure 2.6.

2.5.1.1 FDD

FDD allows simultaneous communication on different frequency bands. Delay is therefore not affected and this is the reason why it is widely deployed in cellular communications. It is also used in Long-Term Evolution (LTE) communications where assigning two different channels between uplink (UL) and downlink (DL) to prevent possible interference. However, this means a significant drop in spectral efficiency. Indeed, FDD requires no less than twice the spectrum of TDD. Considering the urgent need for spectrum saturation and optimization of frequency resources, this is a major limiting factor. Finally, since the

characteristics of the channel change according to the assigned frequency, the techniques used in areas such as MIMO or beamforming becomes more complex. For example, for LTE communication, the allocation of different frequencies will mean different processing at the UL and DL levels.

2.5.1.2 TDD

TDD is designed to assign different communication times for transmitters and receivers on the same and unique frequency band. Therefore, it alternately transmits and receives by assigning variable time intervals. The advantage of TDD is the use of a single frequency resource for transmission and reception. In addition, TDD communication does not require channel separation or frequency guard bands. Most wireless transmission techniques, such as Wifi, Bluetooth, or Zigbee, use TDD. In addition, due to cost constraints and insufficient spectrum, TDD is also adopted by some cellular systems, such as China's TD-LTE system. The downside is that the successful implementation of TDD requires a very precise timing system on the transmitter and receiver ends to prevent time slots from overlapping or interfering with each other. Since the terminal is forced to wait to receive the message before starting the transmission, the use of TDD will also increase the end-to-end delay. Delay time can be a crucial criterion, this method is therefore not suitable for some specific communication conditions such as vehicular communications.

2.5.1.3 FD and its advantages

As mentioned earlier, the traditional wireless communication system is based on the HD mode. However, in order to benefit from the advantages of FDD and TDD while avoiding the drawbacks of both, the FD mode is considered. This mode is a combination of these two modes, which allows simultaneous transmission and reception on the same frequency band. The principle of FD is not new as it has been successfully used in wired communications. This principle is produced by the coupling between the transmitter and receiver cables. That will bring about the problem of echo. However, this echo is relatively weak, it is easy to achieve the performance required for cancellation [55].

The FD mode features several advantages, the main benefit is to improve throughput. In fact, compared with HD mode, using FD theoretically can double the bit rate. In the following, we will focus on the advantages of FD radios over HD radios:

- **Increased throughput**:

FD operation doubles the theoretical bandwidth of the connection. If a link normally runs at 1 Mbps but can work in FD mode, it really has 2 Mbps of bandwidth (1 Mbps in each direction). It may be difficult to double the performance in a real application scenario, because communications usually do not involve sending lots of data in both directions at once. However, we certainly get better throughput than in a HD mode.

- **End-to-end delay reduction**: A FD node can begin transferring before the end of reception, which is particularly interesting for relay modes and can significantly reduces the end-to-end delay of delivering packets.

- **Reliable primary user detection**:

  For cognitive radio networks (CRN), dynamic spectrum access needs to be carefully designed to minimize interference and delay to the main (licensed) users. One of the main challenges of dynamic spectrum access is to determine when secondary (unlicensed) users can use the spectrum. In HD mode, the secondary user cannot immediately detect the existence of the primary user, because he cannot detect the spectrum while transmitting. The adoption of FD mode can solve this problem [30].

- **Collision avoidance**: Although the carrier sense multiple access with collision avoidance (CSMA/CA) protocol has been shown effective in the WiFi networks, it suffers from the problem of long collision duration. Nowadays, WiFi networks are based on the HD technique because users cannot perform carrier sense and collision detection during the transmission, unlike the CSMA/CD protocol in Ethernet. Consequently, if a collision happens between transmitting users, they cannot detect it and still transmit the collided data packets. By taking advantage of the FD techniques, each user can sense the spectrum and determine whether other users are occupying it while transmitting its own data simultaneously, which is necessary to avoid collisions with FD nodes that do not perform carrier detection [116].

- **Hidden node problem**: In wireless networks, the hidden node problem or hidden terminal problem occurs when a node can communicate with a wireless access point (AP), but cannot communicate directly with other nodes that are communicating with that AP. Consider a scenario where multiple nodes wish to transmit their data to a common access point. If a FD communication between this AP and a hidden node is already established, then the other nodes in the network "listen"

to the transmission of the access point and thus delay their transmission to avoid collisions [85].

- **Improve physical layer security**: Due to the openness of the wireless channel, the communication content may be intercepted by a third side which may be a malicious one., so high-level data encryption is usually used to ensure a safe transmission. In recent years, physical layer security has attracted the attention of the industry. The idea of physical layer security is to dynamically change the physical characteristics of the wireless channel to make the wireless signal more difficult to be intercepted. Figure 2.7 shows an anti-eavesdropping FD transmission scheme [28, 140, 142]. While receiving the signal, the transceiver releases the interference signal of the same frequency. At the same time, the same-frequency FD receiver understands the prior information of the interference signal, and through self-interference cancellation (SIC), it will not have an impact on the reception of useful signals. However, the eavesdropper does not know the prior information of the interference signal, so it cannot suppress all the interference signals which increase the difficulty of intercepting the signal, thereby ensuring the security of the physical layer transmission, this method is so called self-jamming.

The advantages of FD radios are listed above, but the reason why FD is still in the experimental stage is its SI problem. The main limitation impacting FD transmission is the strong SI signal generated by the transmitting antenna to the receiving antenna of

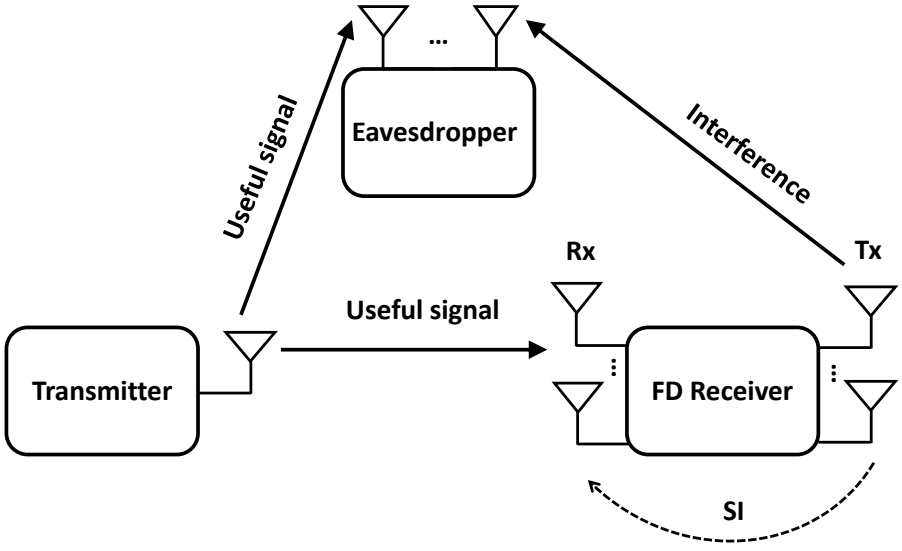

Figure 2.7: Anti-eavesdropping FD transmission scheme

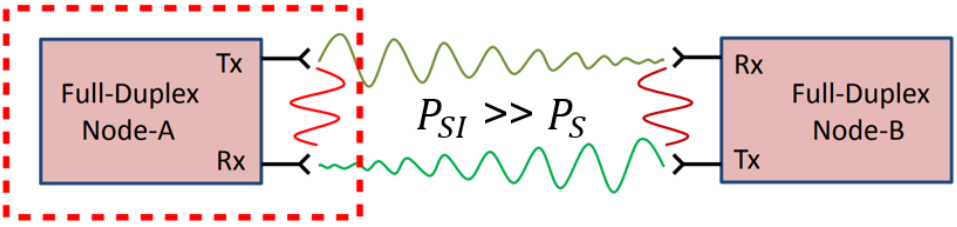

Figure 2.8: Illustration of the self interference principle in FD radios. The SI signal (in red) has a level much bigger than the distant one (in green).

the same node. Moreover, the power of the SI signal is much greater than the power of the signal of interest. In order to have a higher efficiency in this type of communication, the SI signal must be reduced to receiver's noise level. For example, in a WiFi system, the transmit power can be as high as 20 dBm, and the noise level of the receiver is -90 dBm, which roughly, requires a total of 110 dB of SIC to make the FD system operate properly. If SIC is not sufficient, the residual SI will reduce the signal-to-noise ratio and degrade the system performance.

2.5.2 Self-Interference cancellation

As mentioned previously, even though the theoretical FD principle is promising, successfully conceiving FD-based systems is a complex subject. Several SIC solutions are introduced in this section to ensure FD performance. In general, they can be divided into two categories: passive cancellation and active cancellation.

2.5.2.1 Passive cancellation

Passive cancellation consists in studying the characteristics of propagation and antennas to increase propagation loss of SI signal. The effect of SIC depends on the antenna pattern, antenna layout and shielding material. By summarizing the existing passive cancellation methods, they can be divided into the following types according to their principles:

- **Use of directional antennas**: The directional antenna method refers to the use of different directional antennas for transmission and reception to suppress SI. Due to the directivity of the directional antenna, the main lobe of the antenna pattern is higher than the side lobes (usually > 10dB), thereby reducing SI. The literature [43, 44] applies this method to achieve SIC of around 25 dB.

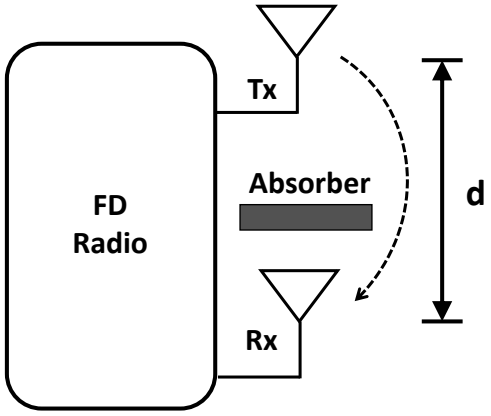

Figure 2.9: Block diagram of passive cancellation using separation and shielding of antennas

- **Separation and shielding of antennas**: As shown in Figure 2.9, the most intuitive method of reducing SI is to increase the distance between the transmitting and receiving antennas of the same node. Indeed, increasing the distance between the two antennas amounts to obtain a greater attenuation and thus reduce the signal power at the receiving part [51]. Moreover, the shielding between the transmitting and receiving antennas increases the SIC level. It has been demonstrated in [44] that when the distance between the antennas is 50cm (with carrier frequency of 2.4 GHz), 27.9dB can be suppressed without absorbing shielding; 48dB can be suppressed with absorbing shielding.

- **Polarization**: The polarization of electromagnetic waves refers to the property that the direction of electric field changes with time. According to the rotation direction of the electric field intensity, it can be divided into left-handed polarization and right-handed polarization. According to the shape, it can be divided into linear polarization, circular polarization, and elliptical polarization [50]. According to the vector composition principle of the electric field, the electric field can be decomposed into the vector composition of two orthogonal electric fields. Therefore, two antennas placed with an angle of 90 degrees can receive two orthogonal components of electromagnetic waves. By employing this principle, SI can be suppressed between $22-70$ dB [44, 52, 64, 68].

- $\lambda/2$ **spacing**: This method uses two transmitting antennas and one receiving antenna. The principle consists in placing the two transmitting antennas at distances

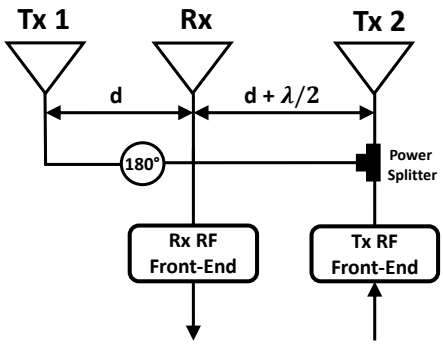

Figure 2.10: Block diagram of passive cancellation based on $\lambda/2$ spacing

of d and $d + \lambda/2$ from the receiving antenna, as shown in Figure 2.10 (where λ represents the wavelength). The idea is to simultaneously transmit the same signal in order to obtain a destructive sum at the receiving antenna. As the second antenna is shifted by half a wavelength of the center carrier frequency, the two signals will arrive in phase opposition and cancel each other out [31, 32, 58]. The cancellation can be theoretically possible to significantly eliminate the SI signal. In [31], this method has been proved to achieve 30 dB of SIC. Theoretically, the residual SI signal after SIC $r_{\text{res}}(t)$, is given by

$$r_{res}(t) = \sqrt{P_{t1}}\sqrt{L_1}x(t)e^{j2\pi f_c\left(t+\frac{d_1}{c}\right)} + \sqrt{P_{t2}}\sqrt{L_2}x(t)e^{j2\pi f_c\left(t+\frac{d_2}{c}\right)} \tag{2.8}$$

where $x(t)$ is the unit power BB transmit signal, P_{t1} and P_{t2} are the transmit power of the two signals from the two transmitting antennas respectively, L_1 and L_2 denote the attenuations experienced by the two transmitting signals before arriving at the receiving antenna, d_1 and d_2 represent the distance from the two transmitting antennas to the receiving antenna respectively. f_c represents the center carrier frequency and c is the speed of light. If $d_2 = d_1 + \lambda/2$, these two signals add destructively and hence the SI signals can be nulled. However, this method is nevertheless compromised by the presence of multipaths which change according to the position of the antennas. These multipaths can have remarkable gains which cannot be controlled and lead to the degradation of the cancellation performance.

2.5.2.2 Active cancellation

In order to reduce the interfering signal below the noise level, active cancellation methods are further analyzed. Active cancellation aims to exploit the knowledge of its own

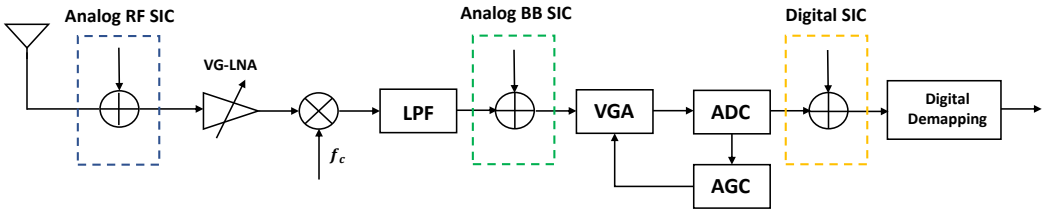

Figure 2.11: Classical receiver end of FD radios with possible SIC placements

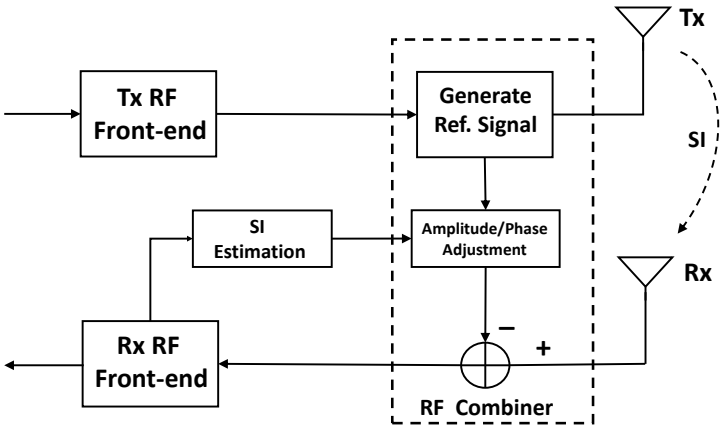

Figure 2.12: Block diagram of classical analog RF SIC

transmission and emulate the over-the-air SI channel to craft a cancellation signal and then subtract it in the receiver end. Based on the SIC being implemented before or after the Analog-to-Digital converter (ADC), the active cancellation is classified as active analog cancellation and active digital cancellation as shown in figure 2.11 [133].

- **Analog RF SIC**: Active analog RF SIC refers to reconstructing the SI signal in the RF analog domain, and then subtracting the SI from the received signal as shown in Figure 2.12. In the literature on analog RF SIC, SI can be suppressed of about 20 up to 70 dB [16, 29, 31, 39, 81, 89, 103, 134].

- **Analog BB SIC**: Although the passive cancellation and Analog RF SIC could significantly reduce the received SI, even up to 20 - 70 dB, the residual SI is still strong enough to mask the weak desired signal from the distant radio node. Furthermore, the ADC has a very limited dynamic range (DR) which is defined as the ratio between the largest possible input (full-scale voltage) to the smallest possible input (the least significant bit or quantum voltage). When the dynamic range is exceeded, the quantization noise of the converter could bury the weaker

signal. Therefore, we can further cancel the residual SI as much as possible before it goes through the ADC. It has been presented in [65, 66] that 10 dB more of SIC can be achieved by the implementation of analog BB SIC.

- **Digital SIC**: Digital SIC refers to the realization of SIC in the digital domain (after ADC) as shown in Figure 2.13. The benefit of digital domain cancellation is the increased flexibility in terms of modeling and parameter estimation, which facilitates the use of advanced SI signal models. This means that the significant analog impairments can be explicitly included in the modeling within the digital canceller. The residual SI after digital SIC $r_{\mathrm{DSIC_{res}}}(n)$ can be expressed as ,

$$\begin{aligned} r_{\mathrm{DSIC_{res}}}(n) &= \mathrm{ADC}\left\{\left\{\left[\mathrm{DAC}\{x(n)\}e^{j(2\pi f_c t+\phi_t)}\right] * h_{si}(t)\right\}e^{-j(2\pi f_c t+\phi_r)}\right\} - x(n)\circledast\widetilde{h}_{si}(n) \\ &= x(n)\circledast h_{si}(n)e^{j(\phi_t-\phi_r)} - x(n)\circledast\widetilde{h}_{si}(n) \\ &= x(n)\circledast h_{si}(n)\left[e^{j(\phi_t-\phi_r)}-1\right] + x(n)\circledast\left[h_{si}(n)-\widetilde{h}_{si}(n)\right] \\ &= x(n)\circledast h_{si}(n)\left[e^{j\Delta\phi}-1\right] + x(n)\circledast\Delta h_{si}(n) \end{aligned} \tag{2.9}$$

where $x(n)$ is the transmit digital signal, ϕ_t and ϕ_r are the transmitter phase offset and the receiver phase offset respectively ($\phi_t - \phi_r = \Delta\phi$), $\widetilde{h}_{si}(n)$ is the estimate of the SI channel $h_{si}(n)$, $\Delta h_{si}(n)$ represents the SI channel estimation error. ADC(χ) and DAC(χ) denote the perfect conversion of analog signal $\chi(t)$ to digital signal $\chi(n)$ and digital signal $\chi(n)$ to analog signal $\chi(t)$ respectively.

As it can be concluded from the Eq. 2.9, the SI can be completely mitigated if the phase difference $\Delta\phi$ between the transmitter and receiver is zero and perfect channel estimation, i.e. $\widetilde{h}_{si}(n) = h_{si}(n)$, could be obtained. Comprehensive simulation and measurement results evaluating the performance of the proposed digital cancellation solutions are presented in [72, 77, 87, 120, 135], the measurements incorporate also different analog SI suppression techniques. It has been demonstrated that digital SI cancellers are able to suppress the SI to the level of the receiver noise floor, thereby facilitating true FD operation. Korpi et al. [53, 73, 75, 79] employed digital SIC complemented by nonlinear digital cancellation processing, the results show that the residual SI level is pushed down to the noise floor of the demonstration system, despite the harsh nonlinear nature of the SI. These findings indicate that deploying the FD principle can indeed also be feasible in mobile devices, and thus be one potential technology in, for example, next generation communication and beyond radio systems. In [75], more than 100 dB of

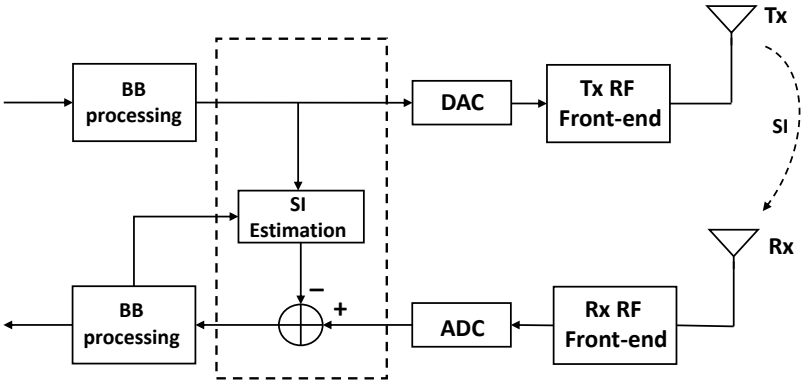

Figure 2.13: Block diagram of classical digital SIC

SI cancellation is obtained which is one of the highest amounts of cancellation reported in the existing literature.

2.5.3 Combination of spatial modulation and full duplex

The above-mentioned research on the FD system is basically based on a single-input single-output (SISO) system. In order to enhance the spectral efficiency and reliability of FD systems, MIMO techniques, such as V-BLAST architecture, can be employed. While MIMO systems offer the benefit of both diversity and multiplexing gains, they suffer from a high power consumption owing to power-hungry RF chains. Moreover, when there is more than one active transmit antenna in the MIMO systems, it is also required to cope with the ICI at the receiver side. Therefore, the complexity of the detection algorithm exponentially increases with the number of transmit antennas under ICI, and the multipath channel of MIMO systems will inevitably lead to a significant increase in the complexity of SIC. However, SM activates only one transmit antenna for one symbol period, there is only one data stream of SI for the receiving antenna. SM can be a solution suitable to avoid the disadvantages like high power consumption, ICI and high complexity detectors. Some recent studies have analyzed the performance of the systems which are applying both FD and SM techniques. The implementation complexity is much lower than that of the multi-stream MIMO. Besides, the spectral efficiency can be improved compared to the FD-SISO system. The superiority of the full duplex spatial modulation (FDSM) system has been studied in [63, 70, 99, 106, 138] theoretically and by simulations. In [63], it has been demonstrated that FDSM shows a higher spectral efficiency in comparison with conventional FD and MIMO-HD in the

entire SNR region. In particular, the authors in [99] studied the performance of FDSM systems in drone communication applications, where several drones act as FD relays. The proposed solution has exhibited robustness both to the SI encountered in FD systems and to strong LOS signals.

In the following chapters, we will first introduce the SM system from a simulation level, and then introduce the S; system with the addition of FD radio.

CHAPTER 3

SPATIAL MODULATION SYSTEM WITH CSI DETECTOR

3.1 Introduction

The FDSM system has the modulation and transmission mode of SM and the simultaneous transmission and reception function of FD. In this chapter, we are committed to construct a SM system by simulation firstly. That is, each side has only the transmitting or receiving function, and then the system performance is evaluated, which lay the foundation for the future addition of the FD function.

SM uses the active state of antennas as a support for the transmission of information, which effectively simplifies the problems of inter-channel interference in the traditional MIMO scheme. It was explained in [109] that, compared to the V-BLAST (Vertical Bell Laboratories Layered Space-Time) system, the SM receiver does not require a continuous interference cancellation step in order to handle inter-channel interference, and has low system complexity. Moreover, the use of a unique RF link greatly reduces the cost of a SM system.

In the literature, the authors in [60] present the performance analysis of a SM scheme in the case of a ML (Maximum Likelihood) detector (i. e. optimal detector). However, in their study, the channel model is a basic Additive White Gaussian Noise (AWGN) one. Furthermore, the performance analysis over the more complex channel models has been presented in [36] and [13]. However, most of the previous studies assume that perfect CSI is available at the receiver, which may be difficult to implement in real time. The

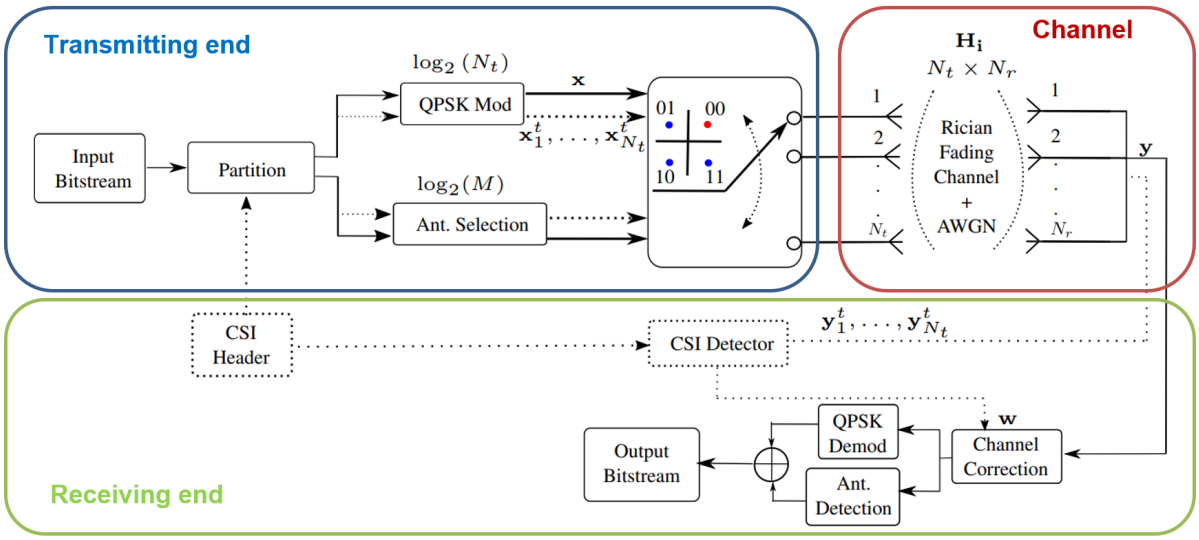

Figure 3.1: $N_t \times N_r$ SM system model with a CSI Detector

difficulty is even greater in scenarios with mobility, where there is high relative speed between the emitter and the receiver. Hence, this assumption is unrealistic. Furthermore, several authors [11, 118] have studied the effects of the channel estimation errors on the SM performance. In [18], it analyzes the performance of SM in the presence of channel estimation errors by introducing different variances of the estimation errors. However, to the best of the author's knowledge, studies on the design of the CSI detector are still lacking.

In this chapter, we propose a SM system with a CSI detector. It is no longer assumed that a perfect CSI can be obtained at the receiving end. The CSI is considered to be degraded by the AWGN noise. In order to study the performance of the proposed system, Advanced Design System (ADS) - Matlab system co-simulations will be performed. More precisely, the performance of the SM over the time-varying Rician fading channel will be analysed.

The remainder of this chapter is structured as follows. In Section 3.2, the system and channel models will be discussed, and the channel model together with the channel estimation strategy will be pointed out. The ADS-Matlab co-simulation results are presented in Section 3.3. Section 3.4 summarizes this chapter.

3.2 SM system model

A SM system model over the time-varying Rician fading channel with a CSI detector is presented in Figure 3.1. Here N_t is the number of emitting antennas and N_r is the number of receiving antennas. The SM architecture can be divided into three main parts:

1. **Transmitting end:** Here, the input bitstream is divided into two parts. One part is used for the antenna selection and the other one is used in order to form the symbols. As a header, the other N_t sets of data are sent for the CSI estimation.

2. **Channel:** A $N_t \times N_r$ channel model is built. The activated antenna transmits the modulated symbols through a time-varying Rician fading channel. Besides, an AWGN noise is also considered.

3. **Receiving end:** Here, the CSI from the detector is used for the antenna detection. Then, each received symbol is demodulated. The resulting bits from the antenna detection are concatenated with the ones from the demodulation step, thus forming the output bitstream.

3.2.1 SM modulator

The input bit stream is divided into N groups. Each group has $\log_2(N_t) + \log_2(M)$ bits, where M is the number of the distinct symbols that the transmitter can send. The transmitter activates the corresponding antenna according to the first $\log_2(N_t)$ bits of the input bitstream. The rest $\log_2(M)$ bits are used in order to form the M-ary signal constellation. In other words, the transmission SM scheme allows simultaneously transmitting two types of symbols: (1) classical IQ-symbols of a M-order QAM modulation, (2) spatial bits or symbols related to the index of the transmit antenna.

Therefore, a block of $\log_2(N_t) + \log_2(M)$ bits is mapped into a constellation vector $\mathbf{x}^b(i) \in \mathbb{C}^{N_t}$ i.e., $\mathbf{x}^b(i) = \left[x_1 x_2 \ldots x_{N_t}\right]^T$ by sending the m-th QAM symbol using the i-th antenna. For each symbol period, the signal to be transmitted can be presented as

$$\mathbf{x}^b(i) = \begin{bmatrix} 0 & \ldots & x^b & 0 \end{bmatrix}^T \tag{3.1}$$

where x^b is located in the i-th column.

Besides, in the SM system, there is a limit on the number of the transmitting antennas, which is required to be 2^n, so at least two transmitting antennas are required to ensure the normal operation of the system. This chapter deals with the particular case

of the quadrature phase-shift keying (QPSK) modulation, consequently, $\log_2(M)$=2. A 4×4 SM mapping table is shown in TABLE 3.1.

Table 3.1: 4×4 SM system modulation mapping table

Nt=4,M=4		
Input Bits	Antenna	QPSK Symbol
0000	T_{x1}	$1+J$
0001	T_{x1}	$-1+J$
0010	T_{x1}	$1-J$
0011	T_{x1}	$-1-J$
0100	T_{x2}	$1+J$
0101	T_{x2}	$-1+J$
0110	T_{x2}	$1-J$
0111	T_{x2}	$-1-J$
1000	T_{x3}	$1+J$
1001	T_{x3}	$-1+J$
1010	T_{x3}	$1-J$
1011	T_{x3}	$-1-J$
1100	T_{x4}	$1+J$
1101	T_{x4}	$-1+J$
1110	T_{x4}	$1-J$
1111	T_{x4}	$-1-J$

As mentioned previously, N_t sets of data as a header are transmitted before the random binary sequences for the CSI estimation. Each set $\mathbf{x}_{n_t}$ includes M frames of possible symbols in M-ary modulation. Then we suppose that the number of symbols for each frame is N_f and the total number of symbols in the header for each transmitting antenna ($\mathbf{x}_{n_t}$) is equal to N_F ($N_F = 4N_f$). The structure of the header $\mathbf{x}_{n_t}$ can be given by equation (3.2):

$$\mathbf{x}_{n_t} = \left[\underbrace{s_1 \cdots s_1}_{N_f}, \quad \underbrace{s_2 \cdots s_2}_{N_f}, \quad \cdots, \quad \underbrace{s_M \cdots s_M}_{N_f} \right] \tag{3.2}$$

3.2.2 Channel model

As stated, the symbols are transmitted over a Rician fading channel $\mathbf{H}$, where $\mathbf{H} \in \mathbb{C}^{N_t \times N_r}$. Moreover, an AWGN noise η, is considered.

The Rician fading channel model $\mathbf{H}$ takes into account the presence of the LOS path and the Rice distribution is described by the Rician K-factor. The factor K is defined as the ratio between the main signal power (usually the LOS path signal) and the sum

of the powers of the remaining multipaths. In this particular case, **H** has the following structure:

$$\mathbf{H} = \sqrt{\frac{K}{K+1}} \cdot \mathbf{A} + \sqrt{\frac{1}{K+1}} \cdot \mathbf{V} \tag{3.3}$$

$$K = \frac{P_{LOS}}{\sum P_{NLOS}} \tag{3.4}$$

where **A** is a deterministic matrix and **V** is a stochastic one. Here, A = [1 0 . . . 0] is a vector with all components except first one set to zero.

As stated, an AWGN is taking into account and we add AWGN of the specified noise density to the input signal. The noise power spectral density D can be expressed by the following equation:

$$D = P_s - 10 \cdot log_{10}(R) - E_b/N_0 \tag{3.5}$$

Where P_s is the signal power, E_b/N_0 is the signal-to-noise ratio per bit and $R = 1/T_{bit}$ is the input bitstream data rate. The noise power delivered to the receiving end can be assumed as $D \cdot B_W$, where B_W is the bandwidth.

We assume that the channel parameters change every τ_H seconds, and the output time step is T_{bit} ($\tau_H \gg T_{bit}$). More precisely, the same **H** matrix function is used for a set of τ_H/T_{bit} symbols.

The relation between the output signal **y** and the input one **x** can be written as follows:

$$\mathbf{y} = \mathbf{H_i} \cdot \mathbf{x} + \boldsymbol{\eta}, \quad i \in [1, ..., N_H] \tag{3.6}$$

$$N_H = \frac{N \cdot \left[\log_2(N_t) + \log_2(M)\right] \cdot T_{bit}}{\tau_H} \tag{3.7}$$

where $\mathbf{H_i}$ is a particular realization of **H**, N denotes the total number of symbols, N_H is the maximum number of **H** matrix. $\boldsymbol{\eta}$ is the AWGN noise taken into account. The time-varying channel matrix $\mathbf{H_i}$ is given by

$$\mathbf{H_i} = \begin{bmatrix} h_{1,1}(t,\tau_H) & h_{1,2}(t,\tau_H) & \dots & h_{1,N_t}(t,\tau_H) \\ \vdots & \vdots & \vdots & \vdots \\ h_{N_r,1}(t,\tau_H) & h_{N_r,2}(t,\tau_H) & \cdots & h_{N_r,N_t}(t,\tau_H) \end{bmatrix} \tag{3.8}$$

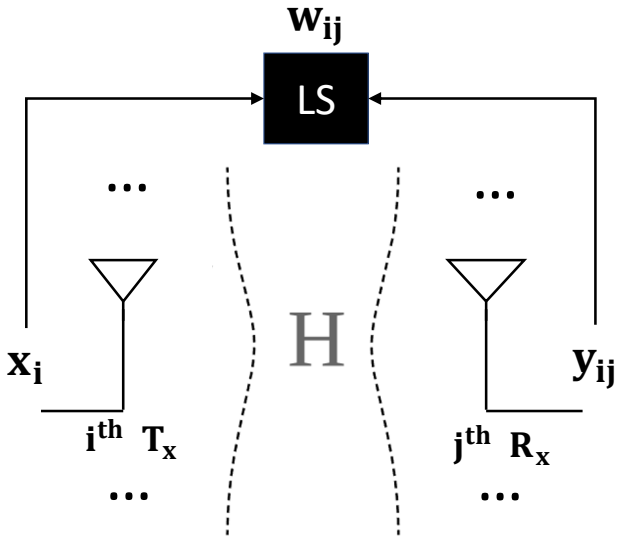

Figure 3.2: CSI detector function by using LS algorithm

3.2.3 CSI detector and demodulator

Since the transmission information bits are respectively mapped in the antenna number and the modulation symbol, it is necessary to detect both the emitting antenna and the transmission symbol. In the detection process of the receiving end, if error occurs in the process of the antenna number detection, the estimated modulation symbol is meaningless. Therefore, the detection of the Tx antenna's number directly impacts the performance of the system, so the receiving end of the SM system needs to be mastered with more complete CSI to better detect the antenna number.

The principle of the CSI detector is based on the Least-Squares (LS) algorithm [46]. The detector calculates the channel matrix elements based on the estimated sampling co-variance matrix. More precisely, we establish N_t sets of the incoming data. Each set is a repeating loop of $\log_2(N_t) + \log_2(M)$ bits. The first $\log_2(N_t)$ bits are fixed and known by the receiver in order to analyze the corresponding channel state. A block diagram of CSI detector function by using LS algorithm with $N_t = N_r = 4$ is shown in Figure 3.2. LS algorithm is applied for the CSI detection depending on calculating the linear relationship between the input and the output. In this situation, each set of the incoming data can get N_r channel states, the total N_t sets can provide the real-time channel matrix H, where $\mathbf{H} \in \mathbb{C}^{N_r \times N_t}$.

The current CSI is used for the correction at the receiving end. The correction matrix

element $\mathbf{w_{ij}}$ is as follows:

$$\hat{\mathbf{w}}_{\mathbf{ij}}^{\mathbf{LS}} = \arg\min_{w_{ij}} \left\| \mathbf{y_{ij}} * \hat{\mathbf{w}}_{\mathbf{ij}} - \mathbf{x_i} \right\|^2 \tag{3.9}$$

$$\hat{\mathbf{w}}_{\mathbf{ij}}^{\mathbf{LS}} = \frac{1}{N_F^2} \cdot \left[\mathbf{x_i} \cdot \mathbf{x_i}^H \right]^{-1} \cdot \overline{\mathbf{y_{ij}}} \cdot \mathbf{x_i}^T \tag{3.10}$$

where $\mathbf{x_i}$ is the modulated symbols sent by the i^{th} transmitting antenna in the header, and $\mathbf{y_{ij}}$ is the transmitting symbols $\mathbf{x_i}$ received by j^{th} receiving antenna. The operator $[\cdot]^H$ denotes the Hermitian transpose and $\overline{[\cdot]}$ denotes the complex conjugate.

Then, maximum likelihood (ML) optimal detection algorithm is applied for index demodulation of the transmitting antenna and the modulated symbols [91]. A low-complexity ML detector is considered, by using the phase difference of different symbols in QPSK. Here, we suppose the initial phase of the QPSK modulation is $\pi/4$, then the symbol $s_n$in this constellation can be expressed as:

$$s_n = A \left[\cos\left(\varphi_n\right) + j \sin\left(\varphi_n\right) \right] \quad n = 1,2,3,4 \tag{3.11}$$

where A is the amplitude of the symbol, and $\varphi_n = (2n-1)\frac{\pi}{4}$. $\hat{n_t}$, $\hat{s}$ are assumed as the estimated activated antenna index and transmitted symbol respectively. Then, we can obtain by ML algorithm:

$$\begin{aligned} (\hat{n_t}, \hat{s})_{ML} &= \arg \min_{n_t \in \mathbf{N_t}, s \in \mathbf{S}} \left(\|\mathbf{yw} - s\|^2 \right) \\ \mathbf{S} &= \{s_1, s_2, s_3, s_4\} \\ \mathbf{N_t} &= \{1, 2, \ldots, N_t\} \end{aligned} \tag{3.12}$$

The demodulation can be divided into two steps. Firstly, the index of transmitting antenna is detected. Here, an example of SM constellation is given in Figure 3.3. To simplify the comprehension, we employ $N_t = 2$ and no phase shift between the two transmitting antennas. The inner and outer circle symbols can be considered as transmitted by Tx1 and Tx2, respectively.

One can remark that the same amplitude of the four symbol points can be obtained for the same transmitting antenna. Therefore, the detection of antenna index can be simplified as the optimization of amplitude.

$$(\hat{n_t})_{ML} = \arg \min_{n_t \in \mathbf{N_t}} (|\mathbf{yw}|^2 - |s|^2) \tag{3.13}$$

The estimated index of transmitting antenna is denoted by $\hat{n_t}$. Then, the optimization issue $(\hat{s})_{ML} = \arg\min_{s \in \mathbf{S}} \left(\|\mathbf{yw} - s\|_2^2 \right)$ can be written as:

$$(\hat{s})_{ML} = \arg \min_{s \in \mathbf{S}} \left(\left| \tilde{y}_{\hat{n_t}} - s \right|^2 \right) \tag{3.14}$$

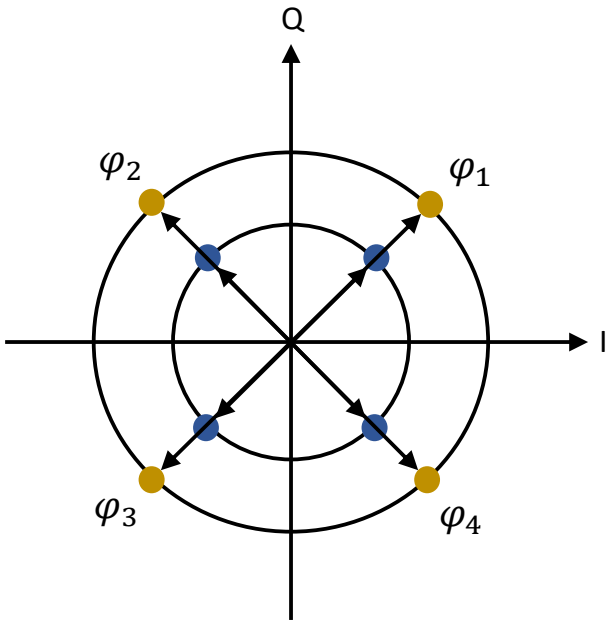

Figure 3.3: Constellation of SM modulation with QPSK and $N_t = 2$ (no phase shift)

where $\tilde{y}_{\hat{n}_t} = \mathbf{yw}$. $\hat{y}_{\hat{n}_t}$ and s can be denoted as $\tilde{y}_{\hat{n}_t} = r_{\hat{n}_t} e^{j\theta_{\hat{n}_t}}, s = e^{j\varphi}$ ($A = 1$ is assumed for simplification) in polar form, then $(\hat{s})_{ML}$ can be expressed as

$$\begin{aligned}
(\hat{s})_{ML} &= \arg\min_{s\in\mathbf{S}} \left(\left| \tilde{y}_{\hat{n}_t} - s \right|^2 \right) \\
&= \arg\min_{\varphi\in\Psi} \left| r_{\hat{n}_t} e^{j\theta_{\hat{n}_t}} - e^{j\varphi} \right|^2 \\
&= \arg\min_{\varphi\in\Psi} \left(r_{\hat{n}_t} e^{j\theta_{\hat{n}_t}} - e^{j\varphi} \right) \overline{\left(r_{\hat{n}_t} e^{j\theta_{\hat{n}_t}} - e^{j\varphi} \right)} \\
&= \arg\min_{\varphi\in\Psi} \left(\left| r_{\hat{n}_t} \right|^2 + 1 - 2 r_{\hat{n}_t} \cos\left(\theta_{\hat{n}_t} - \varphi \right) \right) \\
\Psi &= \{\varphi_1, \varphi_2, \varphi_3, \varphi_4\}
\end{aligned} \tag{3.15}$$

If the $\hat{n}_t$ is firstly detected, the optimization of the symbol has the form as follows:

$$\begin{aligned}
(\hat{\varphi})_{ML} &= \arg\max_{\varphi\in\Psi} \left(\cos\left(\theta_{\hat{n}_t} - \varphi \right) \right) \\
0 \le \theta_{\hat{n}_t} < 2\pi, &\quad 0 \le \varphi < 2\pi
\end{aligned} \tag{3.16}$$

We can conclude that $0 \le \left| \theta_{\hat{n}_t} - \varphi \right| < 2\pi$. This optimization can be divided into two cases:

For $0 \le \left| \theta_{\hat{n}_t} - \varphi \right| < \pi$:

$$(\hat{\varphi})_{ML} = \arg\min_{\varphi\in\Psi} \left| \theta_{\hat{n}_t} - \varphi \right| \tag{3.17}$$

For $\pi \leq \left|\theta_{\hat{n}_t} - \varphi\right| < 2\pi$:

$$(\hat{\varphi})_{ML} = \arg\max_{\varphi \in \Psi} \left|\theta_{\hat{n}_t} - \varphi\right| \tag{3.18}$$

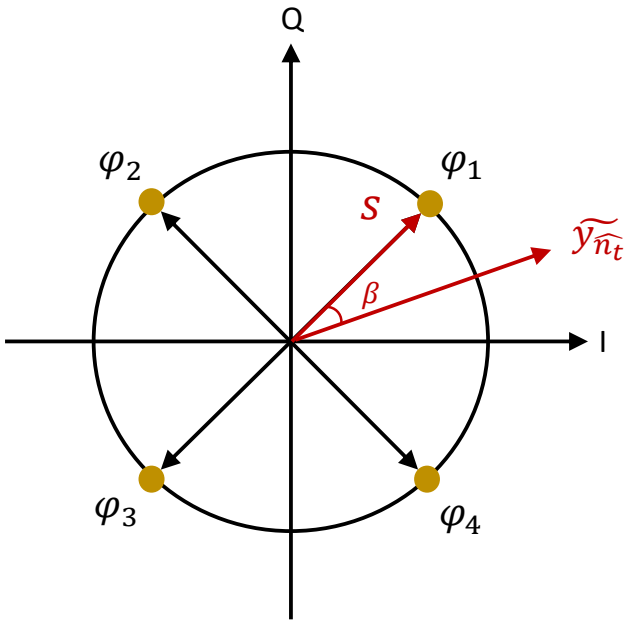

Figure 3.4: ML detection method for QPSK symbols

The principle of ML method to detect QPSK symbol can be explained in Figure 3.4. Here, β is assumed as the difference between $\theta_{\hat{n}_t}$ and φ. One can remark that the closer the symbol point s to $\tilde{y}_{\hat{n}_t}$, the smaller value in (3.15) is. In other words, if the angle β between $\tilde{y}_{\hat{n}_t}$ and s is smaller, then the value of $\cos\left(\theta_{\hat{n}_t} - \varphi\right)$ is larger. Once $\hat{\varphi}$ is estimated, the transmitting QPSK symbol can be directly demodulated.

Therefore, we can conclude the demodulation as follows: (1) Detect transmitting antenna index: the most likely transmitting antenna is the antenna giving the smallest amplitude difference between the received corrected symbol and one of the four QPSK symbols. (2) Estimate digital modulation symbol: because of using the QPSK modulation, only four possible symbols exist. The detection is simplified by calculating the phase difference β. (3) The binary values corresponding to the estimated QPSK symbol are concatenated with the binary values obtained by identifying the emitting antenna to recover the transmitting bitstream.

3.3 Simulation results and discussion

A simulator of the SM scheme (Figure 3.1) is built in order to extract the performance in terms of BER variation with respect to Eb/No, which is the energy per bit over the noise power spectral density. We simulate the transmitting and receiving ends on Keysight's ADS and implement digital signal processing and part of the detection algorithm on Matlab. The simulation parameters are gathered in Table 3.2.

Table 3.2: Simulated SM system parameters

Parameter	Value
Carrier frequency	2.4 GHz
Signal Power	-10 dBm
Modulation type	QPSK
Data rate	10 Mbit/s
Total number of input bits	10^6
Number of symbols of frame for CSI estimation	10^3

3.3.1 CSI detector evaluation

The BER performance of the considered SM system is evaluated in two aspects. The performance with proposed CSI detector is firstly compared with that under the perfect CSI.

From Figure 3.5, one can remark that the increase of the number of emitting antennas will increase the BER. More precisely, the BER performance of the 2×2 SM system is better than that of the 4×4 SM system. This is because there are only two possible transmitting antennas in the 2×2 SM system compared with four possibilities in the 4×4 SM system. In other words, the detection will be relatively easier. On the other side, the proposed channel estimation slightly increases the BER compared to the case where the perfect CSI is considered. However, it can be considered that the difference of BER performance between the system with perfect CSI and the system with imperfect estimated CSI is at an acceptable level.

3.3.2 Rician K-factor evaluation

The BER performance is then analyzed under different values of Rician K-factor. Five typical values are considered: K=1 dB, K=5 dB, K=10 dB, K=20 dB, K=60 dB, which from the weak LOS path environment to the LOS-led environment. The BER performance of

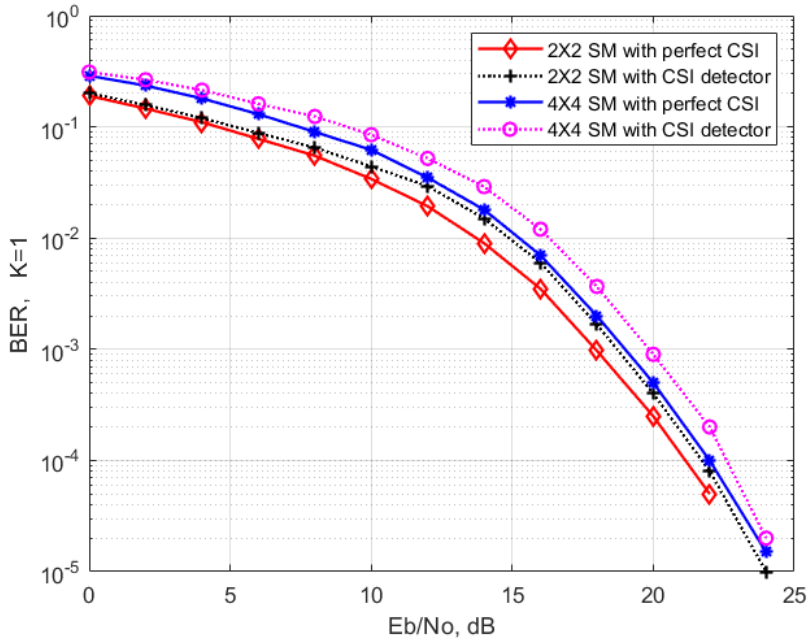

Figure 3.5: BER performance of the 2×2 and 4×4 SM system with the perfect and realistic CSI detector over time-varying Rician fading channel

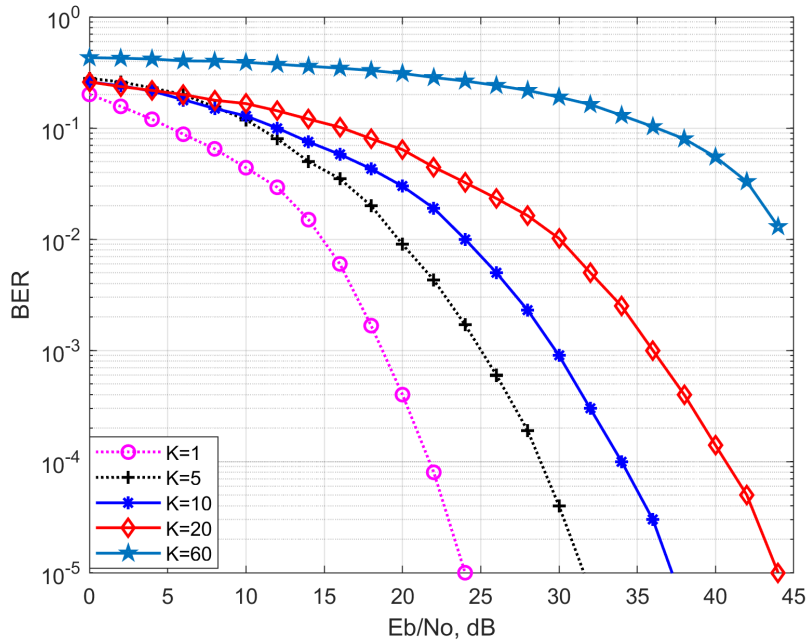

Figure 3.6: BER performance of the 2 × 2 SM system with the realistic CSI detector and for different Rician K-factor

the 2×2 and 4×4 with the realistic CSI detector for different Rician K-factor is shown in Figure 3.6 and Figure 3.7, respectively.

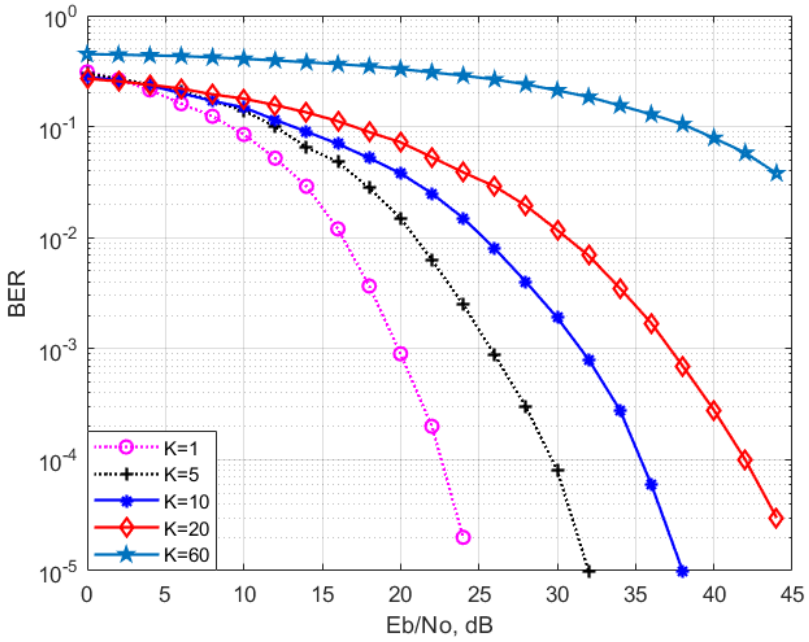

Figure 3.7: BER performance of the 4×4 SM system with the realistic CSI detector and for different Rician K-factor

From these two figures, one can remark that the SM system over a Rician fading channel offers better performance with the smaller values of K. This can be explained because the difference between the $N_t \times N_r$ values in the channel matrix $\mathbf{H}$ is minimal if the K factor is significant, which leads to imprecision in the antenna detection. In other words, if the CSI difference between each channel is assumed to be negligible, and all $N_t \times N_r$ elements in the channel matrix $\mathbf{H}$ are equal, then the BER of detecting the transmitting antenna will remain at 0.5. Hence, the more multipaths in the channel, the better we can detect the emitting antenna.

3.4 Summary

In this chapter, a SM system over the time-varying Rician fading channel was presented. A complete SM system is modeled and simulated by integrating ADS with Matlab software, including the transmitting end, channel model and the receiving end. The modulation module as well as the channel model were introduced. In particular, a time-varying CSI detector for the channel estimation was designed instead of assuming the

availability of the perfect CSI at the receiver. Moreover, the index of transmitting antenna and symbol are detected respectively by employing a low complexity ML detection method. System simulation results indicate that the detector error is acceptable with the proposed CSI detector and the considered ML method, especially when the Rician K-factor is small.

CHAPTER 4

SIMULATED FULL DUPLEX SPATIAL MODULATION SYSTEM

4.1 Introduction

With the development of mobile communication technology, the number of users and data traffic in wireless communications is overgrowing. Moreover, due to the limitation of electromagnetic wave propagation characteristics, the wireless spectrum resources used to support the mobile environment can not be increased endlessly. As stated previously, one of the solutions to overcome this problem is the FD technology. Compared to FDD or TDD, FD can double the spectral efficiency. However, FD will bring strong SI, which severely affects the communication quality. For this reason, SIC has always been the core issue of FD development.

As mentioned earlier, SM is introduced as a new MIMO technology that uses the active state of antennas as a support for the transmission of information [37]. The superiority of the FDSM system has been theoretically studied in [63, 70, 138]. Since SM uses a single antenna for the transmission, there is only one data stream of SI for the receiving antenna. The implementation complexity is much lower than that of the multi-stream MIMO. Besides, the spectral efficiency can be improved compared to the FD-SISO system. As the core difficulty of FD communication, SIC can be implemented by passive suppression and active cancellation. Active cancellation includes analog SIC and digital SIC. Passive suppression maximizes the attenuation of the SI signal by

adjusting the transmitting/receiving antenna direction or antenna position, coupling, etc. Recent research [23, 112] has reduced the strength of SI to an acceptable level by combining the passive suppression and active cancellation, which allows to implement a real FD radio. The key to active analog cancellation is the SI estimation. More precisely, a signal is transmitted as a cancellation signal, which is inverted with SI and has the same frequency. The amplitude and phase of the cancellation signal are adjusted by SI estimation. After SIC in the analog domain, there is still a residual SI, which can be further reduced by using algorithms implemented in digital domain which is optional. For the single SI channel, as in the FDSM system case, if SI estimation can be exact, analog cancellation can reduce SI to the noise level. Therefore, the SI estimation results in different accuracy of SIC, which indeed impacts the performance of the whole FDSM system.

Previous studies [135, 136] analyze the performance of the FD system based on analog cancellation. The performance analysis of the FD system with imperfect SIC has been presented in [34, 133]. However, few publications are available in the literature that discusses the BER performance issue of the FDSM system. The article [69] highlights the better performance of the FDSM system compared with the SM system under imperfect channel estimation. However, it analyzes BER performance by merely defining the constant λ ($0 \leq \lambda \leq 1$) which represents the quality of the channel estimation.

In this chapter, we propose a FDSM system over the Rician fading channel with an SI estimator. More precisely, ADS - Matlab system co-simulation will be performed in order to study the performance of the proposed system under different accuracies of SIC. Furthermore, the performance of the FDSM system will be compared with that of the traditional FD system.

The remainder of this chapter is organized as follows. In Section 4.2, the system model is presented in detail. The channel model, the SI, together with the cancellation strategy, are mentioned. The following section discusses the ADS-Matlab co-simulation results to analysis and evaluate the system performance. Section 4.4 summarizes the results of this chapter and draws conclusions.

4.2 FDSM system model

In this chapter, we describe a 2×2 FDSM system over a Rician fading channel, especially with a channel correction module and a SIC module. Two nodes (namely Node A and Node B) with the same functions are considered. Due to the characteristics of FD

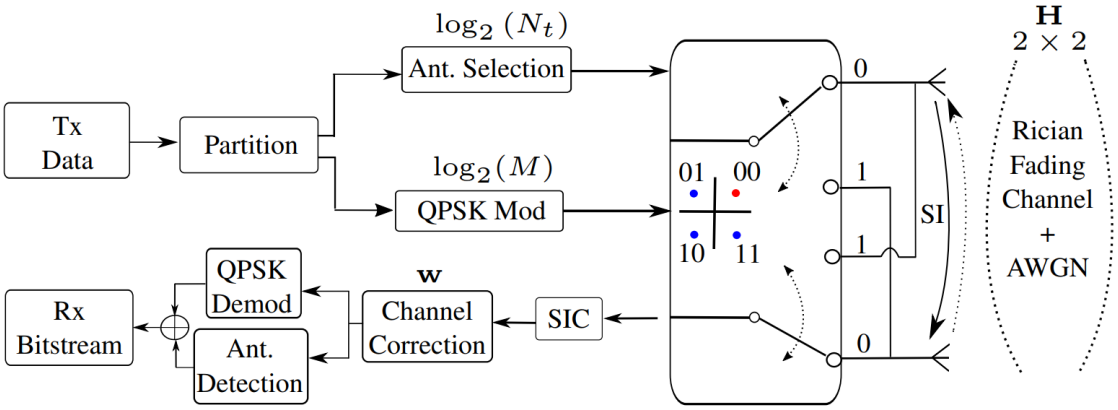

Figure 4.1: Block diagram of a 2 × 2 FDSM system: node A

communication system, both ends of the system have the same functions of simultaneous emission and reception. Consequently, we only show the structural characteristics of one end. The antenna used for emitting or receiving is determined by the SM mapping of input bitstream. The block diagram of this system at Node A is presented in Figure 4.1.

As we can remark, one antenna at node A is used to transmit and the other one is used to receive simultaneously for each symbol period. The system will be presented in three main parts as follows: modulation and demodulation part, channel model and channel correction module part, self-interference and cancellation module part.

4.2.1 Modulation and demodulation

As discussed in Chapter 3, the SM modulation method is also employed at the transmitting end in this FDSM system. A brief description is reviewed here. Firstly, the input bit sequence is divided into N groups. Each group has $\log_2(N_t)+\log_2(M)$ bits, where N_t is the number of antenna at each node, M is the number of distinct symbols that the transmitter is able to transmit. The first $\log_2(N_t)$ bits of each group are employed to select the transmitting antenna and the remaining $\log_2(M)$ bits are employed for the QPSK modulation. We can achieve the desired spectral efficiency by using different modulation methods and configuring different numbers of antennas. In our model, N_t=2, M=4, hence three bits are transmitted for each output time step. An example is given in Figure 4.1, the first 3 bits of the input bitstream are 000. In this case, we enable the first antenna for transmitting, and the other is connected to the receiving end. The symbol

that we transmit is 00, which is in the first quadrant of the constellation scheme. The precise mapping table of the proposed FDSM system is given in Table 4.1:

Table 4.1: 2×2 FDSM system modulation mapping table

Nt=4,M=4		
Input Bits	Antenna	QPSK Symbol
000	T_{x1}	$1+j$
001	T_{x1}	$-1+j$
010	T_{x1}	$1-j$
011	T_{x1}	$-1-j$
100	T_{x2}	$1+j$
101	T_{x2}	$-1+j$
110	T_{x2}	$1-j$
111	T_{x2}	$-1-j$

The demodulation process that we are talking about here is the process of recovering the received bit stream after the SIC module and the channel correction module. Since QPSK modulation is applied, we have only four possibilities for demodulated symbols. The demodulation is divided into two steps, where the transmitting antenna is determined at first. Then, the minimum distance is calculated between the receiving symbol and the four possible modulation states in order to discover the most possible passing channel. The channel matrix of the 2×2 FDSM system is in the form $\mathbf{H} \in \mathbb{C}^{2\times 2}$, where the receiving antenna at each node occupies two channels. The two possible demodulated corrected symbols will be compared to the four possible symbols to find the minimum difference. The low-complexity ML optimal detector is considered to achieve the above function.

- **Antenna index detection**: The modulated QPSK symbol before passing channel is denoted by $s(n)$, with the form:

$$\begin{aligned} s_n &= A\left[\cos\left(\varphi_n\right) + j\sin\left(\varphi_n\right)\right] \\ \varphi_n &\in \left\{\frac{\pi}{4}, \frac{3\pi}{4}, \frac{5\pi}{4}, \frac{7\pi}{4}\right\} \end{aligned} \tag{4.1}$$

The estimated $(\hat{n_t})_{ML}$ by the help of ML can be expressed as

$$\begin{aligned} (\hat{n_t})_{ML} &= \arg\min_{n_t \in \mathbf{N_t}} (|\tilde{y}_{n_t}|^2 - |s|^2) \\ \mathbf{N_t} &= \{1,2\} \\ s &\in \{s_1, s_2, s_3, s_4\} \end{aligned} \tag{4.2}$$

where the received after correction and SIC is presented by $\tilde{y}_{n_t}$, has the form:

$$\tilde{y}_{n_t} = \tilde{A}_{n_t}\left[\cos\left(\tilde{\theta}_{n_t}\right) + j\sin\left(\tilde{\theta}_{n_t}\right)\right] \tag{4.3}$$

Therefore,

$$(\hat{n_t})_{ML} = \arg\min_{n_t\in\{1,2\}}(\tilde{A}^2_{n_t} - A^2) \tag{4.4}$$

- **Symbol detection**: As presented in Section 3.2.3, the symbol detection is simplified by the optimization of the phase shift of $\tilde{y}_{n_t}$. So, we can obtain

$$(\hat{\theta})_{ML} = \arg\min_{\varphi_n\in\{\frac{\pi}{4},\frac{3\pi}{4},\frac{5\pi}{4},\frac{7\pi}{4}\}}(|\tilde{\theta}_{n_t}|^2 - |\varphi_n|^2) \tag{4.5}$$

- **Recover bitstream**: We suppose that the binary bit $B_{\hat{n_t}}$ represents the antenna index, $B_{\hat{\theta}}$ represents the symbol, where $B_{\hat{n_t}} \in \{0,1\}$, $B_{\hat{\theta}} \in \{00,01,10,11\}$. The recovered bitstream B_{out} for each symbol can be expressed as $B_{out} = [B_{\hat{n_t}}, B_{\hat{\theta}}]$, which denotes that $B_{\hat{\theta}}$ is concatenated with $B_{\hat{n_t}}$.

To summarize, the proposed algorithm is summarized in Algorithm 1.

Algorithm 1: Demodulation for FDSM system

procedure Recover the input bitstream for FDSM system

1. $\tilde{y}_{n_t}, s \rightarrow \tilde{A}_{n_t}, A, \theta_{n_t}, \varphi_n$
2. $\tilde{A}_{n_t}, A \rightarrow \hat{n_t}$
3. $\theta_{n_t}, \varphi_n \rightarrow \hat{\theta}$
4. $\hat{n_t}, \hat{\theta} \rightarrow B_{\hat{n_t}}, B_{\hat{\theta}}$
5. $B_{\hat{n_t}}, B_{\hat{\theta}} \rightarrow B_{out}$

end procedure

This detection method has been applied in the SM system before (3.2.3). However, the complexity is half in this FDSM system compared with SM system. The reason is that only one antenna is used for receiving at each node, which reduces the number of the possible passing channels.

4.2.2 Channel model and channel correction module

The time-varying channel is employed in our system. The channel model and the channel correction module mentioned in this section are supposed in the time range of $(0, \tau_H)$, where the channel model is assumed to be changeless.

4.2.2.1 Propagation channel model

A Rician fading channel model **H** is considered between two nodes, where the Rician factor is equal to K. Additionally, an AWGN noise η is considered.

$$\mathbf{y} = \mathbf{H}\mathbf{x} + \boldsymbol{\eta} \tag{4.6}$$

$$\mathbf{H} = \begin{bmatrix} h_{1,1} & h_{1,2} \\ h_{2,1} & h_{2,2} \end{bmatrix} \tag{4.7}$$

The channel model has been presented in detail in Section 3.2.2. Our efforts have already focused on the performance of a SM system over this channel model. It demonstrated that a lower Rician factor does not degrade the performance of the system. Instead, it increases the accuracy of the detection due to the distinct difference between channels, which brings a better BER performance. Therefore, a low Rician factor can be applied under the premise of including a channel correction module.

4.2.2.2 SI channel model

As a consequence of the proximity between the transmitting and receiving antennas, the power of the LOS path dominates the power of the SI channel H_{si}. Thereore, the characterization of the SI channel is quite different from that of the multipath fading channel. In this way, the SI channel is assumed to be a one-path channel or a multi-path channel with a high Ricean K-factor. In this thesis, the SI channel model is assumed as a one-path channel. Besides, self-interference-to-noise ratio (INR) is introduced as the power ratio of the received SI signal to the receiver thermal noise, in order to evaluate the SI power. In a practical sense, we can understand the influence of the changes with INR as that of the changes with the distance between the two nodes on the performance of the system.

4.2.2.3 Channel correction module

The function of the channel correction is a method attempting to recover the transmitting signal. The perfect CSI can be obtained under the condition that the detection symbols are enough and there are no nonidealities effects. The estimated correction matrix is denoted by $\hat{\mathbf{w}}$, where

$$\hat{\mathbf{w}} = \begin{bmatrix} \hat{w}_{1,1} & \hat{w}_{1,2} \\ \hat{w}_{2,1} & \hat{w}_{2,2} \end{bmatrix} \tag{4.8}$$

$$\hat{\mathbf{w}} = \arg\min_{w} \|\mathbf{y} * \hat{\mathbf{w}} - \mathbf{x}\|^2 \tag{4.9}$$

Instead of implementing a CSI detector, we assume that CSI of the Rician fading channel can be sufficiently obtained for the channel correction module, in order to more intuitively see the impact of SIC on the system performance, i.e.

$$\mathbf{y} * \hat{\mathbf{w}} = \mathbf{x} \tag{4.10}$$

4.2.3 Self-interference and cancellation module

Here, we define the power ratio of the received SI signal to the receiver thermal noise as INR. The received SI signal P_{SI} is expressed as

$$P_{SI}(dBm) = P_S(dBm) + \mathrm{INR}(dB) - E_b/N_0(dB) \tag{4.11}$$

where P_S is the power of the received signal which is emitted from the node B, E_b/N_0 is energy per bit over the noise power spectral density.

The vast majority of existing methods for SI channel estimation are based on the LS algorithm. The specific method supposes that we shield the transmitting signal from the other node. There is only one SI channel at a single node, from the transmitting end to the receiving end, which significantly reduces the channel estimation difficulty. The different numbers of detection symbols result in different accuracy of estimation. We can analyze the relationship between these two factors to select the best amount of detection symbols. The expression of the channel estimated by the LS method $\hat{\mathrm{H}}_{si}$ can be represented as follows:

$$\hat{\mathrm{H}}_{si} = \left(\mathbf{x}^H\mathbf{x}\right)^{-1}\mathbf{x}^H\mathbf{y} \tag{4.12}$$

where $\mathbf{x}$ is the modulated symbol sent by the transmitting end at each node, $\mathbf{y}$ is the symbol received by the receiving end at the same node. The operator $[\cdot]^H$ denotes the Hermitian transpose and $\overline{[\cdot]}$ denotes the complex conjugate.

We integrate the estimator described in equation (4.12) into the receiving chain in order to evaluate its performance. To analyze the SI channel estimation impact, we assume a perfect knowledge of the propagation Rician fading channel $\mathbf{H}$. Once the CSI (i.e. the amplitude and phase) of the SI signal is estimated, a signal with the same amplitude but the inverse phase is generated as the SI signal of regeneration, to perform the active analog cancellation.

4.3 Simulation results and discussion

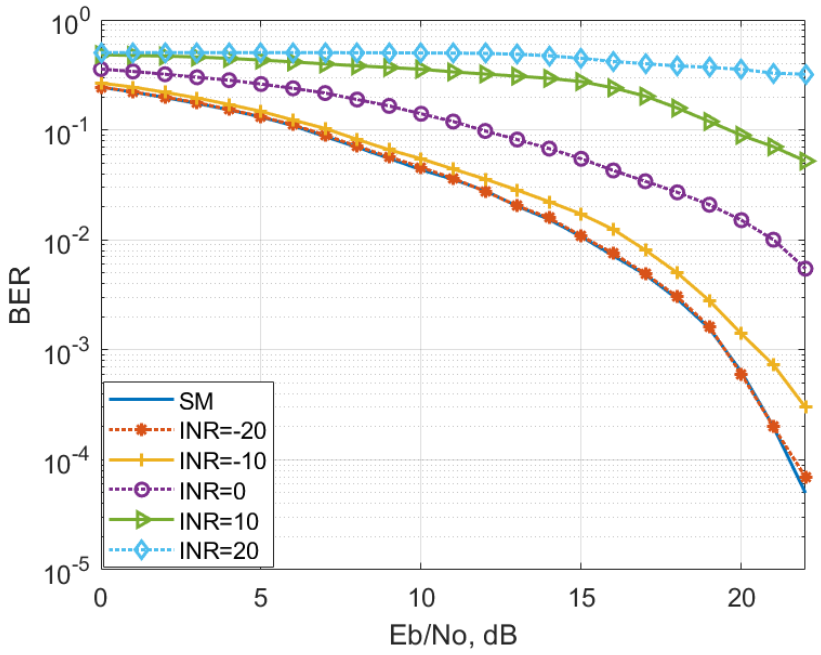

Figure 4.2: BER performance of the FDSM system without SIC

A FDSM simulator based on Keysight's ADS and Matlab software is built in order to study the BER performance. In parallel, the FD system is also simulated to compare with the FDSM system. The FD system is a FD-SISO communication applying QPSK modulation and with the same system parameters as the proposed FDSM system. Three different scenarios are taken into account. Firstly, the effect of SI on system performance without SIC is analyzed. Secondly, we study the impact of the accuracy of SIC in the case of imperfect SI estimation. Finally, a complete FDSM system is constructed by introducing an estimated SI. A time-varying fading channel environment with $K = 1$ is considered in simulation. The remaining simulation parameters are gathered in Table 4.2.

4.3.1 Without SIC

The BER performance of the FDSM system and the FD system without SIC are given in Figure 4.2 and Figure 4.3.

We can remark that with a low Eb/No, the BER of the FD system is better than that of the FDSM system, which can be explained by the significant increase in the difficulty

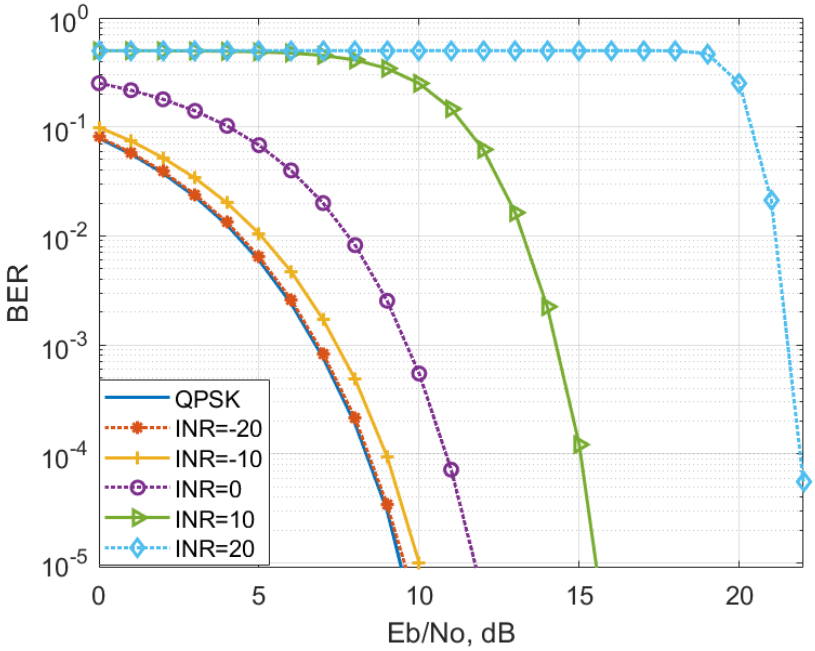

Figure 4.3: BER performance of the FD system without SIC

Table 4.2: Simulated FDSM system parameters

Parameter	Value
Carrier frequency	2.4 GHz
Signal Power	-10 dBm
Modulation type	QPSK
Data rate	10 Mbit/s
Total number of input bits	$3 \cdot 10^5$

of detecting the transmitting antenna caused by SI for the FDSM system. When INR = -20 dB (i.e. SI power is much lower than thermal noise power), the performance of the FDSM system can be basically equivalent to the performance of a 2×2 SM system. The performance of the FD system is theoretically consistent with that of a conventional QPSK modulation HD system. When INR $\geq$ 10 dB (i.e. SI power is much higher than thermal noise power), due to $P_{SI} > P_S$, the BERs of the two systems are maintained at approximately 0.5 while Eb/No is at a low level. In addition, we also find that the FD system is more sensitive than the FDSM system. Even a small evolution of Eb/Nb in the FD system will have a big impact on BER. We can conclude that the lack of SIC will degrade the BER performance of FD and FDSM systems, especially with a larger INR and a lower Eb/No.

4.3.2 SIC with different accuracy level

Two factors are defined to evaluate the errors that occur in the SI estimation. The factor σ represents the difference of the amplitude between the actual SIC and the perfect SIC, and is expressed in dB. The factor θ represents the difference of the phase between the actual SIC and the perfect SIC, and is expressed in degrees of angle. Figure 4.4 and Figure 4.5 present the different accuracies of SIC in terms of the variation of σ and θ for INR = 20, 40, 60, 80 under Eb/No = 10 (dB scale). We emphasize an interesting result in these 3D figures. As INR increases every 20 dB, we can reduce the x-axis and the y-axis value range to 10% each time to maintain the z-axis value at the same level. In other words, when INR increases by 20 dB, the sensitive response to σ and θ of the two systems is multiplied by ten.

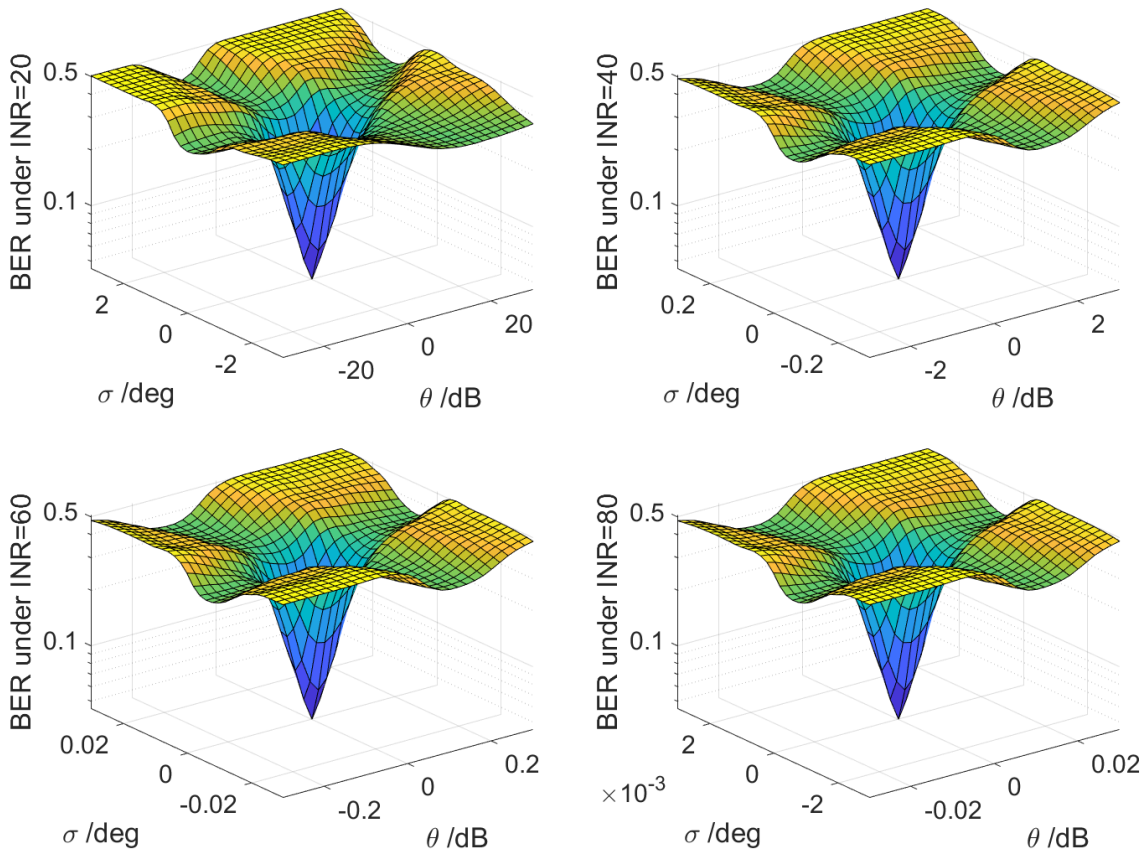

Figure 4.4: BER performance of the FDSM system with estimation errors for different INRs under Eb/No=10 dB

We also notice that although the FD system performs better than the FDSM system when there is no error (or small error), as σ and θ increase, the BER performance of

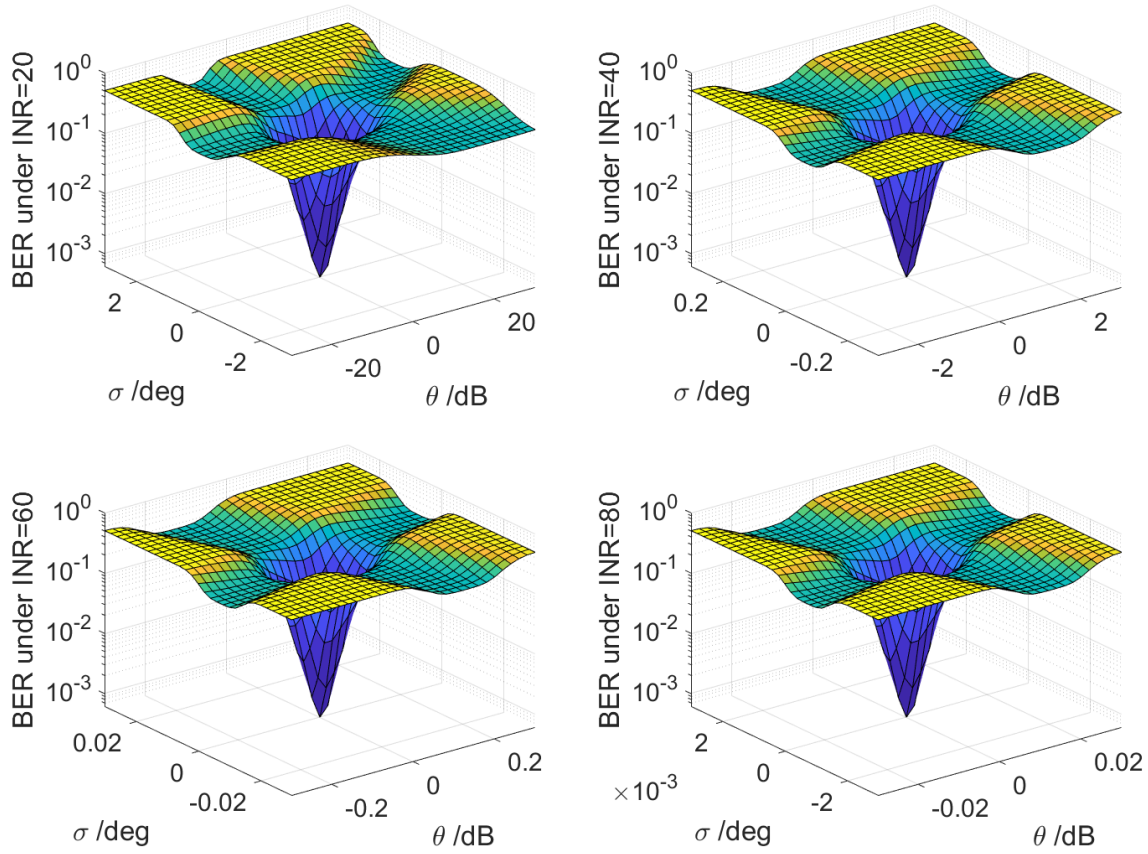

Figure 4.5: BER performance of the FD system with estimation errors for different INRs under Eb/No=10 dB

the FDSM system can reach the same level as the FD system, and even better. Figure 4.6 gives a typical example that shows the difference of the BER value between FDSM and FD system for INR=40 dB under Eb/No=10 dB. The area with a value greater than zero (yellow area) represents that the BER of the FDSM system is below the BER of the FD system. This finding makes sense because it is impossible to avoid errors in the SI estimation. The FDSM system not only improves the spectral efficiency but also has a performance that is not lower than the FD system when errors increase in the supposed propagation case.

4.3.3 With a real SI detector

The performance of the SI estimation is evaluated in this section. As mentioned in Section 4.2.3, an essential factor impacting the accuracy of SI estimation is the number of the detection symbols. Figure 4.7 gives the BER performance with real SI estimation

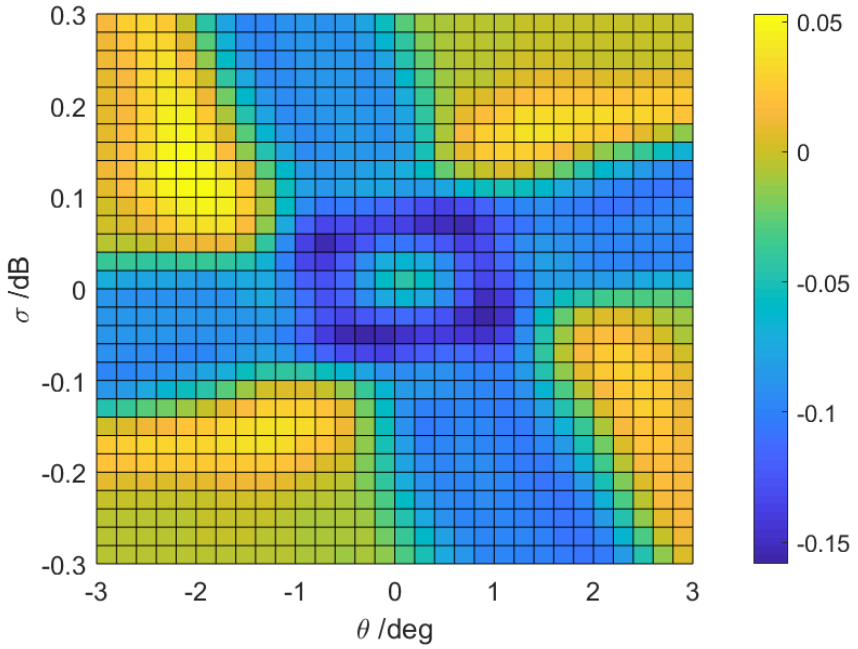

Figure 4.6: BER difference between FDSM and FD systems for INR=40 dB under Eb/No=10 dB

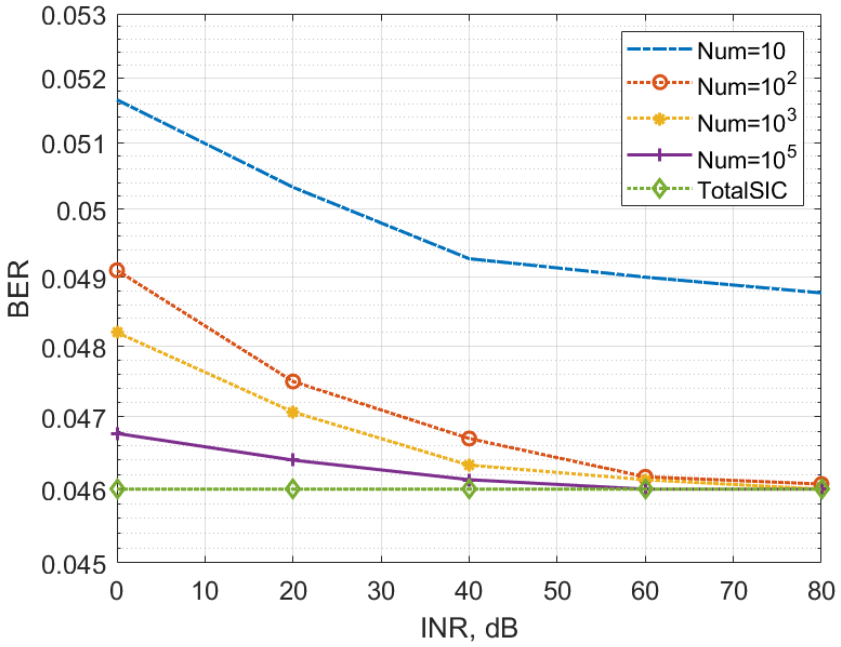

Figure 4.7: BER performance with SI estimation for different INRs and number of detect symbols under Eb/No=10 dB

for the different INR and the different number of detection symbols under Eb/No=10 dB.

As the INR increases, the BER of the FDSM system is slightly reduced due to the better SI estimation. This result corresponds to our previous conclusions on studying the FD system in [135]. Besides, one can conclude that increasing the number of detection symbols can improve the performance of the system. However, the lower amount of detected symbols does not make the system perform poorly but at an acceptable level especially in the case of high INR.

4.4 Summary

In this chapter, a study of a 2×2 FDSM system is presented. The study is performed in simulation, by using an ADS-Matlab co-simulator. We introduced different modules (antenna selection module, modulation, demodulation, channel correction module, SI estimation, SIC module, etc.) in order to complete this simulation framework. The impact of SIC accuracy on the BER performance for different INRs was highlighted. We can conclude that an acceptable BER performance needs to maintain the SI estimation error within a small range. The performance of the FDSM system is worse than the FD system when there is no error or are minor errors. However, the lower sensitivity makes the FDSM system maintain a BER performance close to the FD system and even better than the FD system in the case of large estimation errors. Besides, the detector with different numbers of detection symbols has a lower impact on the performance when INR is large. In other words, when INR is large, it is possible to reduce the number of detection symbols to improve transmission efficiency and complexity of detection.

CHAPTER 5

FULL DUPLEX SPATIAL MODULATION SYSTEM IN PRESENCE OF RF NONIDEALITIES

5.1 A classical RF front-end

The RF front-end is a core component of wireless communication devices. It is the fundamental component that converts wireless electromagnetic waves and binary digital signals into each other where the A/D and D/A conversion is included in the radio front-end. The transmitter RF front-end is used to upconvert the analog baseband signal into an RF signal suitable for transmission over a wireless channel, while the receiver RF front-end is used to downconvert the RF signal into a baseband one. A simplified architecture of the traditional Zero-IF is given in Figure 5.1.

In a Zero-IF RF front-end, the received RF signal is directly downconverted to a baseband signal, i. e. a signal around the DC component. Since the RF carrier and the local oscillator (LO) have the same center frequency, the biggest weakness of this architecture is that leakage from the LO to the mixer can lead to self-mixing, which results in an offset at the output of the time-varying direct conversion mixer. The RF front-end consists of components such as power amplifiers (PAs), low-frequency noise amplifiers (LNAs), filters, and switches. The PA is used to amplify the RF signal in the transmit channel; the filter is used to retain the signal in a specific band and filter out the signal outside this specific band; and the LNA is used to amplify the RF signal in the receive channel. During the practical signal transmission, there is a possibility of signal

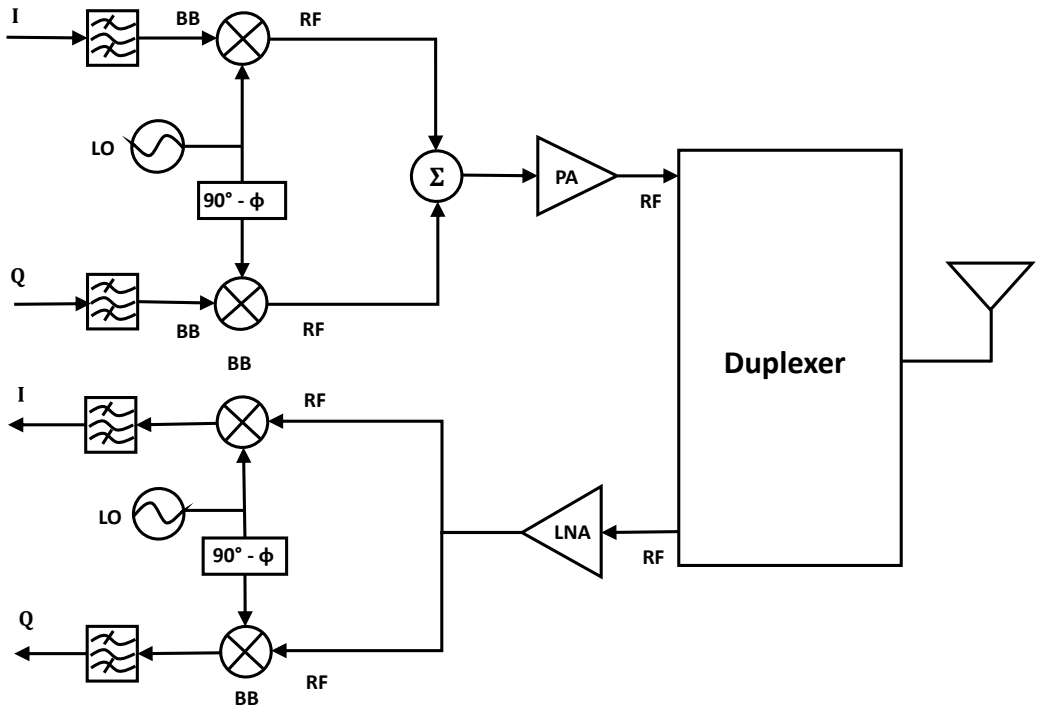

Figure 5.1: Typical architecture of the Zero-IF RF front-ends

loss and distortion due to the non-ideal nature of these components. RF impairments typically encountered in design and implementation include limited mirror rejection due to I/Q imbalance, nonlinear distortion due to PA of the mixer at the transmitter, LNA and receiver, and the phase noise arising from the rapid, short term, random phase fluctuations that occur in a signal. For example, the Zero-IF radio front-end presented here is sensitive to IQ imbalance.

For instance, MAX2830 [2] direct conversion, zero-IF, RF transceiver is a RF front-end solution which is designed for 2.4GHz to 2.5GHz 802.11g/b WLAN applications and the internal structure of its integrated circuit is shown in Figure 5.2. It contains the frequency transposition part, the amplification part (PA, LNA), the frequency synthesis, and a switch for antenna diversity. The targeted applications for this type of radio front-end are WiFi, mobile communications, etc. As an example, this radio front-end is employed in one of the versions of USRP (Universal Software Radio Peripheral), which is well known in the software-defined radio world. As can be seen, the circuit contains all the active functional blocks and some of the filters of an homodyne (or zero-IF) transceiver. To have a complete solution, it is necessary to add a band filter, quartz, and some passive components. The maximum bandwidth of the carried signals is 20

MHz. The circuit also contains 16 programmable registers which are used to modify the parameters of each functional block.

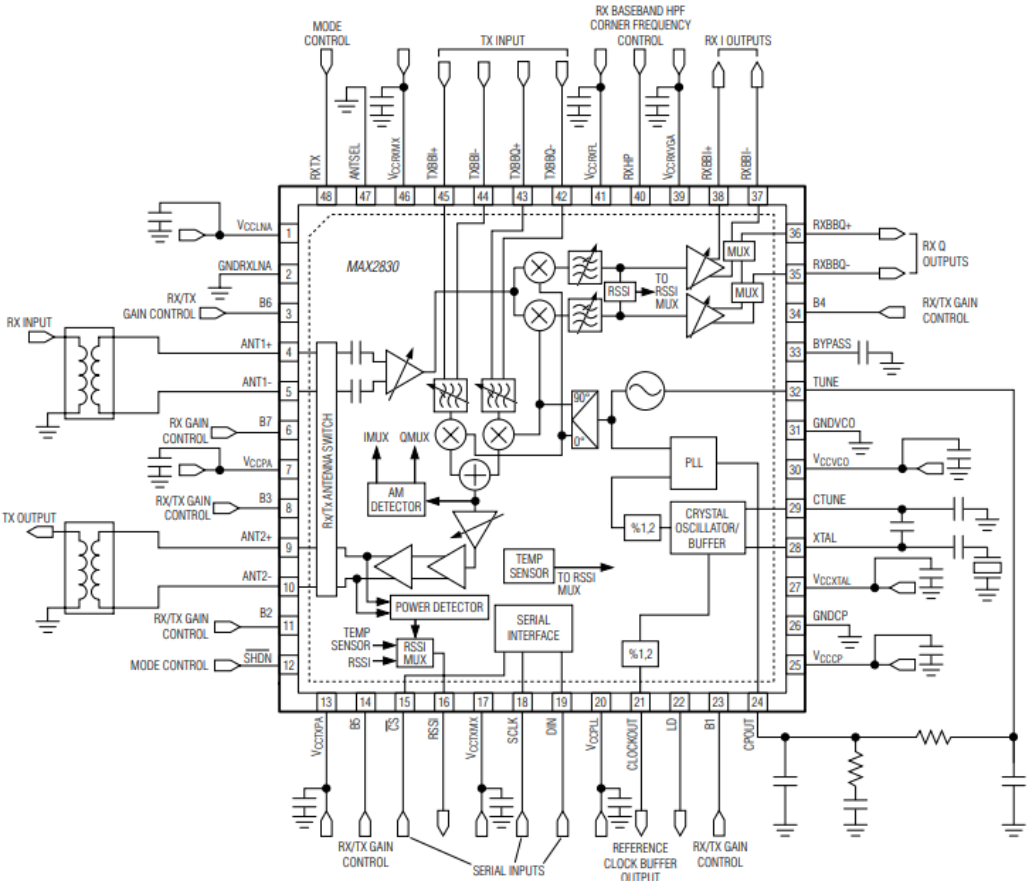

Figure 5.2: Typical operating circuit of MAX 2830 [2]

5.2 Imperfections of FDSM system

The core issue of the FDSM system is to attenuate both SI signal and the associated noise components. However, several constraints limit the performance of SI mitigation. The reasons for these limitations represent a number of factors including IQ imbalance, phase noise, power amplifier's nonlinearity, and switch response delay which is caused by antenna selection. In practice, if high system performance is expected, the imperfections generated in the front-end of transmitter and receiver must be considered. Due to the high power difference between the power levels of the SI signal and the signal of interest, compared with the latter, even slight distortion in the former may seriously

impact the system performance, while the latter will be weakened due to the much longer propagation distance. Moreover, the antenna switch is switched just before the generation of each symbol, and remains at the same position during the entire symbol generation process. In fact, there may be a delay between the instruction and the actual completion of the switch. Moreover, a power loss of the transmitting signal will be caused by the switch. In this section, we present in the following the various limits that impact the system performance.

5.2.1 IQ imbalance

The information is transmitted by modulating an RF carrier. The signal from the transmitter is usually received as a modulated signal in the receiver. In modern digital communication systems, the modulated signal includes an in-phase component and a quadrature one. There is always a certain amount of deviation in the correct alignment of the in-phase and quadrature components of the modulated signal. This difference may appear in the amplitude and phase of the in-phase and quadrature components of the signal. Figure 5.3 describes the phase and amplitude imbalances of the up and down conversion RF systems respectively. In the in-phase path and the quadrature path, the phase mismatch factor ϕ and the amplitude mismatch ε factor are introduced. However, in terms of amplitude and phase, the analysis is often only concerned with their amplitude difference and whether the phase is orthogonal. Therefore, in order to facilitate the analysis, one of the channels is used as the amplitude and phase reference, and the gain and phase deviation are placed in the other path, so as to obtain the demodulated signal through the quadrature demodulation method. The IQ imbalance that occurs in the modulation process is taken as an example here. After orthogonal demodulation, the two path signals are synthesized to obtain the signal $x(n)$:

$$\begin{aligned} x(n) =& A\cos\theta + j(A(1+\varepsilon)\sin(\theta-\phi)) \\ =& A((1-j(1+\varepsilon)\sin\phi)\cos\theta + j(1+\varepsilon)\cos\phi\sin\theta) \\ =& A(\alpha\cos\theta + j\beta\sin\theta) \end{aligned} \tag{5.1}$$

where $a = 1-j(1+\varepsilon)sin\phi$, $\beta = (1+\varepsilon)\cos\phi$, A is denoted by the ideal amplitude of I/Q path, ε is the amplitude mismatch factor, ϕ is the phase mismatch factor. θ represents the phase information of the modulated signal where $\theta = j\cdot 2\pi f_c + \phi$ and f_c is the carrier frequency, the time-varying nature of θ is not considered here. Obviously, when there is

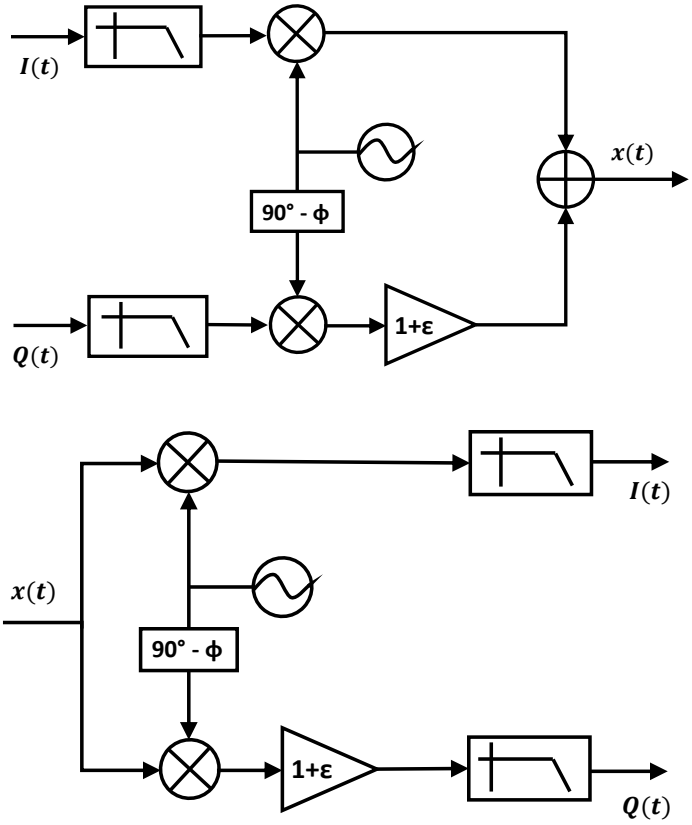

Figure 5.3: IQ mismatch in the quadrature modulation and demodulation process

no mismatch error, i.e. $\varepsilon = \phi = 0, \alpha = \beta = 1$. As

$$\begin{aligned} \alpha &= \frac{\alpha+\beta}{2} + \frac{\alpha-\beta}{2} \\ \beta &= \frac{\alpha+\beta}{2} - \frac{\alpha-\beta}{2} \end{aligned} \tag{5.2}$$

We can obtain

$$\begin{aligned} x(n) =& A\left(\frac{\alpha+\beta}{2}(\cos\theta + j\sin\theta) + \frac{\alpha-\beta}{2}(\cos\theta - j\sin\theta)\right) \\ =& A\left(\frac{\alpha+\beta}{2}e^{j\theta} + \frac{\alpha-\beta}{2}\mathrm{e}^{-j\theta}\right) \end{aligned} \tag{5.3}$$

From equation (5.3), it can be seen that when there is an amplitude or phase mismatch, the complex signal $x(n)$ not only contains the required signal component $A\mathrm{e}^{-j\theta}$, but also contains a component with different amplitudes that mirrors the frequency of the desired signal. In the actual application process, the image signal is caused by the IQ imbalance, and its magnitude is directly proportional to the severity of the phase and

amplitude mismatches between the I and Q paths. To characterize and quantify the image suppression performance of a direct-conversion (homodyne, synchrodyne, or zero-IF) transmitter or receiver , the image rejection ratio (IRR) is typically applied which is denoted by the ratio of the required signal level to the image signal level. It is defined as:

$$IRR = \frac{|(\alpha+\beta)/2|^2}{|(\alpha-\beta)/2|^2} = \frac{[1+(1+\varepsilon)\cos\phi]^2+((1+\varepsilon)\sin\phi]^2}{[1-(1+\varepsilon)\cos\phi)^2+((1+\varepsilon)\sin\phi)^2} \tag{5.4}$$

A more exhaustive presentation of IQ imbalance is given in [104]. For a HD system presented in [104], the system performance can be acceptable for an IRR up to -25 dB [4]. However, such IQ imbalance will cause a considerable degradation in FD system since the presence of SI. The impact of IQ imbalance on the SIC performance has been analyzed in [73, 83].

5.2.2 Phase noise

Local oscillator (LO) is one of the core components of the receiver. The homodyne (or zero-IF) receiver uses one or several LOs to move the input signal to the intermediate frequency before demodulation. For an ideal receiver, these frequency conversions will not cause distortion of the input signal. However, for the actual receiver, the phase noise of LO will distort the received signal, thereby reducing the overall performance of the receiver. An ideal oscillator can be described mathematically by a sine wave:

$$V = \cos(\omega_0 t) \tag{5.5}$$

The actual oscillator appears as amplitude noise modulation $n(t)$ and phase noise modulation $\theta_n(t)$:

$$V_0 = (1+n(t))\cos(\omega_0 t + \theta_n(t)) \tag{5.6}$$

Here $n(t)$ and $\theta_n(t)$ are both random processes. The amplitude modulation power is much smaller than the phase noise modulation power. In addition, the receiver mixer usually works at a saturated input power, which will reduce its sensitivity to changes in the amplitude. Therefore, the amplitude noise of the LO has little effect on the performance of the receiver and is usually ignored. The mixer in the ideal receiver multiplies the RF input and the LO input to get its sum-frequency and difference-frequency. Assuming that the input signal is an unmodulated carrier, and the LO is modulated by phase noise, the output frequency is the sum or difference frequency of the unmodulated carrier frequency and the LO frequency. A typical phase noise spectrum of a free running oscillator is shown in Figure 5.4. The phase noise is "transferred" to the RF signal, which manifests

itself as phase modulation of the unmodulated carrier. This effect is also applicable to the case of the modulated signal. Phase noise causes additional noise in the signal demodulator, and its degree of influence depends on the modulation type. For a FD mode system, the effect of oscillator phase noise has been analyzed in [110].

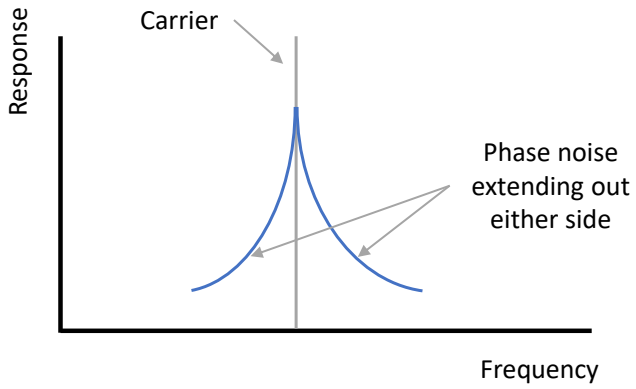

Figure 5.4: Typical phase noise spectrum of a free running oscillator

5.2.3 Nonlinear distortion

As discussed in [86], the main sources of nonlinearity in the system are the PA at the transmitter side [78]. The nonlinear PA brings a major challenge to maintain acceptable SIC capability. For an ideal linear PA, its input power $r_{in}(t)$ and output power $r_{out}(t)$ satisfy a linear relationship, can be expressed as

$$r_{\text{out}}(t) = g r_{\text{in}}(t) \tag{5.7}$$

Where g is the ideal gain, $r_{in}(t)$ and $r_{out}(t)$ are the signal voltages of the PA output and input, respectively. An ideal linear PA can increase all input signals by the same gain, and there is a fixed phase shift between input and output. Moreover, it has no memory effect, that is, the output of the PA depends only on the instantaneous input samples, not any previous samples.

The nonlinear behavior of the PA includes two main components: static nonlinearity and memory effect [48]. Static nonlinearity is also called memoryless nonlinearity, which corresponds to the distortion produced by PA without considering the memory effect.

For memoryless nonlinear PA, the relationship between input and output signals can be expressed by Taylor polynomials as:

$$V_{\text{out}}(t) = g_1 V_{\text{in}}(t) + g_2 V_{in}^2(t) + g_3 V_{in}^3(t) + \ldots + g_n V_{in}^n(t) \tag{5.8}$$

where $g_1, g_2, \ldots, g_n$ are the coefficients of Taylor polynomial. $V_{\text{in}}(t)$ is denoted by the input of PA, expressed as

$$V_{in}(t) = a\cos(\omega t), \quad \omega = 2\pi f t \tag{5.9}$$

where a and f represent the amplitude and the frequency of the input signal respectively. If only the first three terms of Taylor polynomials are taken into account, we can obtain

$$V_{\text{out}}(t) = \frac{g_2 a^2}{2} + (g_1 a + \frac{3g_3 a^3}{4})\cos(\omega) + \frac{g_2 a^2}{2}\cos(2\omega) + \frac{g_3 a^3}{4}\cos(3\omega) \tag{5.10}$$

In fact, though there are several terms (DC term, the fundamental term, the second-order harmonic term and the third-order harmonic term) in the output signal, only the fundamental term $(g_1 a + \frac{3g_3 a^3}{4})\cos(\omega)$ is useful and need to be extracted. When a is a minor value, it can be assumed that

$$\frac{3g_3 a^3}{4} \approx 0 \tag{5.11}$$

Hence, the gain of this PA g_{PA} is approximated to g_1, otherwise,

$$g_{\text{PA}} = g_1 + \frac{3g_3 a^2}{4g_1} \tag{5.12}$$

It can be concluded that the gain of PA decreases as the input power increases in the nonlinear PA case. Here our study of nonlinearity considers only the case of a single signal (for harmonic distortion). A different scenario in RF design occurs if two sources of interference accompany the desired signal [107]. This scenario represents the actual situation and reveals nonlinear effects that may not appear in harmonic distortion or desensitization tests. If two sources of interference at ω_1 and ω_2 are applied to a nonlinear system, the output will typically show components that are not harmonics of those frequencies, a phenomenon called "intermodulation", caused by the "mixing" (multiplication) of the two components. The third-order intercept (IP3) point is proposed to capture the intermodulation behavior of the circuit and thus becomes a rule-of-thumb measure to estimate nonlinear PA.

In general, it is necessary to make the PA work in a nonlinear state to improve its energy efficiency. In this way, the linearity of the PA is not guaranteed. These nonlinearities are assumed to have an impact on the SNR and ACPR (Adjacent Channel Power Ratio), which can cause degradation of the BER to a certain degree.

5.2.4 RF Switch imperfections

RF switch is used to switch between transmitting and receiveing antennas, or in more advanced transmitters and receivers, is used to switch between transmiting antennas or receiving antennas. For example, switching between receiving antennas enables antenna diversity techniques. A RF switch in the SM modulation part of the FDSM system is shown in Figure 5.5. Here, the switch controller executes the command to select the desired antenna to transmit data. In an ideal situation, when the antenna selection switch controller receives a change command, the time for the switch to change from one state to another state is assumed as zero. However, in practice, there is a response delay between the command and the reaction. The switching time will influence the transmission rate and the system performance, especially in the case of high data rate [117].

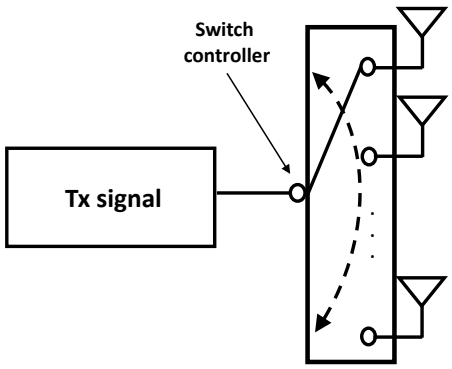

Figure 5.5: RF switch

Moreover, the switch insertion loss could be another issue that degrades the system performance [54]. The insertion loss of the RF switch means that the signal will be attenuated though the switch. This attenuation is mainly reflected in the amplitude of the constellation. Isolation is another key indicator of RF switch performance, i.e., the degree of attenuation between the input and output of the circuit. Additionally, isolation is a measure of how effectively a switch is turned off.

Table 5.1: Parameters of commercial RF switches: switching time, insertion loss and isolation

Switch Product	Switching time	Insertion loss	Isolation
TS72421K	0.65 μs	0.45 dB	20 dB
MM5120	< 10 μs	0.35 dB	25 dB
BGS12SN6	60 ns	0.25 dB	33 dB

Here we provide as reference three types of commercial RF switches with regard to switching time, insertion loss and isolation, the models are TS72421K (Tagore Technolog) [7], MM512 (Menlo Micro) [8] and BGS12SN6 (Infineon) [1].

We can conclude from Table 5.1 that current on-market RF switching time can be controlled at the μs level, insertion loss is generally within 0.5dB, and isolation is generally greater than 20dB.

5.3 Effect of the receiver's nonidealities

5.3.1 Introduction

In general, impairments of the radio front-end such as IQ imbalance and phase noise strongly impact the transmission performance. For FD systems, the strength of residual SI after SIC directly influences the quality of the transmission. Moreover, receiver nonidealities will affect the accuracy of the SI estimation, which also have an impact on system performance. Digital estimation and compensation of IQ imbalance for FD system is presented in [132] and [137]. As the SI signal is much stronger than the signal of interest, the influence of the receiver nonidealities on SI signal will significantly increase the system's BER. The authors of [26] proved that IQ imbalance is also a critical issue for SM-based transmission. In [27] the performance of a SM system in presence of IQ imbalance has been studied via computer simulations and analytical derivations.

In the previous chapter, the BER performance of the FDSM system as function of different SIC accuracies has been studied. However, receiver front-end was considered ideal. The work considering the impact of the receiver nonidealities on the FDSM system is still lacking. Moreover, no estimation and compensation approaches for strong SI with impairments are proposed for FDSM systems. Channel estimation and SIC are still open problems for FDSM systems, especially in presence of receiver nonidealities.

As introduced in the previous section, the disparities of the characteristics of compo-

nents constituting the radio front-end induce IQ imbalance and phase noise, which are the two main factors causing receiver nonidealities.

In this section, we study 2×2 FDSM systems over a Rician fading channel in the presence of radio front-end nonidealities. We consider a receiver structure to cope with IQ imbalance and phase noise for this FDSM system.

The remainder of this section is divided as follows: the 2×2 FDSM system model is introduced in 5.3.2. Also, the receiver and the SI estimation algorithm are explained in detail. Section 5.3.3 presents a comparison between the BER performance of system with different levels of nonidealities and no receiver imperfection. A summary is given in section 5.3.4.

5.3.2 FDSM System architecture and receiver radio front-end

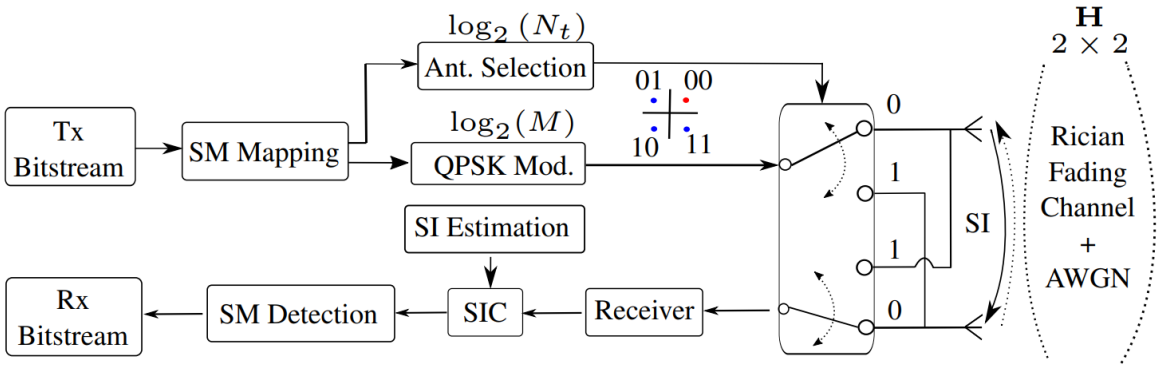

Figure 5.6: 2×2 Full Duplex Spatial Modulation system: node A

Both nodes of the FDSM system (i.e. node A and node B) have emitting and receiving capabilities. The structure of node A in the 2×2 FDSM system is given in Figure 5.6, and here a nonideal receiver front-end is taken into acount. As stated in the previous chapter, the incoming data bitstream is divided into groups of $\log_2(N_t M)$ bits. N_t represents the number of antennas at each node, M represents the modulation order of the complex constellations. In the particular case studied here, $N_t = 2$ and $M = 4$. Depending on the incoming bit combination, an analog switch selects one of the two antennas. The antenna that is not selected is used for signal reception. The other 2 bits determine the symbol of the QPSK modulation to be transmitted. The transmitted signal passes through a 2×2 sized Rician fading channel modeled by the matrix $\mathbf{H}$.

We suppose that node A and node B transmit simultaneously over the same communication channel. At node A, while transmitting the modulated signal, the second antenna

receives the signal from the node B together with the SI signal, where the power level is much higher than the signal of interest. Consequently, the received signal from node B experiences a strong interference. The incoming signal together with the SI one are transposed in BB by an analog radio front-end supposed to be impacted by IQ imbalance and phase noise.

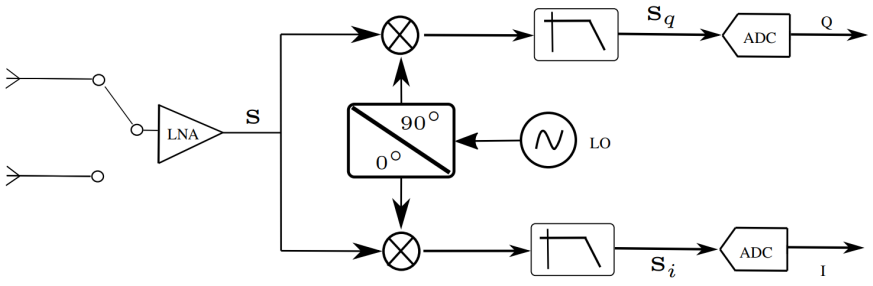

Figure 5.7: 2×2 Full Duplex Spatial Modulation system: the receiver side of the radio front-end

The simplified architecture of the receiver's analog part of the radio front-end is shown in Figure 5.7. As discussed previously, in practice, the total gain on the in-phase I and quadrature Q paths of the radio front-end RF are not exactly equal. Similarly, the 90° phase shift of the LO for the Q path may also be inaccurate. When the analog part of the radio front-end does not respect the power balance and the orthogonality between the I and Q branches, IQ imbalance occurs. The IQ imbalance can be described by two parameters: the amplitude imbalance ε and the phase orthogonality imbalance θ. To be better understood, the effect of the IQ gain imbalance (ε) and the IQ phase imbalance (θ) on the QPSK constellation is shown in Figure 5.8. The figure shows that IQ gain imbalance leads to a rectangular stretch along the ideal I/Q axes, while IQ phase imbalance causes a rectangular stretch along a 45° line.

The simulation results of a QPSK constellation deformation in presence of different scenarios of IQ imbalance is shown in Figure 5.9. For an amplitude imbalance ε in dB and a phase orthogonality imbalance θ in degree, a θ-angle and ε-dB deformation will occur. In this case, 4 dB and 20° are selected as the absolute value of the gain imbalance and the phase imbalance respectively. It should be noticed that for real transmissions, the IQ imbalance is much smaller (e.g. phase error of ±0.35° and gain imbalance of ±0.1 dB for Max 2830 [2]). Moreover, the phase noise $\phi(t)$ of LO may also degrade the performance of the radio front-end.

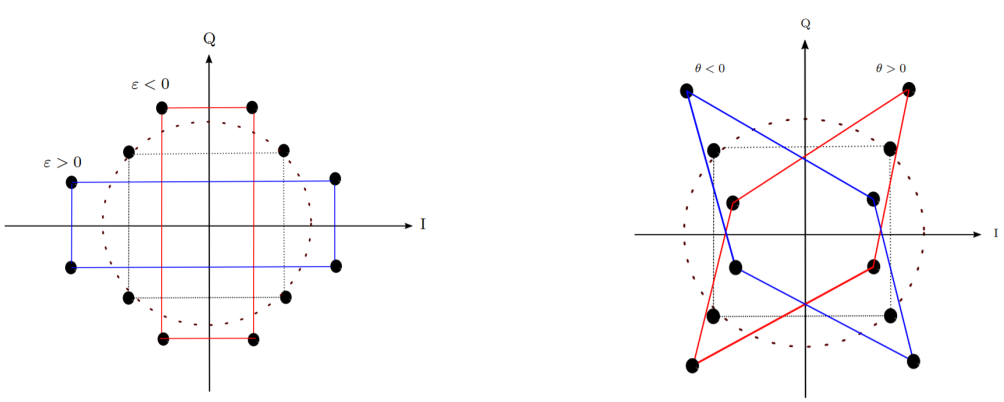

(a) with IQ Gain imbalance (b) with IQ Phase imbalance

Figure 5.8: QPSK constellation with IQ gain and phase imbalance

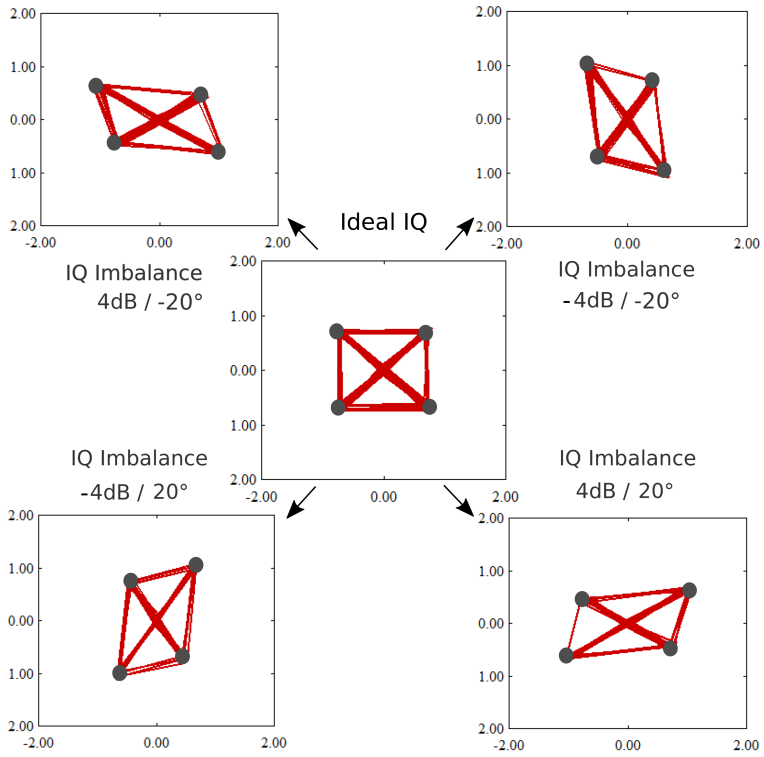

Figure 5.9: Deformation of a QPSK constellation in presence of different scenarios of IQ imbalance

S is the incoming mixed signal which combines the SI signal and the signal of interest, the signals $\mathbf{S}_i$ and $\mathbf{S}_q$ impacted by the gain and phase imbalance and by phase noise in

time domain are given by (5.13) :

$$\begin{cases} \mathbf{S}_i = \left(1+\frac{\varepsilon}{2}\right)\cos\left(\omega_c t + \frac{\theta}{2} - \phi(t)\right)\cdot\mathbf{S} \\ \\ \mathbf{S}_q = \left(1-\frac{\varepsilon}{2}\right)\cos\left(\omega_c t - \frac{\theta}{2} - \phi(t)\right)\cdot\mathbf{S} \end{cases} \tag{5.13}$$

where $\omega_c = 2\pi f_c$, and f_c is the frequency of the receiving signal.

As the SI signal strength is higher than the useful one (the one transmitted by the remote node B), the impact of IQ imbalance and phase noise on the system performance mainly comes from its impact on SI signal.

SIC is implemented after the frequency translation (in BB). A LS estimator is proposed for cancelling the SI together with the impact of the receiver nonidealities on SI. More precisely, the SI channel and the nonidealities are not actually separated, the two parameters are estimated at the same time.

During the estimation phase, we assume that only the SI signal is present and Node B does not transmit. This is a reasonable constraint given the difference between the power level of the remote signal and the power level of the SI signal. Nevertheless, we designed a dedicated framework for estimating the auto-interference channel parameters. The estimated channel matrix $\widetilde{\mathbf{H}}^*$ between the generating SI signal $\mathbf{x}$ and the receiving signal $\mathbf{y}$ is given by (5.14):

$$\widetilde{\mathbf{H}}^* = \left(\mathbf{x}\cdot\mathbf{x}^H\right)^{-1}\cdot\mathbf{y}\cdot\mathbf{x}^H \tag{5.14}$$

where:

$$\begin{cases} \mathbf{x} = [x[0], \quad x[1], \quad \cdots \quad x[N-1]]^t \\ \mathbf{y} = [y[0], \quad y[1], \quad \cdots \quad y[N-1]]^t \end{cases} \tag{5.15}$$

and:

$$x[n] = A(n)e^{j\varphi_{si}}. \tag{5.16}$$

Here A, φ_{si} represent the amplitude and the phase of the SI signal, respectively. N is the number of symbols that are employed for the SI estimation.

Consider $\mathbf{H}_{si}$ the actual SI channel and $\mathbf{H}_{in}$ the channel taking into account the nonidealities. The theoretical relation $\mathbf{H}^*$ between $\mathbf{x}$ and $\mathbf{y}$ can be defined by φ_{si} and $\mathbf{H}_{in}$:

$$\begin{aligned} \mathbf{H}^*(n) = \mathbf{H}_{si}(n)\cdot\mathbf{H}_{in}(n) = \mathbf{H}_{si}(n)\cdot((1+\tfrac{\varepsilon}{2}) \\ \cos(\omega_c t + \tfrac{\theta}{2} - \phi(t)) + j(1-\tfrac{\varepsilon}{2})\cos(\omega_c t - \tfrac{\theta}{2} - \phi(t))) \end{aligned} \tag{5.17}$$

As stated, compared to the main signal transmitting from the other node, the SI signal strength is much higher, so even a small IQ imbalance on the SI signal can have a great impact on the system's performance. We propose an estimation after the receiver front-end where an estimation of both the SI signal and nonideal impact on the SI signal can be guaranteed. The difference between the estimation of channel before ($\widetilde{\mathbf{H}}^{*\mathbf{1}}$) and after the receiver front-end ($\widetilde{\mathbf{H}}^{*\mathbf{2}}$) is taking into account the nonidealities.

$$\begin{aligned} \widetilde{\mathbf{H}}^{*\mathbf{1}} &= \widetilde{\mathbf{H}}_{\mathbf{si}}(\mathbf{n}) \\ \widetilde{\mathbf{H}}^{*\mathbf{2}} &= \widetilde{\mathbf{H}}_{\mathbf{si}}(\mathbf{n}) \cdot \widetilde{\mathbf{H}}_{\mathbf{in}}(\mathbf{n}) \end{aligned} \tag{5.18}$$

The two different residual signals are given in the equation (5.19) and the equation (5.20). $\mathbf{S}_r^1$ and $\mathbf{S}_r^2$ represent residual signal for the estimation before and after the receiver front-end respectively. Here B, φ_s are the amplitude and the phase of the useful signal from node B, respectively. For the first case, the coefficient ρ_1 of the SI signal cannot be completely eliminated. However, it can be seen that the non-negligible influence of the impairments on the SI signal can be eliminated in the second case under ideal conditions ($\rho_2 = 0$). Therefore, with an ideal estimation, the mixed signal after SIC has the same power level as the signal of interest, which means the BER performance of the FDSM system with cancellation will be at the same level as the SM system.

$$\begin{aligned} \mathbf{S}_r^1(n) &= A(n)e^{j\varphi_{si}(n)} \cdot \mathbf{H}^*(n) + B(n)e^{j\varphi_s(n)} \cdot \mathbf{H}_{\mathbf{in}}(n) \\ &\quad - A(n)e^{j\varphi_{si}(n)} \cdot \widetilde{\mathbf{H}}^{*\mathbf{1}} \\ &= A(n)e^{j\varphi_{si}(n)}(\mathbf{H}^*(n) - \widetilde{\mathbf{H}}^{*\mathbf{1}}) + B(n)e^{j\varphi_s(n)} \\ &\quad \cdot \mathbf{H}_{in}(n) \\ &= A(n)e^{j\varphi_{si}(n)}(\overbrace{\mathbf{H}_{si}(n) \cdot \mathbf{H}_{in}(n) - \widetilde{\mathbf{H}}_{si}(n)}^{\rho_1}) \\ &\quad + B(n)e^{j\varphi_s(n)} \cdot \mathbf{H}_{in}(n) \end{aligned} \tag{5.19}$$

$$\begin{aligned} \mathbf{S}_r^2(n) &= A(n)e^{j\varphi_{si}(n)} \cdot \mathbf{H}^*(n) + B(n)e^{j\varphi_s(n)} \cdot \mathbf{H}_{in}(n) \\ &\quad - A(n)e^{j\varphi_{si}(n)} \cdot \widetilde{\mathbf{H}}^{*\mathbf{2}} \\ &= A(n)e^{j\varphi_{si}(n)}(\mathbf{H}^*(n) - \widetilde{\mathbf{H}}^{*\mathbf{2}}) + B(n)e^{j\varphi_s(n)} \\ &\quad \cdot \mathbf{H}_{in}(n) \\ &= A(n)e^{j\varphi_{si}(n)}(\overbrace{\mathbf{H}_{si}(n) \cdot \mathbf{H}_{in}(n) - \widetilde{\mathbf{H}}_{si}(n) \cdot \widetilde{\mathbf{H}}_{in}(n)}^{\rho_2}) \\ &\quad + B(n)e^{j\varphi_s(n)} \cdot \mathbf{H}_{in}(n) \end{aligned} \tag{5.20}$$

Moreover, the four symbols of the QPSK modulation are impacted by IQ imbalance in different ways. For example, for a positive amplitude mismatch and a clockwise phase mismatch, the amplitudes of symbols in the first and third quadrants increase and the phase shifts rotate in a counterclockwise direction. The symbols in the second and fourth quadrants change in opposite direction. Hence, a judgment on the quadrant where the symbol is located is also necessary before the SIC module.

The remaining signal after SIC will pass through a SM detection module to detect the transmitting antenna and symbol. We assume that a perfect CSI of the Rician fading channel between node A and node B can be obtained in this section to ensure SIC quality as the single variable for judging system performance. Finally, the output bitstream is generated by combining the transmitting bits coded by the antenna selection and coded by the QPSK modulation. More details of the demodulation module can be found in Chapter 3.

5.3.3 System performance results

The performance in the presence of nonidealities at the receiving end is analyzed by taking into account: the impact of the IQ imbalance under different noise levels, the BER performance with estimation under IQ imbalance, and the BER performance under different phase noise levels. The system parameters of this simulation framework (e.g. frequency, data rate, etc.) is the same as shown in Table 4.2.

5.3.3.1 Impact of IQ imbalance

The impact of IQ imbalance under different ratios of energy per bit (E_b) to the spectral noise density (N_0) is studied in this part. An ideal SI detector by applying LS algorithm is supposed at this point. The system's BER performance without IQ imbalance under E_b/N_0 = 10, 15 and 20 dB is shown in Table 5.2.

Table 5.2: FDSM system performance with ideal IQ

E_b/N_0	Number of input symbols	BER
10	10 000	0.04459
15	10 000	0.01147
20	10 000	0.00040

The FDSM system performance within the corresponding range of the gain and phase imbalance has been evaluated. This evaluation is made taking into account the BER

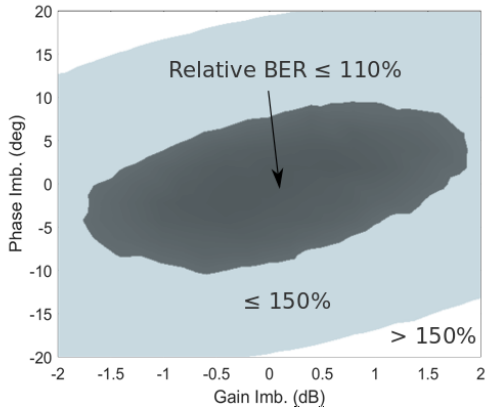

(a) Eb/No=10 dB

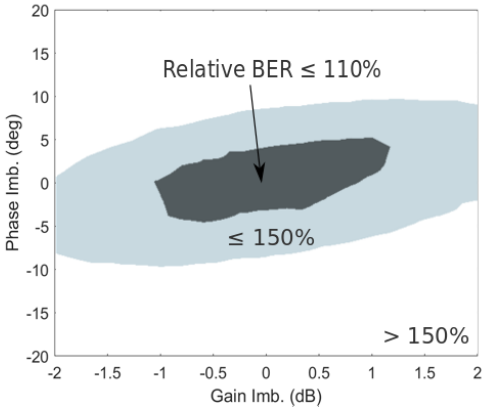

(b) Eb/No=15 dB

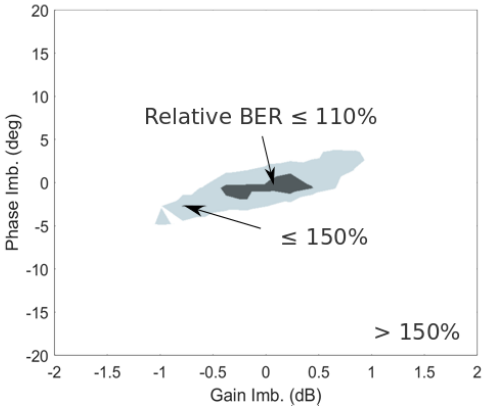

(c) Eb/No=20 dB

Figure 5.10: Relative BER under Eb/No=10 dB, 15 dB and 20 dB.

values presented in table 5.2. The variation of the gain imbalance is (-2 dB, 2 dB) and the variation of the phase imbalance is (-20°, 20°). This range selection is large enough to cover the IQ imbalance of commercial RF front-ends.

The relative BER (ratio between BER with IQ imbalance and BER with ideal IQ) is introduced to study the impact of varying IQ imbalance.

It can be observed in Figure 5.10 that the system is more sensitive to IQ imbalance as E_b/N_0 increases. The reason is that when the E_b/N_0 is large, the system is less impacted by the noise and it can maintain high performance. In the absence of IQ imbalance, the BER can reach 10^{-4} when E_b/N_0 = 20 dB. Therefore, even a small imbalance will have a great impact on the system performance in this situation. On the contrary, when E_b/N_0 is small, the thermal noise has already a large impact on the system performance and the addition of IQ imbalance will not create a substantial gap.

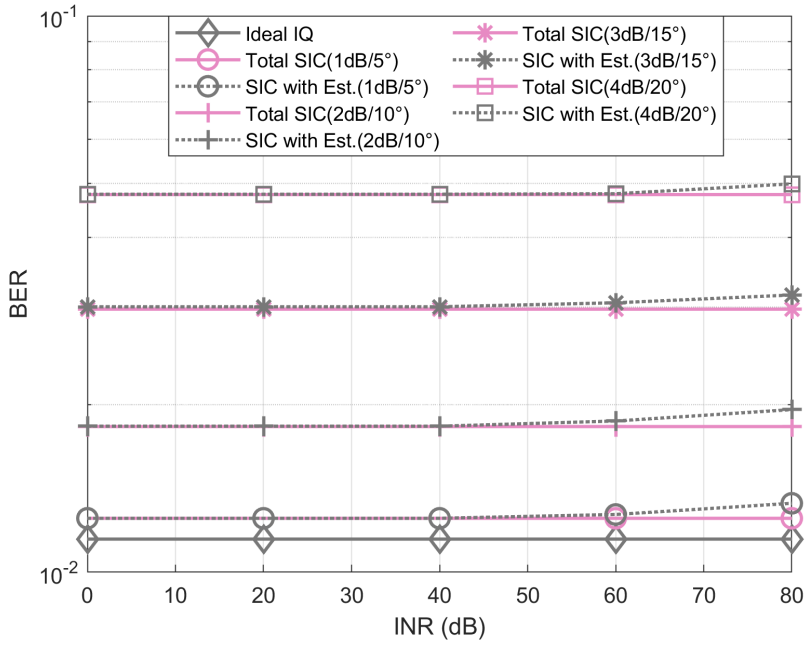

Figure 5.11: BER performance with LS estimator compared with total SIC under Eb/No=15 dB. The number of symbols for SI estimation $N = 1000$

5.3.3.2 BER performance with estimation under IQ imbalance

The BER performance with the proposed LS estimator under $E_b/N_0 = 15$ dB is shown in Figure 5.11. Self-interference-to-noise Ratio (INR) is introduced to measure the strength of the SI signal. The BER performance of the proposed estimator is compared with the total SIC for different IQ imbalance levels. IQ imbalance is considered as the only nonidealities effect in this case. The BER performance of the FDSM system with total SIC is equivalent to that of the SM system. It can be remarked that even if the INR is high (i.e. the SI and its additional signal which is due to the IQ imbalance are both much larger than the signal of interest), the system can still maintain the performance at an acceptable level. The simulation results correspond to the theoretical analysis in equation (5.20), where the value of ρ_2 can be considered as nearly equal to zero with the proposed estimator.

For comparison, the BER performance with the proposed estimator for the conventional SM system while varying E_b/N_0 and for different levels of IQ imbalance is presented in Figure 5.12. The BER performance for the FDSM system under INR = 40 dB while varying E_b/N_0 and for different levels of IQ imbalance is presented in Figure 5.13. When comparing the two BER variations, one can remark that the FDSM system

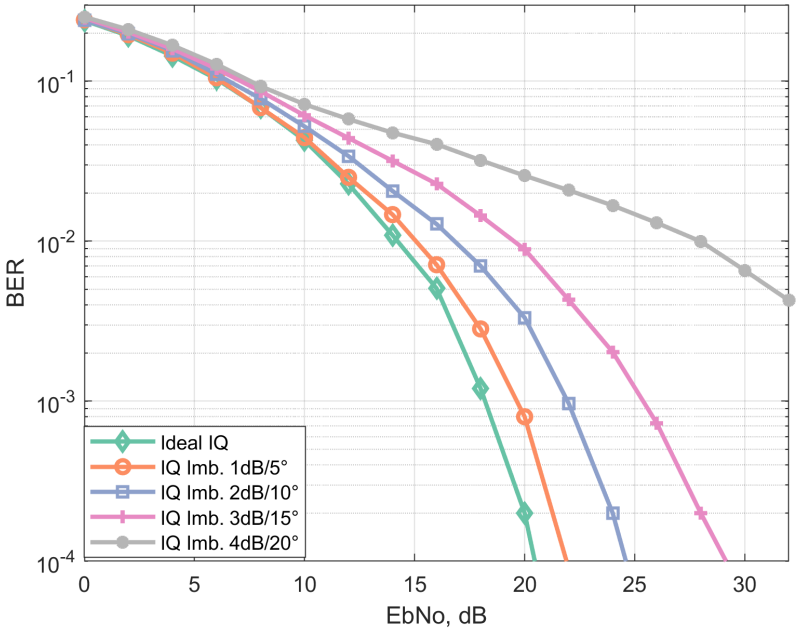

Figure 5.12: BER performance of SM system for different IQ imbalance levels

has a slightly degraded BER performance, i.e. SIC can reach an acceptable level.

5.3.3.3 BER performance under different phase noise levels

The phase noise level of the receiver's local oscillator (LO) is another factor that can degrade the overall FDSM system performance. In order to study its impact, several phase noise levels are considered (Table 5.3). The PN1 corresponds to the phase noise of the NI PXIe-5646R RF vector signal transceiver (VST), the instrument employed for the measurement campaigns.

Table 5.3: Data of different phase noise levels

PN(dBc/Hz) Freq.(kHz) / Level	0.1	1	10	100	1000
Phase Noise Level 0 (PN0)	No phase noise				
Phase Noise Level 1 (PN1)	-83	-101	-104	-115	-143
Phase Noise Level 2 (PN2)	-63	-81	-84	-95	-123
Phase Noise Level 3 (PN3)	-53	-71	-74	-85	-113
Phase Noise Level 4 (PN4)	-43	-61	-64	-75	-103

The BER performance under different phase noise levels while INR=40 is shown in

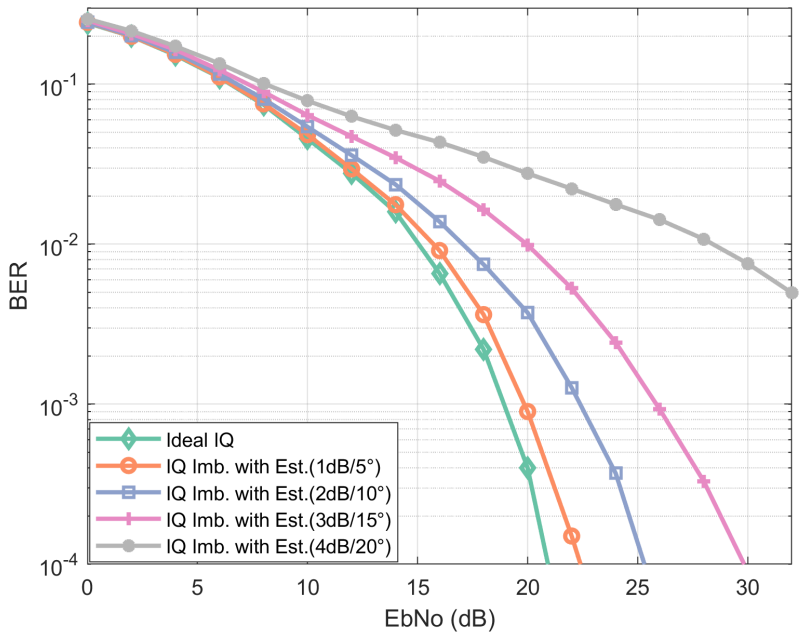

Figure 5.13: BER performance of FDSM system with LS estimator for different IQ imbalance levels

Figure 5.14. The impact of the phase noise on the BER performance is nonlinear. The BER can be kept at an acceptable level until PN3, since with PN4, the BER performance significantly degrades.

5.3.4 Summary

In this section, the performance of the FDSM system has been analyzed in presence of the IQ imbalance and of the phase noise. In theory, even though the SI signal is totally cancelled, the residual signal caused by the receiver nonidealities can significantly degrade the system performance. A LS estimator is proposed to suppress the SI signal received by the imperfect RF receiver. We observed that the system is more sensitive to IQ imbalance at high signal-to-noise ratios. The numerical results show that the proposed estimator can reach an acceptable BER consistent with theory. The phase noise of the instrument employed for the measurement campaigns slightly influences the system BER performance and can be negligibly low.

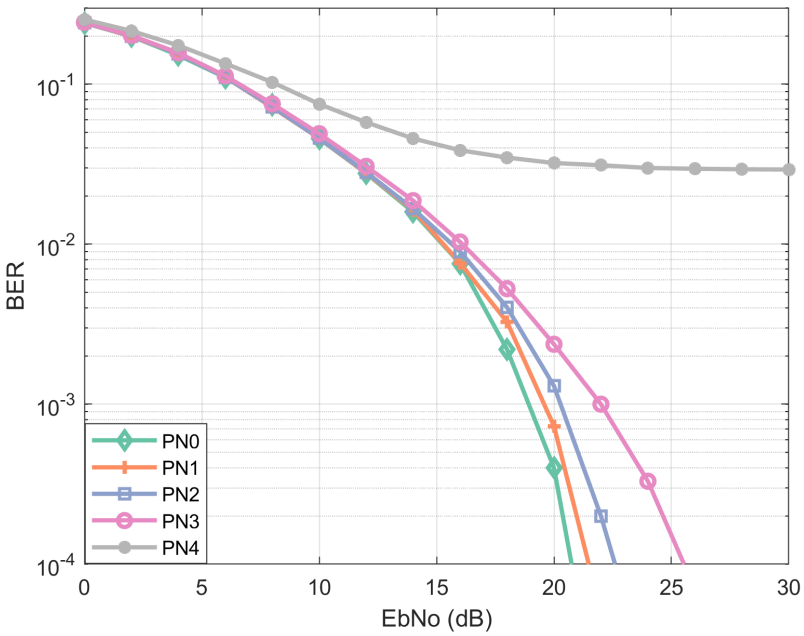

Figure 5.14: BER performance of FDSM system with ideal IQ but different phase noise levels

5.4 Nonlinear distortion effect of PA

5.4.1 Introduction

In addition to the receiver nonidealities, the nonlinear distortion at the transmitting end is also inevitably introduced since the actual hardware is not as ideal as the theoretical assumptions, which causes a gap between the SI signal recovered by the traditional channel estimation and the actual SI signal. The article [76] shows the performance of a FD radio by considering nonlinear RF components. Nonlinear canceller with complexity reduction scheme for FD radios is described in [74][115]. However, nonlinear effects on the FDSM system have been scarcely investigated from the perspective of the power amplifier (PA).

In this section, we analyze especially the nonlinear effects of PA and a digital canceller is employed to suppress the SI signal. Section 5.4.2 presents the considered nonlinear FDSM system model taking into account the PA's non-linear effect, along with the digital canceller specifically adapted for nonlinear PA. The system level simulation results are discussed in Section 5.4.4, after which the summary is given in Section 5.4.5.

5.4.2 System architecture and implementation of digital canceller

The structure of Node A is based on Figure 5.6 but a nonlinear PA is considered in the emission chain. For ease of understanding, we divide Node A into three parts.

5.4.2.1 Transmitting part

In our model, the antenna selected by the switch will transmit the QPSK symbols, and the other antenna will be used to receive the signal from the other node. Before transmitted by the selected antenna, the modulated signal will be amplified by the PA which may impact the communication performance by its nonlinear behavior.

Nonlinear distortions produced by the transmitter's PA is one of the nonidealities of RF chain which become a significant issue in a FD transceiver when using cheaper and less linear power amplifier. In order to study this impact, we choose the low-cost PA of the type CC2595 from Texas Instruments [9] and apply its model in the FDSM's system level simulation. The CC2595 has a typical gain of 24 dB, its operating frequency range is between 2400 MHz and 2483.5 MHz and the typical output power is $P_{out} = 20.7$ dBm.

A simulation model of CC2595 is built by ADS software according to the datasheet [9]. The simulation results of this model are presented in Figure 5.15. Here Gain represents the amplifier's gain in dB; P_{out} denotes the output power; PAE represents the power-added efficiency. PAE is denoted by the ratio between the effective output power and the DC input power, which is a metric for rating the efficiency of a PA. As can be remarked from this figure, the -1dB compression point is obtained for input power levels of about -6 dBm and the corresponding output power level is 17 dBm, as presented in the CC2595's datasheet.

In order to incorporate the PA's nonlinear effect, the performance of the canceller will be evaluated for PA's input power levels greater than -6 dBm.

5.4.2.2 Channel environment

As presented in 4.2.2, the main channel between two nodes is defined as a 2×2 sized Rician fading channel. SI channel is supposed to be a single-path one delay channel where the direct path dominates the SI channel. Besides, INR is the power ratio of the received SI signal to the receiver thermal noise, in order to evaluate the SI power. A large range ([-20 dB, 80 dB]) INR is applied to represent the different levels of SI power for the receiving end. In a practical sense, we can understand the influence of the

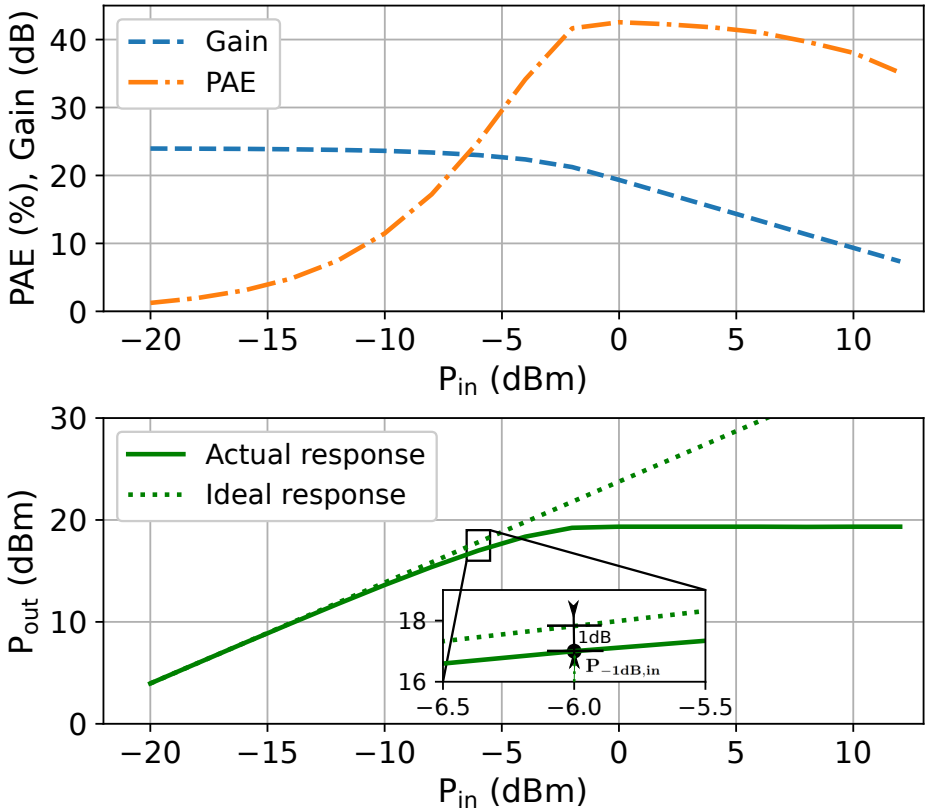

Figure 5.15: CC2595 PA's typical characteristics in simulation

changes with INR as that of the changes with the distance between the two nodes on the performance of the system.

5.4.3 Receiving part: digital canceller

The signal received at node A (x_n^a) is the combination of two parts: one from node B and the other is SI. Precisely, the received signal (s_n) from node B after passing the Rician fading channel and the SI (s_n^{si}) generated by the transmitting part from its own node (node A). The nonlinear signal distortion produced by PA has significant effects on SI signal. Here, the nonlinear signal model is supposed as a simple memoryless polynomial model. For higher accuracy, a model with memory such as parallel Hammerstein model can also be supposed as shown in [74][78]. A study on the memoryless polynomial model is firstly taken into account, where the signal S_n^a received by the antenna can be given as follows.

$$S_n^a = s_n + s_n^{si} + \eta \tag{5.21}$$

with the received SI signal s_n^{si} given as

$$s_n^{si} = h_n \cdot (s_n^a)_{PA} \tag{5.22}$$

where η corresponds to the AWGN noise, h_n denotes the SI channel taken into account PA nonlinearities and s_n^a is the input signal of PA at node A. $(s_n^a)_{PA}$ represents the output signal of PA, given as

$$(s_n^a)_{PA} = \sum_{k=0}^{K} p_k \cdot s_n^a \cdot |s_n^a|^k \tag{5.23}$$

where p_k is the complex-valued coefficient of the PA polynomial model and $K+1$ is the maximum order of the polynomial. In general, only odd-orders are considered because only odd-order distortion will appear around the received signal [38]. Hence, the odd-order polynomial model can be presented as

$$\begin{aligned}(s_n^a)_{PA} &= \sum_{k=0}^{K} p_k \cdot s_n^a \cdot |s_n^a|^{2k} \\ &= \sum_{k=0}^{K} p_k \cdot i_{2k+1}(s_n^a)\end{aligned} \tag{5.24}$$

where i_{2k+1} is a function of s_n^a, is equal to $s_n^a \cdot |s_n^a|^{2k}$.

The combined signal is transposed in BB by an analog radio front-end. We assume the rest of the radio front-end is ideal to ensure that the PA's nonlinearities are the unique nonideality taking into account, since the nonlinear distortion is mainly caused by the PA in the transmitting part [78]. A nonlinearity digital canceller is employed after the analog-to-digital conversion at the receiving part for the cancellation of both SI and PA nonlinearties. The idea for this canceller is to regenerate an estimated SI signal. This estimator is based on the Least Square (LS) algorithm, the signal $\hat{x}_n$ after the cancellation is given as

$$\hat{x}_n = x_n^{a^*} - \hat{s}_n^{si^*} \tag{5.25}$$

where $x_n^{a^*}$ is the digital signal after passing the radio front-end and $\hat{s}_n^{si^*}$ is the estimated SI based on the LS algorithm.

$$\begin{aligned}\hat{s}_n^{si^*} &= \sum_{k=0}^{K} h_n \cdot \hat{p}_k \cdot i_{2k+1}(s_n^a) \\ &= \sum_{k=0}^{K} \hat{w}_k \cdot i_{2k+1}(s_n^a)\end{aligned} \tag{5.26}$$

The estimator aims to calculate the weights $\hat{w}_k$ which minimize the power of signal after SIC, $\hat{x}_n$, which guarantees the recovery of the signal of interest. $\hat{w}_k$ is assumed as the complex-valued coefficient of both the SI channel and the PA polynomial model and is given as

$$\hat{\mathbf{w}}_\mathbf{k} \overset{\text{def}}{=} [\hat{w}_1 \quad \hat{w}_3 \cdots \hat{w}_{2K+1}]^\mathbf{T} \tag{5.27}$$

The received signal matrix $\mathbf{x}^{\mathbf{a}^*}$ with N samples of estimation is presented as

$$\mathbf{x}^{\mathbf{a}^*} \overset{\text{def}}{=} \left[x_n^{a^*} \quad x_{n+1}^{a^*} \cdots x_{n+N-1}^{a^*} \right]^\mathbf{T} \tag{5.28}$$

The input matrix $\mathbf{i}$ is given as

$$\mathbf{i} \overset{\text{def}}{=} \left[\begin{array}{cccc} \mathbf{i}_1 & \mathbf{i}_3 & \cdots & \mathbf{i}_{2K+1} \end{array} \right] \tag{5.29}$$

$$\mathbf{i}_{2k+1} = \left[\begin{array}{l} i_{2k+1}(s_n^a) \\ i_{2k+1}(s_{n+1}^a) \\ \vdots \\ i_{2k+1}(s_{n+N-1}^a) \end{array} \right] = \left[\begin{array}{l} s_n^a \cdot |s_n^a|^{2k} \\ s_{n+1}^a \cdot |s_{n+1}^a|^{2k} \\ \vdots \\ s_{n+N-1}^a \cdot |s_{n+N-1}^a|^{2k} \end{array} \right]$$

Then, we can obtain:

$$\begin{aligned} \hat{\mathbf{w}}_\mathbf{k}^\mathbf{LS} &= \arg\min_{w_k} \left\| \mathbf{x}^{\mathbf{a}^*} - \hat{\mathbf{s}}^{\mathbf{si}^*} \right\|^2 \\ &= \arg\min_{w_k} \left\| \mathbf{x}^{\mathbf{a}^*} - \hat{\mathbf{w}}_\mathbf{k} \cdot \mathbf{i} \right\|^2 \end{aligned} \tag{5.30}$$

$$\hat{\mathbf{w}}_\mathbf{k}^\mathbf{LS} = \left(\mathbf{i}^H \cdot \mathbf{i} \right)^{-1} \cdot \mathbf{i}^H \cdot \mathbf{x}^{\mathbf{a}^*} \tag{5.31}$$

where the operator $[\cdot]^H$ represents the Hermitian transpose.

After the digital cancellation, the signal $\hat{x}(n)$ is going to be detected based on the CSI as prensented in Section 3.2.3. The transmitting antenna index and modulated QPSK symbols are then demodulated. The bit sequence information contained by the QPSK symbols together with the one corresponding with the transmitting antenna index are concatenated to recover the input bitstream.

5.4.4 System performance results

The system performance is evaluated in two steps: one is the BER performance with different INRs, and then we analyze its performance within the linear/nonlinear zone of the PA in terms of Eb/No. The main simulation parameters and the PA characteristics are shown in Table 5.4. As seen in Figure 5.15, the simulated PA works at linear zone or

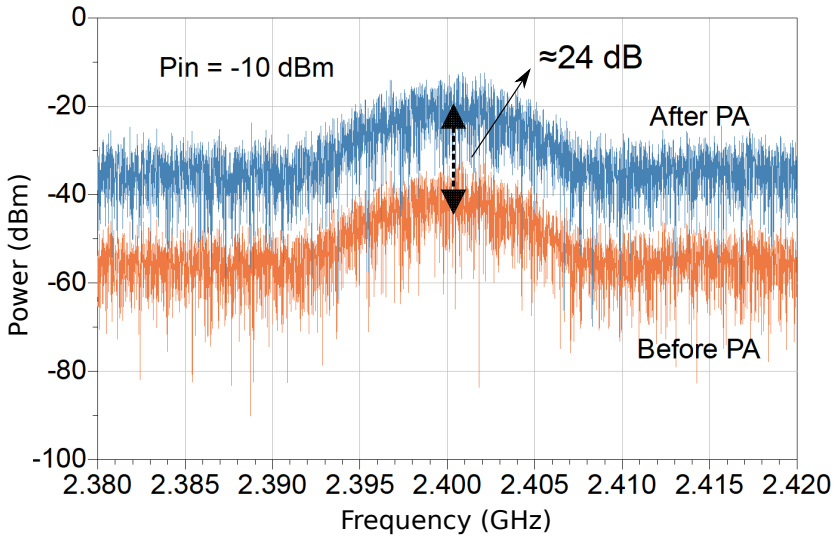

(a) P_{in} = -10 dBm

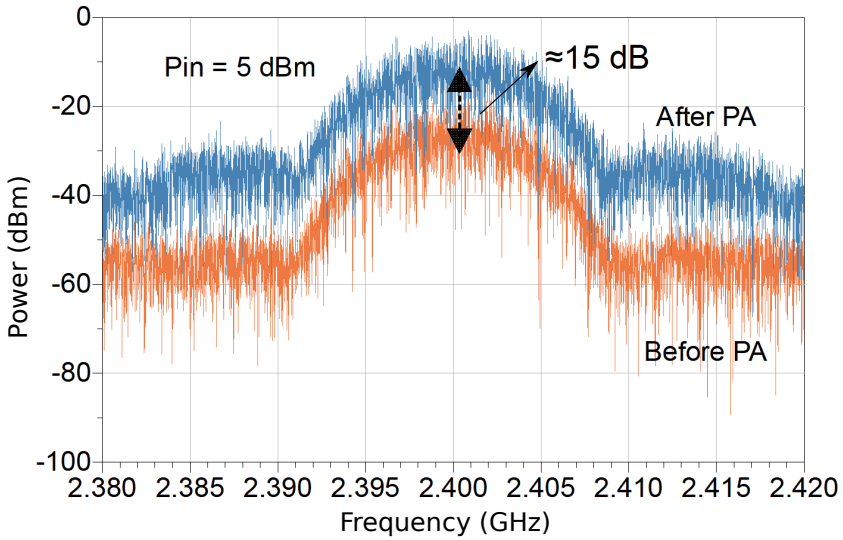

(b) P_{in} = 5 dBm

Figure 5.16: Signal power before and after PA with P_{in} = -10 dBm and 5 dBm

nonlinear zone depending on the input signal power. Therefore, we apply -10 dBm and 5 dBm as the PA's input signal power in order to tackle the linear zone and the nonlinear zone, respectively. The spectrum of the QPSK signals before and after PA in these two cases is shown in Figure 5.16. We remark that the PA gain is about 24 dB with P_{in} = -10 dBm in the linear zone while PA gain is about 15 dB with P_{in} = 5 dBm in the nonlinear zone. We can also observe the spectral increases that occur around the center frequency and that are typical of a nonlinear behavior.

Firstly, three main scenarios are simulated to study the system BER performance

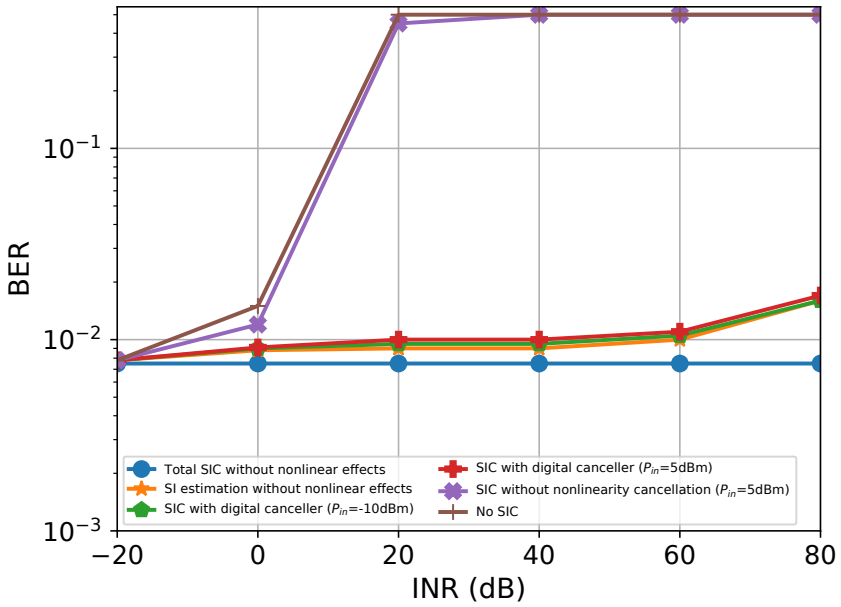

Figure 5.17: BER performance under Eb/No = 15 dB under different scenarios of nonlinearities (number of samples for SI estimation N = 10000)

Table 5.4: Simulated FDSM system parameters with a nonlinear PA

Parameter	Value
Carrier frequency	2.4 GHz
Bandwidth	20 MHz
Symbol rate	10 Mbit/s
Modulation type	QPSK
Crest factor	7.6 dB
PA gain	24 dB
P_{in}	-10 / 5 dBm
P_{out}	14 / 20 dBm
Impulse model	Root raised cosine
Filter type	Nyquist filter
Roll-off factor	0.5

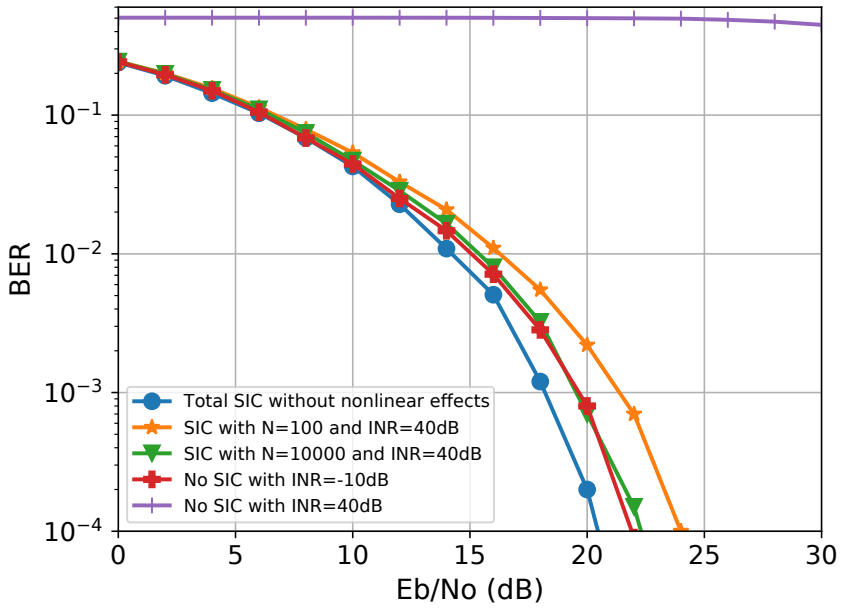

Figure 5.18: BER performance with P_{in} = -10 dBm

with the variation of INR. One is the ideal case with total SIC and without nonlinear effects (perfect knowledge of the CSI). Another is the linear case and SI is estimated. The last is that the proposed digital canceller and the simulated PA are applied. In addition, SIC without nonlinearity cancellation and no SIC as two undesirable situations are simulated to compare the performance. The scenario of total SIC can be assumed to have the same performance of a single SM system. The degradation of BER in other scenarios is due to the incomplete elimination of SI.

The BER under Eb/No = 15 dB under different scenarios is shown in Fig. 5.17. One can remark that with the proposed canceller, no matter which zone the PA is working in, the BER can be maintained at a level equivalent to the ideal one. Moreover, with the increase of INR, BER can be held at the original level and it will increase slightly when greater than 40 dB. Besides, without taking the nonlinearities into account, a noticeable degradation is observed, especially with a high INR.

The number of samples (N) for estimation can also be a main factor impacting BER. The BER performance in the linear zone (P_{in} = -10 dBm) and nonlinear zone (P_{in}= 5 dBm) with the variation of Eb/No is given in Figure 5.18 and Figure 5.19 respectively. We can conclude that increasing N will decline the BER to a certain extent but increases the estimated time. Even in the nonlinear zone, the proposed solution with N = 10000

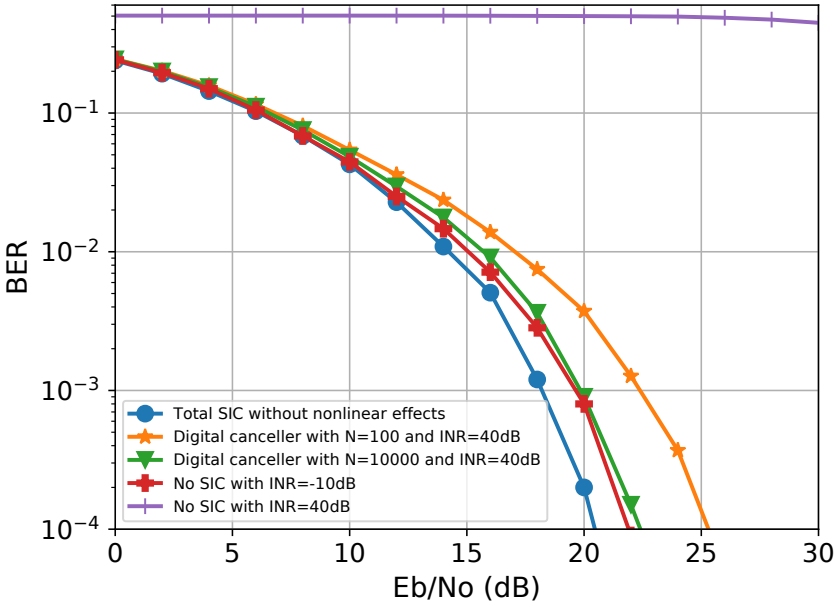

Figure 5.19: BER performance with P_{in} = 5 dBm

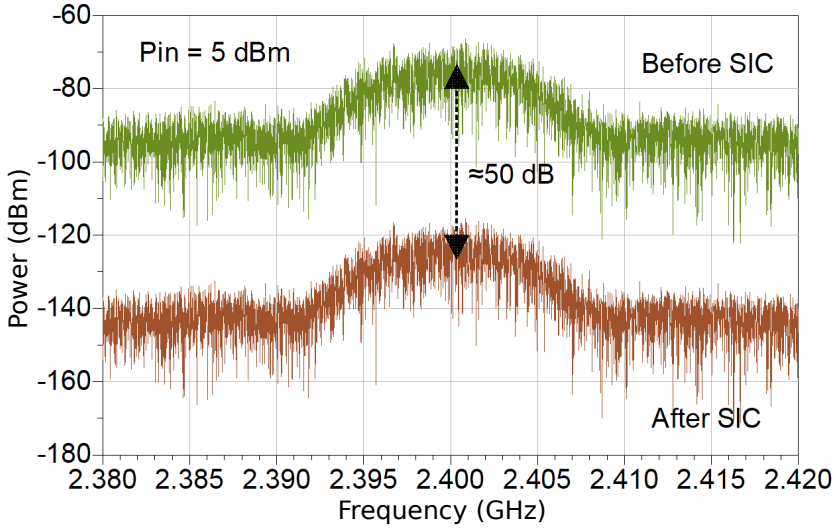

Figure 5.20: SI power before and after digital canceller with INR = 40 dB and P_{in} =5 dBm

can cancel the strong SI (INR = 40 dB) to the comparable level in the case of INR = -10 dB. That indicates SI and the PA's nonlinearity effect is generally reduced to the approximate level of the thermal noise. This conclusion can also be drawn from Figure 5.20, which indicates that the attenuation of SI power is about 50 dB with INR = 40 dB and P_{in} = 5 dBm.

5.4.5 Summary

In this section, the nonlinear effects of a low-cost PA are modeled rigorously and a digital canceller is considered to suppress the SI signal taking into account PA nonlinearities. The reliability of this canceller is demonstrated by comparing the BER performance under different scenarios. The results show that with the considered canceller, when taking into account PA's nonlinear effects and at high SI level, the system performance will only slightly degrade and at a high-accuracy detection level.

5.5 RF switch imperfections

5.5.1 Introduction

At the current state of research involving SM systems, the imperfection of the switch is mostly ignored. In fact, RF switch plays an important role in the RF front-end as a support for the antenna selection of SM systems. RF switch is known in the application of micro electromechanical systems (MEMS) to control circuit on/off conditions. However, the switching time in most MEMS is $2-50\mu s$ [108] that can not satisfy nowadays's high-speed system, which can be longer than the symbol rate of our simulated FDSM system. RF switches are moving in the direction of low switching times in order to meet the needs of today's high-speed systems, such as the three commercial RF switches mentioned in Section 5.3.4, where switching speeds can be kept below 1. To ensure system performance, the switching time must be significantly less than the symbol period. The performance of the switching time can degrade the system overall performance to different levels. Another characteristic of the RF switch is its insertion loss which expresses the attenuation of signal power inserted by the switch. The impact of RF–switch insertion loss on the performance of space modulation techniques has been analyzed in [54]. In addition, for full-duplex systems, switches that do not completely isolate the transmit signal can lead to enhanced SI at the receiving end. Therefore, the isolation degree of the switch is also an important indicator. Overall, efficiency, fast response, accuracy, and high reliability

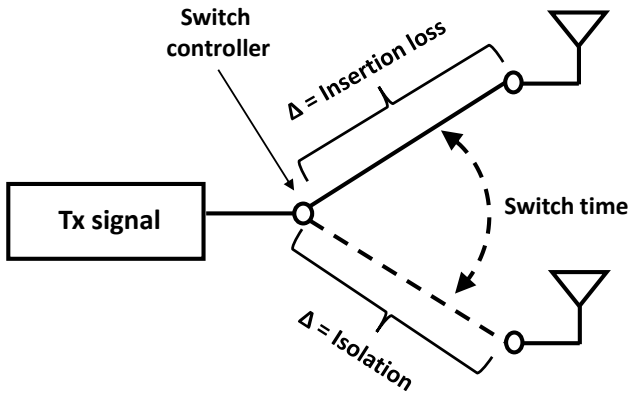

Figure 5.21: RF switch imperfections: switching time, insertion loss, isolation

are the specific requirements for switches in FDSM systems and other modern circuit systems.

In this section, the above mentioned imperfections of RF switch are analyzed. Section 5.5.2 gives the theoretical analysis of the imperfect RF switch. The system level simulation results are discussed in Section 5.5.3.

5.5.2 Imperfection analysis

The positions where the different switching non-idealities (switching time, insertion loss, isolation) occur are shown in Figure 5.21.

For a FDSM system, the RF switch is supposed to choose a transmitting antenna between the N_t antennas. Each antenna being selected can be considered as equal probability, the probability P_s that the switch remains in the original position of antenna n_k for the next symbol transmission (i.e. no switch happens) can be expressed by:

$$P_s = \Pr(n_t = n_k) = 1/N_t, \tag{5.32}$$

On the contrary, the probability P_c that the switch changes the position to transmit the next symbol can be expressed by

$$P_c = 1 - P_s = 1 - 1/N_t. \tag{5.33}$$

For the first case, the symbol transmitting time can be regarded as T_s. For the second case, an additional switch response time T_c should be considered, where the

symbol transmitting time is the sum of T_s and T_c. Therefore, the expected value of the transmitting time for each symbol T_e is given by

$$\begin{aligned} T_e =& P_s T_s + P_c (T_s + T_c) \\ =& \frac{(T_s + T_c) N_t - T_c}{N_t} \\ =& T_s + T_c - \frac{T_c}{N_t} \end{aligned} \tag{5.34}$$

Consequently, the average symbol rate is:

$$R_e = 1/T_e = \frac{N_t}{(T_s + T_c) N_t - T_c} \tag{5.35}$$

From the equation (5.34), we can remark that if the symbol rate and the switching time are fixed, the increase of the transmitting antenna N_t will extend the transmission time. In the ideal case, T_c is equal to 0, which is impossible to realize in the practical system. For the FDSM system, the switching time issue may degrade system performance due to the introduction of SI. We discuss the influence of different switching time values for the FDSM system in Section 5.5.3.

The insertion loss of the switch can be considered to have the similar properties as IQ imbalance but is usually represented as amplitude attenuation distortion, for a given RF switch, the insertion loss between the input and output is fixed.

In addition, for systems with full-duplex radio, the switches in the RF front-end module must meet a high degree of isolation. Because the antenna not selected by the switch will be used as the receiving antenna to receive the signal of interest at the far end, if the system's transceiver isolation is not solved, it may cause the receiving path to fail to operate normally when transmitting, and may cause self-excitation of the receiving path, and even cause damage to the front-end amplifier of the receiving path if it is under high-power conditions.

5.5.3 FDSM system performance results in presence of a realistic antenna switch

The performance of the FDSM system with the switch imperfection effects is analyzed at the simulated system level. The number of transmitting antenna remains at two, which can obtain the shortest average transmitting time of symbol in (5.34) with the same T_s and T_c.

5.5.3.1 With switch response time

The symbol transmission time of the system T_s is set to 3 μs. The switch response time T_c is supposed as one-tenth of T_s, which is equal to 0.3 μs. Therefore, the expected value of the transmitting time for each symbol T_e under this case is equal to 3.15 μs according to the equation (5.34). Moreover, a solution to improve the system performance in presence of the switch response time is proposed. The idea is to change the original symbol rate $1/T_s$ to $1/T_e$ in the demodulation step. The system performance is analyzed under three scenarios: (1) ideal condition with no switch response time; (2) $T_c = 0.1T_s$; (3) changed symbol rate. The BER performance under these three scenarios is shown in Figure 5.22.

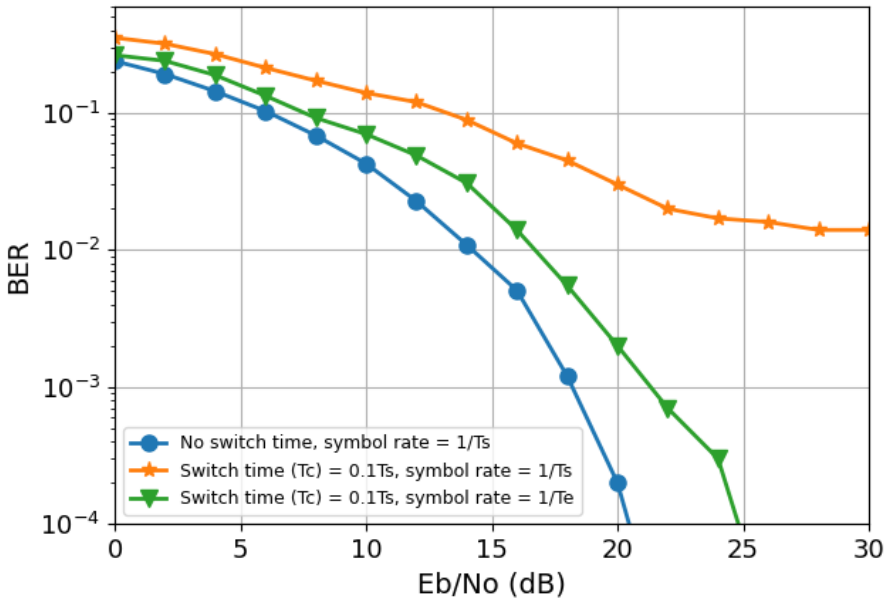

Figure 5.22: BER performance of FDSM system with switch response time

We can conclude from the figure that the BER increases as taking into account the switching time, and the proposed solution can improve the system performance with less errors.

5.5.3.2 With switch insertion loss

The BER performance of the 2×2 FDSM system in the presence of different insertion loss values is shown in Figure 5.23. The first case is the ideal one with no insertion loss, the second is with an insertion loss of 0.5 dB, the third with 1 dB and the fourth with 2

dB. Considering the insertion loss of the switches presented in Table 5.1, a low-quality switch is chosen here to better analyze its impact on the system BER performance. We can remark that the increase of the insertion loss results in the degradation of BER performance. For example, the BER performance with an insertion loss of 2 dB at $Eb/No = 20$ is approximately equal to the BER performance with an insertion loss of 1 dB at $Eb/No = 15$.

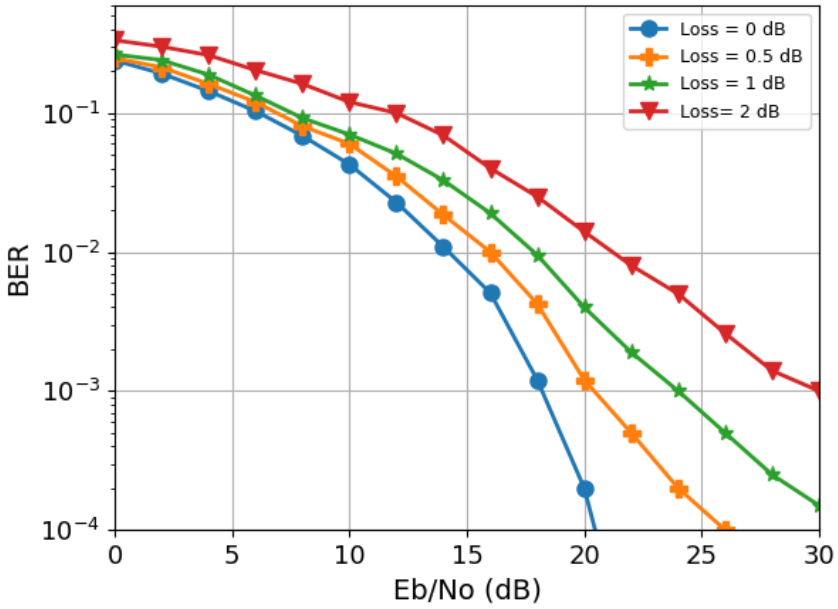

Figure 5.23: BER performance of FDSM system with switch insertion loss

5.5.3.3 With switch isolation

As given in Table 5.1 previously, the isolation of the commercial RF switches can be up to 33 dB. However, this still cannot meet the needs of FD radio, especially with a high INR. Figure 5.24 presents the simplified node A in the FDSM system with switch isolation impact. The power of the signal of interest may be lower than the remaining signal caused by the isolation, which makes the following detection difficult. The solution can be simple by taking into account the signal of isolation when performing the SI estimation and SIC.

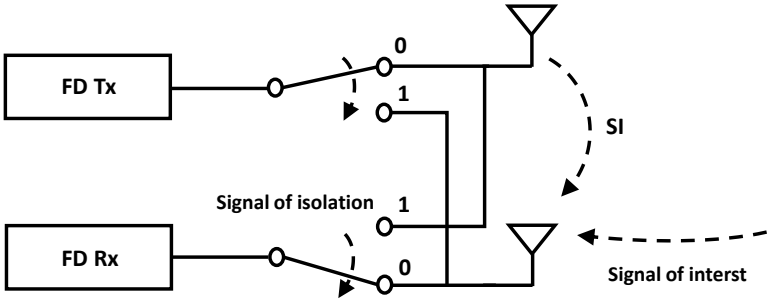

Figure 5.24: Diagram of the simplified node A in the FDSM system with switch isolation impact

5.5.4 Summary

In this section, three switch imperfection effects are considered. We introduce the switch response time, the switch insertion loss and the switch isolation impact. In particular, a solution is proposed to improve the system performance under the case of the switch response time delay, which results in the decrease of BER.

5.6 Summary

In this chapter, the performance of the FDSM system has been analyzed in presence of the IQ imbalance, of the PA's nonlinearity, of the phase noise and of the switch imperfections. We observed that the system is more sensitive to IQ imbalance under low signal-to-noise ratios. The phase noise of the instrument planned for the measurement campaigns slightly influences the system BER performance. Moreover, the nonlinear effects of a low-cost PA were modeled and a digital canceller was considered to suppress the SI signal taking into account PA nonlinearities. Lastly, the imperfection effects of the RF switch are also considered, which includes the switch response time, the switch insertion loss and the switch isolation. Moreover, a method to overcome the switching time imperfection is taken into account.

Other imperfections of the physical layer are neglected in this section, and we can compare and corroborate the results obtained in the simulations through experimental investigations.

CHAPTER 6

EXPERIMENTAL ANALYSIS OF SPATIAL MODULATION SYSTEMS

6.1 Introduction

Although the theoretical analysis and simulation study of SM is global and in-depth, the experiments on SM are very limited. The performance of the SM system by using measured realistic channels is discussed for the first time in [131]. The idea is to simulate the measured urban correlated and uncorrelated Rayleigh fading channels, then the channel measurements are used to analyse the performance of the SM system. However, the RF parts and the propagation environment are still on simulation level in this work. The following implementations [84, 113] have made up for this lack but the propagation environment is a simple LOS channel. To the best of my knowledge, there is no previous work considering a realistic indoor propagation environment for the SM system performance evaluation.

In this chapter, the performance of SM systems is investigated with an experimental testbed in the mixed LOS/NLOS environments. The proportion of LOS and NLOS components is evaluated by the Rician K-Factor. Two methods are employed to perform this study. The first one consists in combining the outputs of two SM sources which transmit the same information but with different amplitudes and phases in order to emulate the direct and complementary paths. The resulting signal is conveyed to the receiver by cable in order to have a precise tuning of the LOS/NLOS communication paths

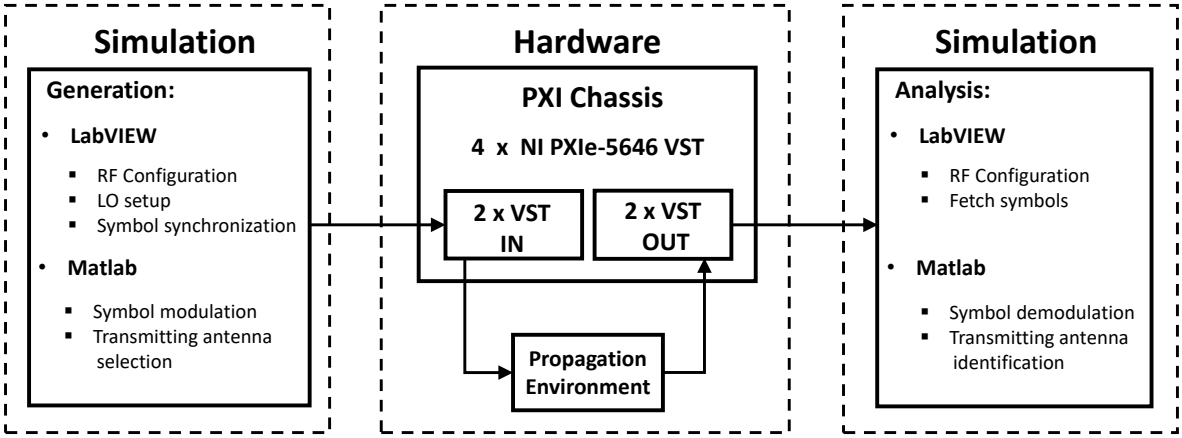

Figure 6.1: Main parts of the experimental setup

in terms of amplitude and phase. The second method consists in the implementation of an over-the-air transmission scenario in an indoor environment. In order to vary the characteristics of the propagation channel, electromagnetic absorbers are inserted between the emitting and the receiving antennas to modify the power level of the LOS signal. A channel sounding method is also applied to evaluate the characteristics of the propagation channel. The performance of the SM system in the practical implementation is compared to the simulation results.

The rest of this chapter is divided as follows: in Section 6.2, the step-by-step operations for the transmitting and receiving parts of the SM system are introduced. Section 6.3 presents the hardware setup together with the implementation of the two propagation environments. Section 6.4 gives the system performance obtained by the proposed experimental testbed in the mixed LOS/NLOS scenarios. Furthermore, the results are compared with those obtained by simulations. Finally, Section 6.5 concludes this chapter and gives some directions for the future work.

6.2 Transmitting and receiving processes of the SM system

The experiment setup can be divided into software and hardware parts, from simulation level and from physical level, respectively. The block functions and the transmission chain are given in Figure 6.1. The SM system is implemented by using four National Instruments (NI) PXIe-5646 VST modules [3] which are programmed by using NI

LabVIEW framework. The VST as a vector signal transceiver is able to transmit and to receive at the same time. Here, to realize a 2×2 SM system, two VST modules are supposed to work for the emission and the remaining two modules are employed for the reception. The four VST modules are integrated into a PXIe chassis which can guarantee the symbol synchronization by configuring the synchronization function. More details on the hardware setup will be presented in Section 6.4.

This section presents the software part of the proposed 2×2 SM system as presented in Section 3. On the generation side, the software programs aims at selecting the bits dedicated to forming digital modulation symbols and the bits dedicated to switching between the transmitting VST modules from the input bitstream. This switching between the two VST's corresponds to the antenna switching in a realistic "SM" implementation. In our case, the QPSK as a digital modulation method is employed. Then, the signal generated by the transmitting VST modules passes through the propagation channel (imposed or over-the-air). The signal received by the VST modules is processed in order to identify the transmitting antenna and to demodulate the QPSK symbols. The VST modules are driven by LabVIEW which is coupled with Mathworks Matlab software. This latter software is employed to implement the complex algorithms of the SM modulation and demodulation in Section 3.2.3.

6.2.1 Transmitting part

Figure 6.2 outlines the step-by-step configuration of the transmitting part. The input data is a random bitstream which will be processed by the SM mapping algorithm. In order to configure the parameters (carrier frequency, modulation type, power level, etc.) of the VST modules, NI-RFSG libraries provided by LabVIEW software are employed. More precisely, NI-RFSG is an instrument driver to configure and operate hardware, to program and generate signals, and to perform modulation tasks using LabVIEW VIs functions [6]. In the following, the main signal processing steps are detailed.

6.2.1.1 Configuration

Once the NI-RFSG session is opened, the carrier frequency and the output power level are configured. The carrier frequency is set up at 868 MHz (inside one of the European ISM band). The output power level can be adjusted as required in the limit range of the VST and the regulations which will be introduced in the following sections. We then configure the generation mode and the reference clock source. The RF signal generator

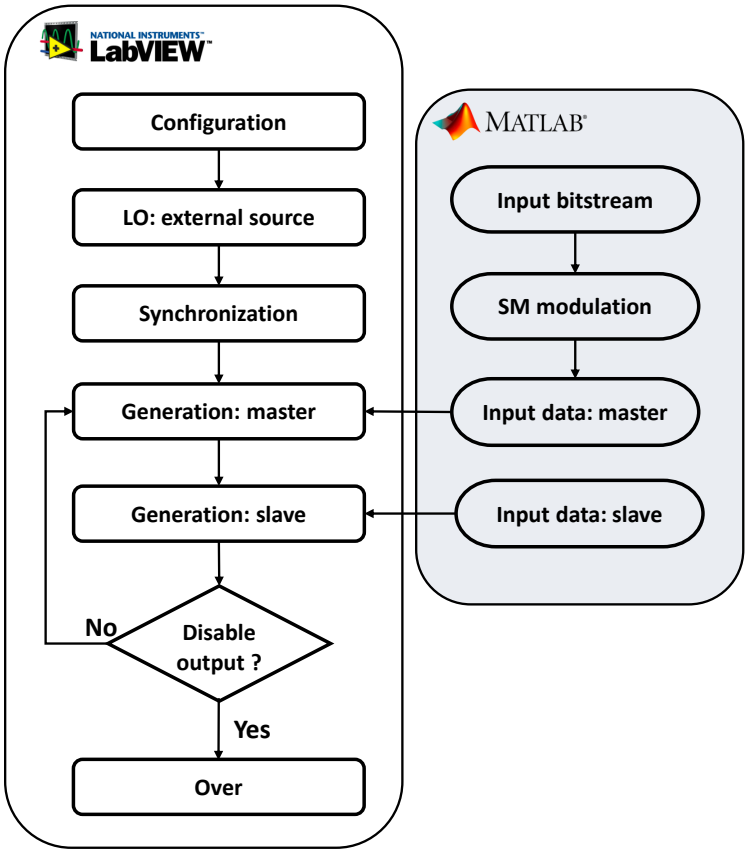

Figure 6.2: A step-by-step process of the SM transmitting part

has also been configured to be able to generate an arbitrary waveform. The reference clock source must be external to the device and we apply the sampled reference clock (SRC) for the synchronization of four VST modules.

6.2.1.2 LO: external source

For the four VST emulating a 2x2 SM transmission, the LO's are supplied by an external source (RF frequency synthesizer) coupled to a 1:4 power divider. Otherwise, another option is to setup the LO's of the four VST modules in a "daisy chain" configuration. An external LO source is applied for our SM system. Firstly, we define the VST corresponding to the antenna index 1 as master device and the VST corresponding to the antenna index 2 as slave device. Moreover, the two VST modules employed at the reception are also set up as slave device. The four VST modules are configured in order to receive the LO from an external source, at the LO input terminals. The employed external source is a

configurable frequency synthesizer. The signal provided by the frequency synthesizer is dispatched to the four VST modules through a 1:4 RF power divider. The coaxial cables are employed to connect the LO inputs of the VST modules to the outputs of the power divider. However, coaxial cables insert different phase shifts, a prior correction is performed in order to guarantee the phase coherence. In general, we always need to ensure that the up-converter center frequencies match on all devices when sharing LOs. Even if the carrier frequency is a multiple of the LO frequency step size, there may be a small amount of LO frequency offset due to the limited resolution of the phase-locked loop (PLL) fractional mode dividers. In our particular case, the VST modules are configured in order to perform a direct conversion. Consequently, both for the emission and for the reception, the intermediate frequency is equal to zero.

6.2.1.3 Synchronization

To perform SM, the symbol synchronization needs to be configured. For the implementation of the synchronization, one of the VST modules takes the role of master and dispatches the clock signal towards the remaining VST modules. The start trigger synchronization should be first configured. Among the applied four VST modules in our system, it is the master device who drives the trigger distribution line. It must be configured to be master for the synchronized sample clock, and a synchronized sample clock distribution terminal must be arranged. For the slave device, the trigger distribution terminal is given. The slave device uses the trigger distribution signal to generate the "sync-start" signal. As done for the master device, an additional step is required to ensure synchronization that a synchronized sample clock distribution terminal must be configured. Moreover, the slave device should be triggered on the rising edge of the "sync-start" signal. Noteworthy, a prior configuration of the trigger bus line need to be done by NI MAX. Basically, whichever module is providing the sample clock, look at what slot it is in, and connect the trigger buses in MAX so that triggers are routed away from that trigger bus.

6.2.1.4 SM modulation

As mentioned before, the input will be processed by the SM mapping algorithm which is given in Figure 6.3. In our case, we have two transmitting antennas ($N_t = 2$), QPSK ($M = 4$) is chosen as the modulation method. As there are four possible symbols for the QPSK modulation, each possible 3-digit ($\log_2(N_t) + \log_2(M) = 3$) binary represents one possible transmitting situation of the SM system. Moreover, P ($P = N_t M = 8$) is given to

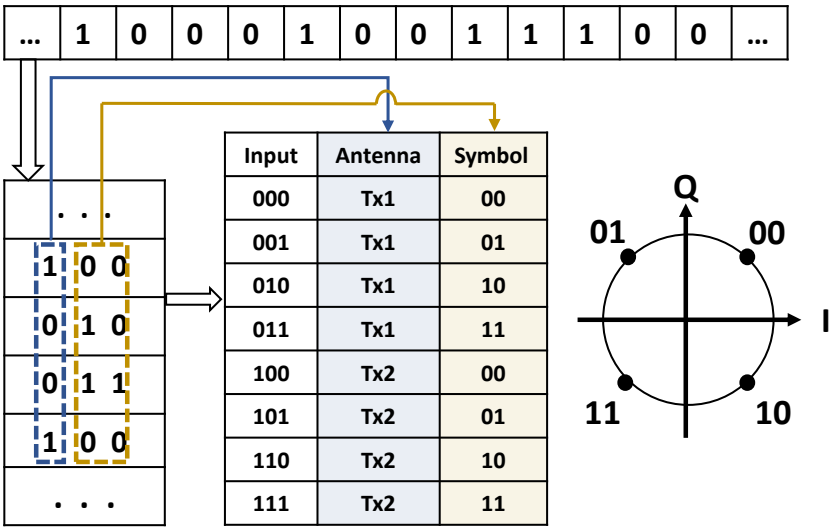

Figure 6.3: SM mapping algorithm for $N_t = 2$ and QPSK modulation

denote the number of possible configurations of the SM. As a header, additional 8 frames of data are added before the random input sequence. This header is employed in order to estimate the propagation channel characteristics (i.e. CSI), which is used at the receiver side for SM demodulation. As shown in the right part of Figure 6.2, the input signals for the two transmitting VST modules need to be prepared. According to the input bitstream, four sets of I and Q values for the master and slave devices are generated.

6.2.1.5 Generation

The two VST modules for the transmission will generate the IQ samples based on the given input, one at a time, with the carrier frequecy of 868 MHz and input power of -20 dBm. The generation is performed continuously, until it is manually stopped. Finally, the outputs of the VST modules are disabled and the NI-RFSG session is closed.

6.2.2 Receiving part

The step-by-step operations of the receiving part are shown in Figure 6.4. This part analyzes the received signal in order to recover the input bitstream. In addition, the bitstream employed at the transmitting part is compared to the one recovered at the receiving part and the BER is calculated. The configuration of the receiving end is performed by using NI-RFSA session in the LabVIEW programming environment. In general, NI-RFSA is an instrument driver to control and configure NI's vector signal

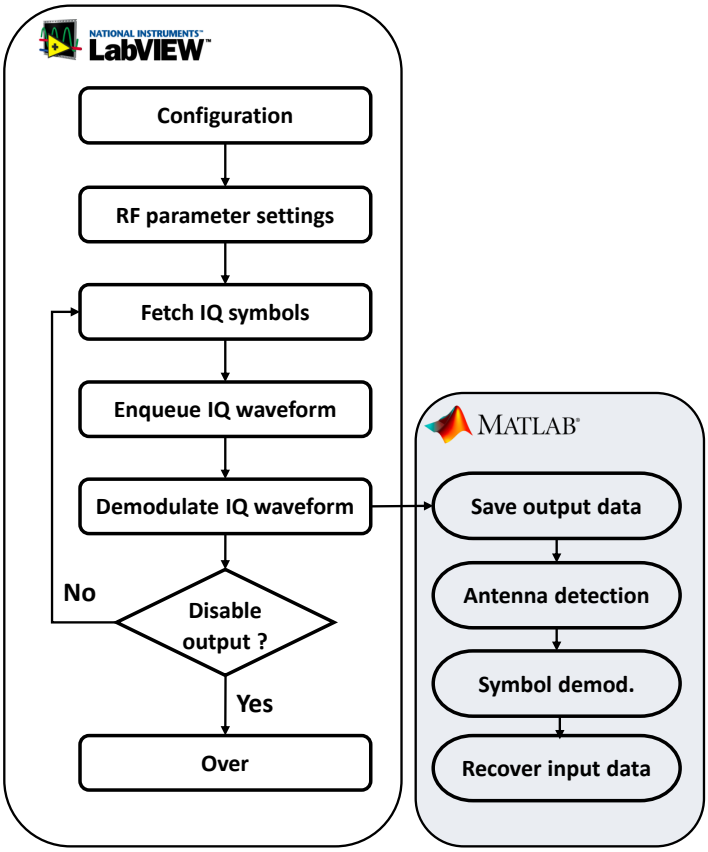

Figure 6.4: A step-by-step process of the SM reception part

analyzers (VSA) [5]. It provides a set of operations and properties which allows the creation of custom metrics or applications that require IQ data. A step-by-step process of the receiving end is described in detail thereafter.

6.2.2.1 Configuration

Once the NI-RFSA session is initialized, we configure IQ acquisition, carrier frequency, reference level and symbol rate for acquisition. The reference level represents the maximum expected power of an input RF signal.

6.2.2.2 RF parameter settings

For the following demodulation, QAM system parameters (e.g. modulation order, symbol map, etc.) are configured firstly, then we generate the matched filter coefficients for pulse-shaping and matched filters applied by the digital demodulation. The raised

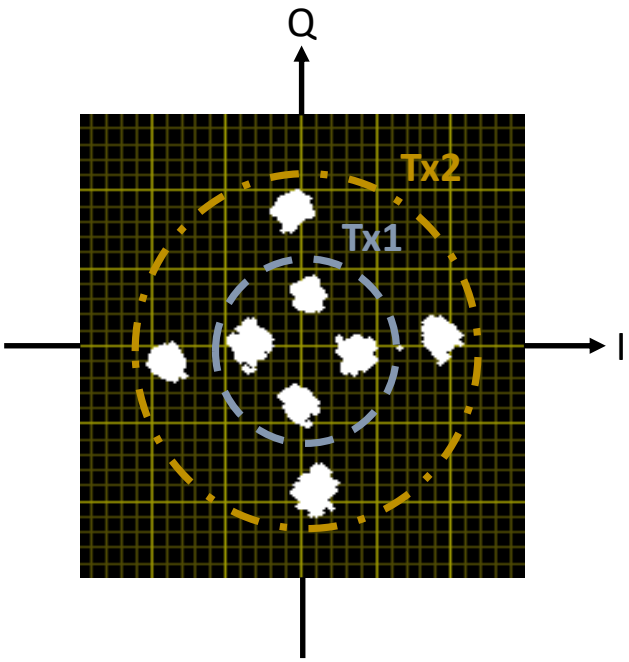

Figure 6.5: Constellation of the received SM signal

cosine filter is applied and the roll-off factor is set at 0.5. Moreover, a synchronization parameter cluster should be constructed. The generated synchronization parameter cluster guarantees that the different symbols which come from the two VST's configured in the receiving part, are received according to the same time base.

6.2.2.3 Fetch and enqueue IQ waveform

After transposing the received signals into BB, the different complex samples generated by the transmitting VST modules are fetched. The producer loop and the consumer loop are constructed. They are employed to fetch and process IQ samples. The producer/consumer model enables two processes to work at the same time, so that for the receiving end, the received signals can be demodulated continuously. We enqueue the IQ waveform acquired in the producer loop and dequeue the IQ waveform in the consumer loop. Next, the input complex-valued waveform is sampled and adjusted to the required IQ rate. Additionally, the number of samples fed into the QPSK demodulation should correspond to an integer number of symbols.

6.2.2.4 QPSK Demodulation

The demodulation is the core step in the RFSA module. Matlab software is introduced to perform the demodulation by the LS algorithm, which has already been demonstrated in Chapter 3 for the simulation implementation of the SM system. The constellation of the received symbols is shown in Figure 6.5. We suppose here Tx1 and Tx2 as the two transmitting antennas. One can remark from the Figure 6.5 that the two QPSK constellations of the signal transmitted by Tx1 and Tx2 are different in terms of amplitude, and a slight rotation between the two constellations is also visible, since the transmission channels between the two transmitting antennas and the receiving ones are quite different.

IQ data waveform for the constellation at the receiving end is shown in Figure 6.6. The scale-like part represents the demodulation result of the P frames of the header. Because the demodulation process is a continuous loop, the header part just follows the previous set of random signals in Figure 6.6. The basis of SM demodulation is to estimate the CSI of the different channels, and then the symbols and the transmitting antenna index can be detected according to the estimated CSI.

As mentioned previously, P frames of data as a header of the transmitted bitstream is prepared for the CSI estimation. The principle of the CSI estimation is based on LS algorithm. Every M frames of the incoming header can get Nr channel states, the total P frames allow us to obtain the channel matrix $\mathbf{H}$, where $\mathbf{H} \in \mathbb{C}^{N_r \times N_t}$. The propagation channel is supposed as an indoor one which is modeled as a Rician fading channel. Here, N_r is the number of the receiving antennas. The Rician fading channel model $\mathbf{H}$ takes into account the presence of the LOS path and the scattered NLOS paths, the proportion of LOS and NLOS paths are evaluated by the Rician K-factor. Additionally, we can increase the accuracy of the estimation by increasing the length of the header, we suppose that the number of symbols for each frame is N_f.

The structure of the header $\mathbf{S}^*$ is given by the following equation:

$$\mathbf{S}^* = \left[\underbrace{s_1 \cdots s_1}_{N_f} \quad \underbrace{s_2 \cdots s_2}_{N_f} \quad \cdots \quad \underbrace{s_P \cdots s_P}_{N_f} \right] \tag{6.1}$$

Therefore, the composition of each frame $\mathbf{S}_p^*$ can be presented as equation (3):

$$\mathbf{S}_p^* = \left[s_p^1, s_p^2, \cdots, s_p^{N_f} \right] \tag{6.2}$$

where $s_p^{n_f}$ denotes one of the P possible symbols transmitted by N_t antennas of the SM modulation. $\hat{\mathbf{w}}$ is assumed as the calculated complex-valued coefficient matrix, which denotes the relation between input signals in the header and the received signal at the

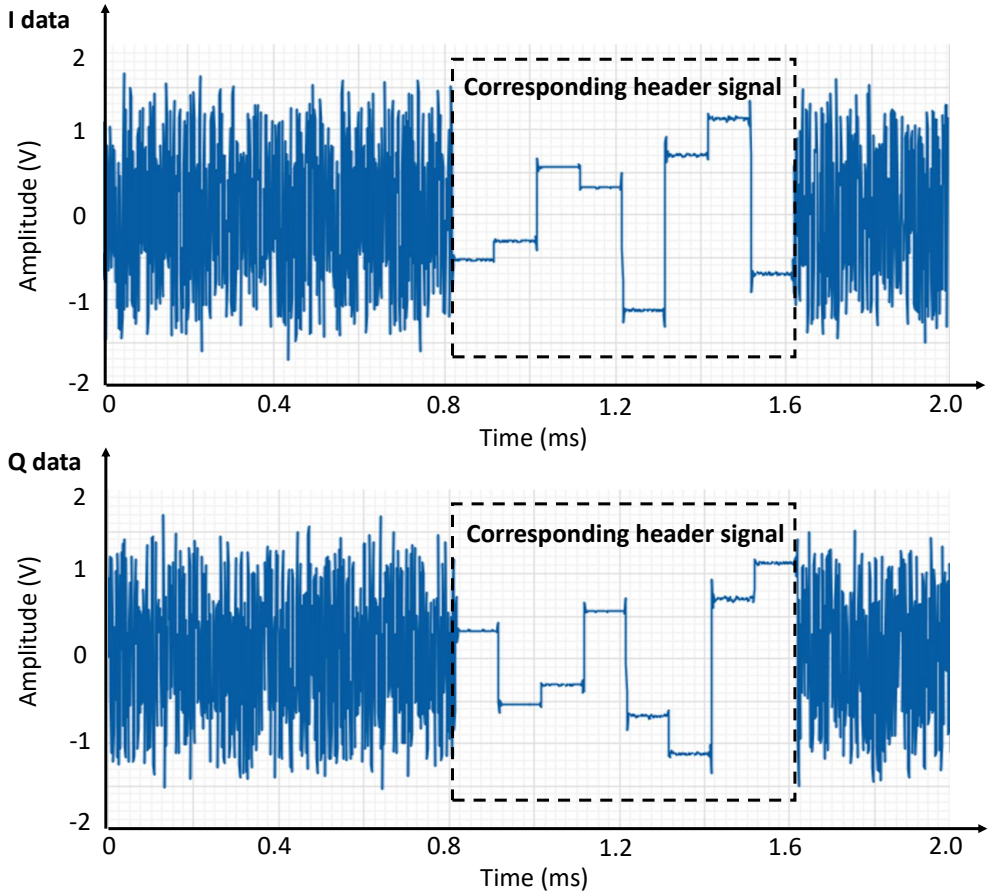

Figure 6.6: The constellation data of the I and Q branches at the receiving end

receiving part.

$$\hat{\mathbf{w}} \overset{\text{def}}{=} [\hat{w}_1 \quad \hat{w}_2 \cdots \hat{w}_P] \tag{6.3}$$

The received signal matrix $\mathbf{y}^*$ for this frame is presented as:

$$\mathbf{y}^* \overset{\text{def}}{=} \begin{bmatrix} \mathbf{y}_1 & \mathbf{y}_2 & \cdots & \mathbf{y}_P \end{bmatrix} \tag{6.4}$$

$$\mathbf{y}_p^* = \left[y_p^1, y_p^2, \cdots, y_p^{N_f} \right]$$

Then, we can obtain the component $\hat{w}_p$ in $\hat{\mathbf{w}}$ according to the LS algorithm:

$$\hat{w}_p^{LS} = \arg\min_{w} \left\| \mathbf{y}_p - \hat{w}_p \cdot \mathbf{S}_p^* \right\|^2 \tag{6.5}$$

$$\hat{w}_p^{LS} = \left(\mathbf{S}_p^{*H} \cdot \mathbf{S}_p^* \right)^{-1} \cdot \mathbf{S}_p^{*H} \cdot \mathbf{y}_p^* \tag{6.6}$$

where the operator $[\cdot]^H$ represents the Hermitian transpose. Once we estimated the CSI, more precisely, the amplitude and phase deformation for the P possible symbols

transmitted by N_t antennas, the necessary information for the detection is ready. For each input signal, a correction of the channel model is performed by using the obtained P components $\hat{w}_p^{LS}$ in the coefficient matrix $\hat{\mathbf{w}}$ to recover the input signal. In our case, we detect the transmitting antenna index firstly according to the difference in amplitude and phase caused by different paths. Once the transmitting antenna is demodulated, the signal will be corrected by applying the estimated CSI. The value of the corrected demodulated signal will be compared to the four possible QPSK symbols to find the minimum difference between the received value and the ideal symbol value. In other words, the most likely QPSK symbol is the one that gives the smallest difference between the received symbol and one of the four ideal QPSK symbols. Finally, the binary values that represent the demodulated QPSK symbols will be concatenated with the binary values that represent the transmitting antenna index to recover input data. Lastly, the VST's inputs are disabled and the NI-RFSA session is closed.

6.3 Hardware setup and propagation environment

6.3.1 Hardware setup

In general, NI PXI platform is designed for measurement and automation applications. It supports high-performance, modular instruments and I/O modules that enable specialized synchronization and critical software functions for test and measurement applications, from hardware validation to production self-testing. As shown in Figure 6.1, the PXI chassis as the hardware assumes the role of transmitting the modulated signals and receiving the signals that have passed through the propagation environment. For our experiments, the NI-PXIe-1085 chassis is equipped with four VST modules of the type PXIe-5646R. Figure 6.7 shows a picture of the PXIe-5646R modules fitting into the NI-PXIe-1085 chassis for the application of our SM system.

The PXIe-1085 Chassis has 16 hybrid slots and incorporates all the features of the PXI specifications, including support for PXI modules with a built-in 10 MHz reference clock, a PXI trigger bus, and a PXI star trigger. Each slot equipped with a VST module in the chassis has the capability of both transmitting and receiving signals by configuring the inputs and the outputs.

A NI PXIe-5646R RF VST module combines the typical RF I/O functions of a vector signal analyzer (VSA) and a vector signal generator (VSG) with NI or user-defined functions. The PXIe-5646R has the particularity of sharing the internal LO between

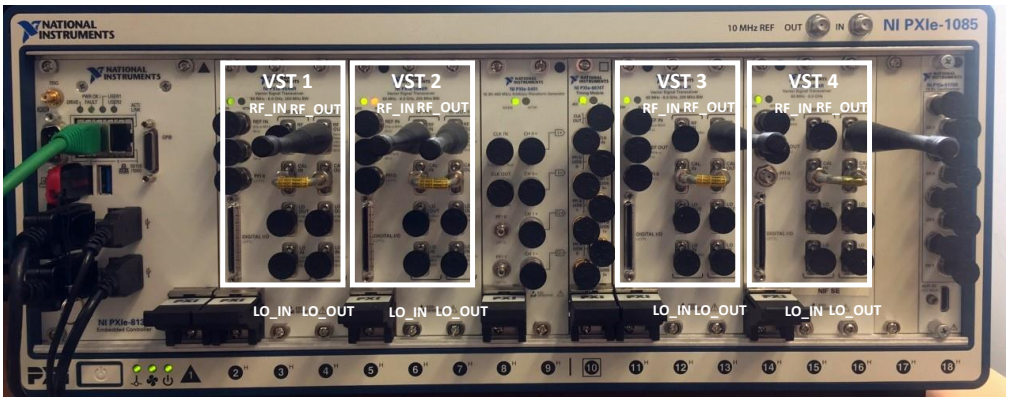

Figure 6.7: NI PXIe-1085 chassis containing four PXIe-5646R VST modules

the emitting and the receiving parts. The RF input and RF output of the PXIe-5646R can operate in a frequency range from 65 MHz to 6 GHz, and have an instantaneous bandwidth of up to 200 MHz. Table 6.1 gives the main parameters of NI PXIe-5646R VST.

Table 6.1: Main Parameters of NI PXIe-5646R VST

Frequency Range	65 MHz to 6 GHz
Bandwidth	200 MHz
Phase Noise (20 kHz offset) < 3 GHz	-99 dBc/Hz
Absolute Amplitude Accuracy (375 MHz to 2 GHz), 15 °C to 35 °C	± 0.35 dB to ± 0.65 dB
Noise Floor Density	-161 dBm/Hz
Maximum Output Power (CW)	+10 dBm
Minimum Output Power	-168 dBm
Modulation Capabilities	Vector Modulation

6.3.2 Propagation environment

For the practical implementation of the SM system, the indoor environment is considered. Besides the LOS component, there are usually NLOS components which may be caused by the complex propagation environment, for example, the reflection of the emitted signal by the objects between or around the transmitting antennas and the receiving ones. The relation between the output $\mathbf{y}$ and the input $\mathbf{x}$ can be written as follows:

$$\mathbf{y} = \mathbf{H} \cdot \mathbf{x} + \boldsymbol{\eta} \tag{6.7}$$

$$\mathbf{H} = \begin{bmatrix} h_{1,1} & \cdots & h_{1,N_t} \\ \vdots & \ddots & \vdots \\ h_{N_r,1} & \cdots & h_{N_r,N_t} \end{bmatrix} \tag{6.8}$$

where the channel matrix $\mathbf{H} \in \mathbb{C}^{N_t \times N_r}$. In our case, $N_t = N_r = 2$. Moreover, an AWGN term η, is considered. The received RF signal $\mathrm{y}_{p,q}(t)$ from Tx antenna element p to Rx antenna element q in this case can be written as:

$$\mathrm{y}_{p,q}(t) = h_{p,q} \cdot x_{p,q}(t) + \eta \tag{6.9}$$

The transmitted signal $x_{p,q}(t)$ is assumed to be the modulated QPSK signal within a symbol duration T_{sym}, then it may take the form:

$$x_{p,q}(t) = \cos(2\pi f_c t + \theta_n), 0 \le t \le T_{sym}, n = 1,2,3,4 \tag{6.10}$$

where the signal phase is given by

$$\theta_n = (2n-1)\frac{\pi}{4} \tag{6.11}$$

Therefore, the received signal $\mathrm{y}_{p,q}(t)$ can be presented:

$$\begin{aligned} \mathrm{y}_{p,q}(t) =& D_{LOS} \cdot \cos(2\pi f_c t + \theta_n) + \\ & \sum_{i=1}^{L} a_i \cos\left(2\pi f_c t + \theta_n + \varphi_i\right) + \eta \end{aligned} \tag{6.12}$$

where D_{LOS} is the amplitude of the direct (LOS) component, f_c represents the carrier frequency and L is the number of NLOS paths. The random variable corresponding to the amplitude of the i^{th} NLOS path signal is denoted by a_i. The inserted phase shift is also considered as a random variable, denoted φ_i.

With the considered propagation environment, two methods have been proposed to generate the scenarios and calculate the Rician K-factor. The first method consists in generating the defined LOS/NLOS scenarios in a controlled environment (by cable). Hence, the precise variation of the LOS and the NLOS power levels is available. The drawback is that only one NLOS path has been implemented. The other strategy is to configure a realistic, over-the-air indoor environment and to measure the channel coefficients by the channel sounding. Thereafter, the two methods are presented in details.

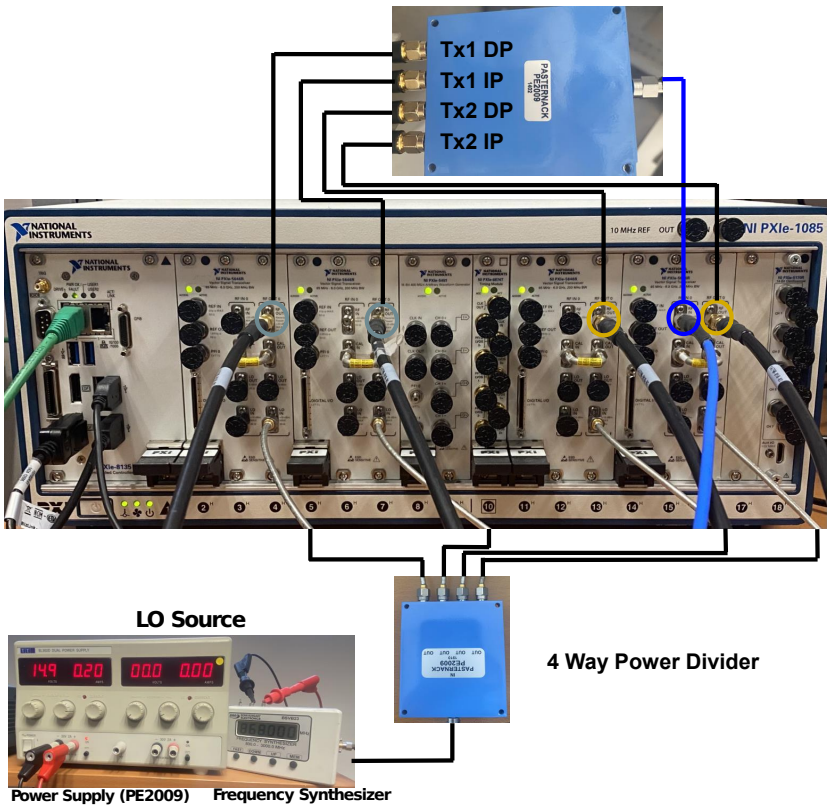

Figure 6.8: Experimental setup of the SM system with controlled propagation environment. In this case, $N_t = 2$ and $N_r = 1$, one LOS path and one NLOS path are configured for each transmission channel

6.3.2.1 SM transmission under a controlled propagation environment

In order to simulate the mixed LOS and NLOS scenarios, it is supposed that there is one direct path and one indirect path, respectively, for each $h_{n_r n_t}$ in the channel matrix $\mathbf{H}$, equation (6.8). In this case, L is equal to 1 in equation (6.12). By definition, we have a Rician K-factor of this multipath:

$$K \overset{\text{def}}{=} |D_{LOS}|^2 / 2|a_1|^2 \tag{6.13}$$

The experimental scenario of the SM system with one LOS path, one NLOS path and two transmitting antennas ($N_t = 2$) is presented in Figure 6.8. Here, the two LOS paths and the two NLOS paths are emulated by the four VST modules configured as transmitters. The outputs of these four VST modules are gathered by a four-way directional coupler. The resulting signal is transmitted to one of the VST modules which is also configured as the receiver. Four coaxial cables having the same electrical length at 868 MHz have been used between the four VST modules and the divider. Few differences may occur since the

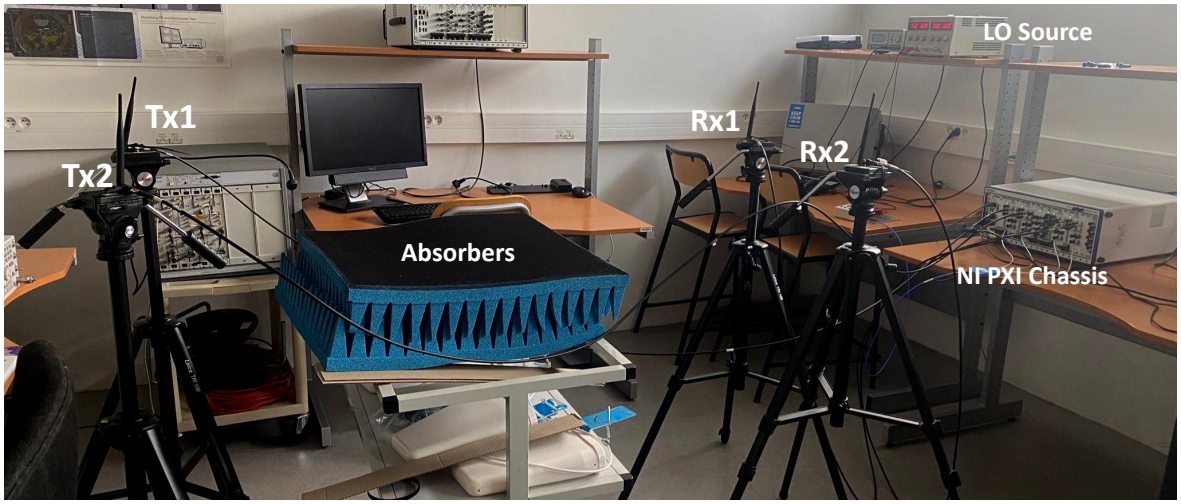

Figure 6.9: Experimental setup of a 2×2 SM system with a realistic propagation environment

phase coherence is not completely respected and, moreover, there are variations in terms of attenuation. Hence, the amplitude and phase errors inserted by the experimental setup are measured and corrected beforehand.

Through this method, we can accurately define the power level of LOS and NLOS components. However, the limitation of this method is obviously that there is only one secondary path.

6.3.2.2 Over-the-air scenario:

In this case, we are employing omnidirectional antennas to transmit and receive signals, where their electrical and radiation characteristics are similar and they are placed at the same height. The separation distance is set to one and a half wavelengths. A picture of the experimental setup implemented for the study of 2×2 SM system is presented in Figure 6.9. Due to our limited indoor area and distance between the transmitting and the receiving antennas, the LOS signal is predominant. In order to bring more complexity (i. e. decrease the K factor), electromagnetic absorbers are placed between the transmitting and the receiving antennas.

In this over-the-air scenario, the channel characteristics are not known in advance. In order to overcome this problem, a channel sounding strategy has been implemented.

The theoretical realization method of the channel sounding is described in [88]. Generally, in a time-varying multipath channel, because of its stochastic behavior, a statistical model may be established and a power delay profile may be introduced. Power

delay profile, also called multipath intensity profile, represents the average relative power as a function of the relative delay of the NLOS paths and it can be measured empirically. By calculating the channel's impulse response, it is possible to obtain the power delay profile and to extract parameters like the mean excess delay (i.e. the first moment of the power delay profile), the root mean square (RMS) delay spread (i.e. the square root of the second central moment of the power delay profile). Moreover, the number of the paths can be determined by properly choosing a power level threshold.

The temporal variation of the channel's model have a corresponding relationship on the temporal variation of the impulse response's multipath components. The channel's output $y(t)$ is found by the convolution between the channel's impulse response $h(t,\tau)$ and its input $x(t)$. Here, the single-input-single-output (SISO) case is introduced to present the channel detection method.

$$\mathrm{y(t)} = \mathrm{h(t,}\tau) * x(t) = \int_{-\infty}^{\infty} \mathrm{h(t,}\tau) x(t-\tau) d\tau \tag{6.14}$$

where $*$ denotes the convolution operator and τ corresponds to the delay. The model of a wireless channel can be represented by

$$h(\mathrm{t},\tau) = \sum_{i=1}^{L} \propto_i (t) \cdot \delta(t-\tau_i) e^{j\varphi_{i(t)}} \tag{6.15}$$

where L is the number of different propagation paths; $\propto_i$ is modeled as a random coefficient with a certain probability density function; the Dirac delta function is denoted by δ; τ_i represents the individual delay of the L multipaths.

In order to determine the channel's model, the core idea is to use the good correlation property of pseudo noise (PN) sequences [98]. Indeed, a PN sequence has been transmitted through the wireless propagation channel, and then the received response is correlated with it in order to calculate the channel coefficients. Assuming that a long-length repetitive PN sequence is transmitted, the channel response is matched and filtered at the receiver. For the impulse testing systems, it is difficult to maintain a uniform spectral density across the entire bandwidth using a single impulse. In this way, impulses with low power levels may be masked by noise, or impulses with high power levels may produce an overload of the receiver stage. Using the uniform energy spectrum over the bandwidth of the PN sequence, the impulse response of the channel can be determined.

As stated, the principle of this method is to apply a PN sequence as the input signal. The cross-correlation of the reference PN sequence and the received PN sequence is given as follows:

$$\begin{aligned} r_{qy}(\tau) &= \lim_{T\to\infty}\frac{1}{T}\int_0^T q(t)\mathrm{y}(t+\tau)dt \\ &= \lim_{T\to\infty}\frac{1}{T}\int_0^T q(t)dt\int_{-\infty}^{\infty}\beta_h(v)q(t-v+\tau)dv \end{aligned} \tag{6.16}$$

where $\beta_h(t)$ is the impulse response, $q(t)$ and $\mathrm{y}(t)$ represent the input PN sequence and output signal, respectively.

Since the output of the system $\mathrm{y}(t)$ is the convolution between the input and the impulse response, we can obtain

$$\mathrm{y}(t) = \int_{-\infty}^{\infty} h(v)q(t-v)dv \tag{6.17}$$

After changing the integration order in the equation (6.16), we have

$$\begin{aligned} r_{qy}(\tau) &= \int_{-\infty}^{\infty} h(v)dv\lim_{T\to\infty}\frac{1}{T}\int_0^T q(t)q(t-v+\tau)dt \\ &= \int_{-\infty}^{\infty} h(v)r_{qq}(t-v)dv \end{aligned} \tag{6.18}$$

The autocorrelation function of the PN sequence (r_{qq}) approximates to a Dirac delta function. Therefore, the cross-correlation can be expressed as

$$r_{qy}(t) = \mathrm{R}\int_{-\infty}^{\infty} h(v)\delta(t-v)dv = \mathrm{R}h(t) \tag{6.19}$$

where R denotes the surface of the impulse function and it is equal to the RMS value of the noise.

By calculating the correlation function of the PN sequence, the parameters of the transmission channel are estimated. In this way, by using the same setup as for the SM system, a simple wireless transmitter-receiver system has been established in order to perform the channel sounding. The PN sequence is sent by using a simple BPSK modulation. Other parameters as the input signal power and the symbol rate are given in Table 6.2. In this way, the channel coefficients can be measured. The Rician K-factor is calculated by

$$K = 10\cdot log_{10}\left(\frac{\max\left((\hat{\propto}_l)^2\right)}{\sum_{l=1}^{L}(\hat{\propto}_l)^2 - \max\left((\hat{\propto}_l)^2\right)}\right)[\mathrm{dB}] \tag{6.20}$$

Where $\hat{\propto}_1 \in \{\hat{\alpha}_1, \hat{\alpha}_2, \cdots, \hat{\alpha}_L\}$, are the amplitudes of the different multipaths.

6.4 SM system's performance evaluation

In this section, we discuss the BER performance of the mentioned SM system under the LOS/NLOS scenarios. The two propagation environment scenarios previously described

are considered. One is the controlled propagation environment and the other is the realistic channel. Due to the hardware limitation, a simple 2x2 SM scenario has been implemented. To compare with the experimental approaches, the simulator of the 2×2 SM transmission scheme presented in chapter 3 was configured with the help of the Keysight ADS and Matlab software. Similar to the experimental implementation, in the simulation setup, a time varying CSI detector is applied to estimate the simulated propagation environment, and 10^6 input binary values are transmitted in order to estimate the BER. The parameters of the experimental system are gathered in Table 6.2.

Table 6.2: Experimental parameters of 2×2 SM system

Parameter	Value
Carrier frequency	868 MHz
Tx number (N_t)	2
Rx number (N_r)	2
Modulation type	QPSK
Symbol rate	10 Mbit/s
Input signal power	-10 dBm
Total number of input binary bits (except header)	10^6
Number of symbols of frame for CSI estimation	10^3
PN sequence order for channel sounding	11
Modulation type for channel sounding	BPSK
Threshold of multipaths (in terms of peak value)	30 dB

6.4.1 Experimental evaluation of the SM transmission over a controlled propagation environment

Firstly, we implement the approach of predefining the propagation environment which is described in Section 6.3.2. For the controlled propagation environment case, we have two hypothetical transmitting antennas. Due to the hardware limitations, we can only consider one hypothetical receiving antenna at a time, so we simulate the 2×1 channel model twice with the same K value, and then combine the two received signals. More precisely, we correct the signals received by the two antennas separately with the help of the estimated CSI as explained in Section 6.2.2. Then the corrected signals are combined and normalized for detection.

The BER performance in a controlled propagation environment is shown in Figure 6.10. We extract the performance in terms of BER variation concerning E_b/N_0, which represents the energy per bit over the noise power spectral density. In addition, we

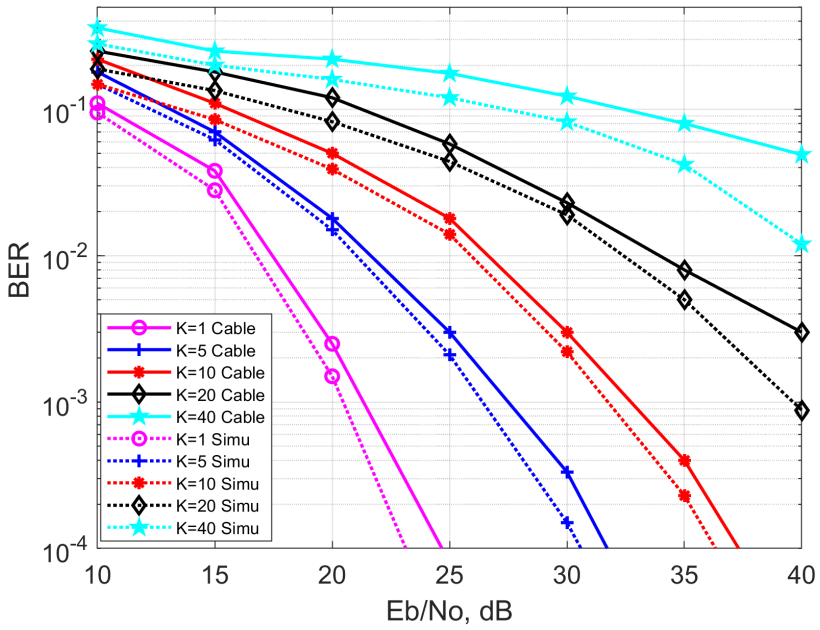

Figure 6.10: BER simulation and experimental results with controlled propagation environment of the SM system under mixed LOS/NLOS scenarios

calculate the real-time SNR by measuring the power in band of the signal and the noise separately to calculate the E_b/N_0. The BER results are given for five different values of Rician K-factor, one corresponds to a scenario nearly without NLOS paths (K= 40 dB) and the others correspond to scenarios with different proportions of NLOS paths. One can remark that the SM system with the proposed CSI estimator performs better for the smaller values of K. From the theoretical point of view, it can be explained by the fact that the difference between the $N_t \times N_r$ values in the channel matrix $\mathbf{H}$ is minimal when the K factor is significant, which makes the antenna detection more difficult.

We can also remark that the experimental results with a controlled propagation environment follow the BER performance of the simulation results. The slight degradation may be caused by the nonidealities of the hardware implementation. The RF parts of the transmitting and receiving end are considered to be ideal in the simulation. However, the nonidealities (e.g. IQ imbalance, phase noise, nonlinearity of the PA, etc.) may occur in the experimental case. The impact of the nonidealities on SM system at the simulation level is discussed in [141] and chapter 3. In addition, the noise power spectral density in the simulation was calculated for a temperature of 25°C and that in reality (experimental part) this temperature is not exactly the same.

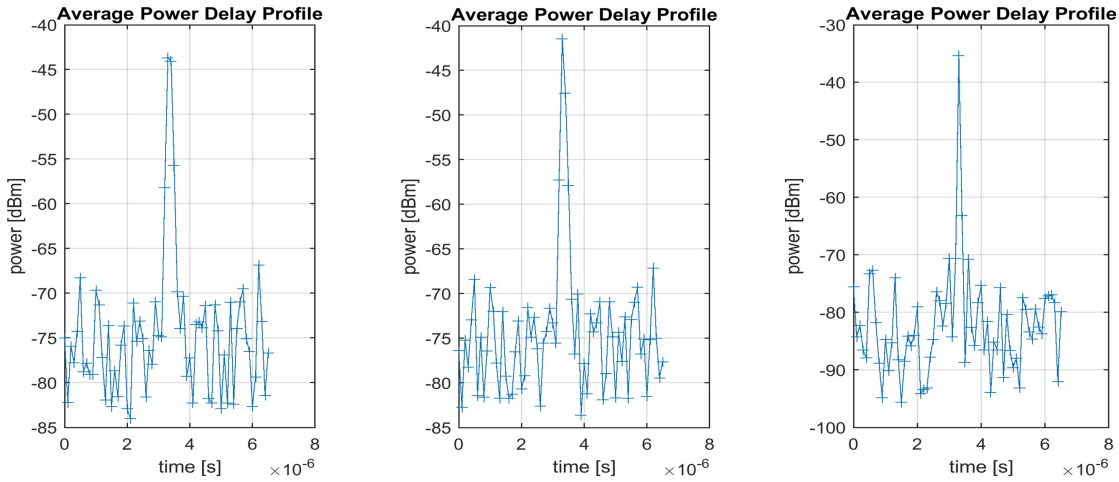

(a) $K = 5.3$ dB (b) $K = 20.1$ dB (c) $K = 39.1$ dB

Figure 6.11: Measured average power delay under $K = 5.3$ dB, 20.1 dB and 39.1 dB

6.4.2 Under realistic wireless scenario

The real propagation environment is illustrated in Figure 6.9. Three typical scenarios are introduced:

- Electromagnetic absorbers block the LOS path.
- The absorbers partially block the direct path (LOS).
- No absorber is placed between the TX and the RX antennas.

By using the method described in Section 6.3.2, the characteristics of the propagation environment have been measured. Three representative values of the Rician K-factor are obtained by the channel sounding under these three mixed LOS/NLOS scenarios: K = 5.3 dB, 20.1 dB, and 39.1 dB. The measurements reveal that when there are no electromagnetic absorbers and the distance between the transmitting and receiving antennas is within 3 meters, the K factor can reach nearly 40 dB. This result indicates that the propagation environment is basely a LOS one. In these three scenarios, the measured average power delays are given in Figure 6.11.

Experimentally, the BER performance under these three mixed LOS/NLOS scenarios is evaluated. The experimental results confronted with the simulation ones are given in Figure 6.12. In the simulation framework, the three Rician K-factor values measured previously are configured. For the three scenarios, a small variation between the simulated and the experimental BER results can be remarked. This variation may come from

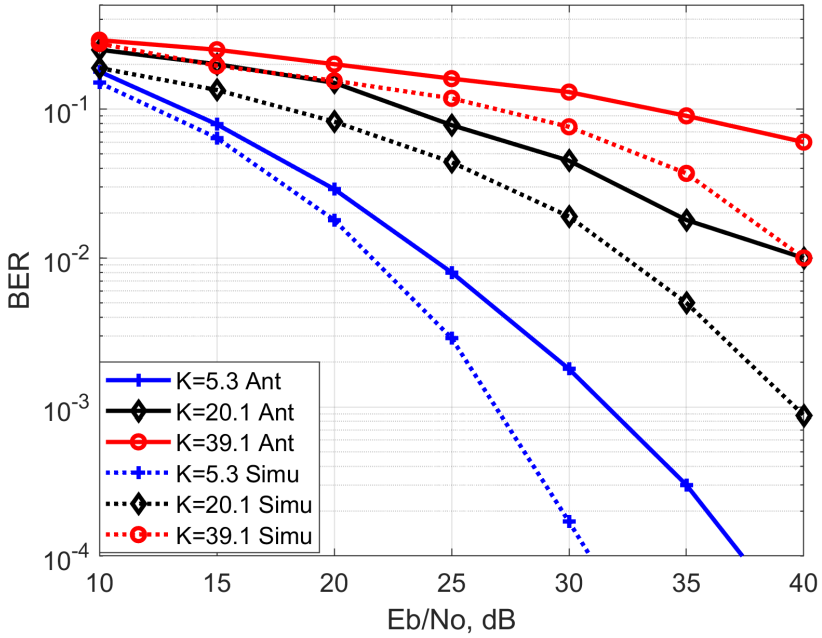

Figure 6.12: BER simulation and experimental results with real propagation environment of the SM system with $N_t = 2$ under three mixed LOS/NLOS scenarios

the nonidealities of the RF part and/or from the accuracy of estimation on the wireless propagation channel model. This variation is more evident when Eb/N0 has a strong value which may be caused by the accuracy on the BER calculations. Moreover, a better performance in terms of BER may be highlighted when a high diversity propagation channel is employed. Indeed, for a given target of BER, it requires a smaller E_b/N_0 for the smaller K value than the higher K value. Generally, we can conclude that the considered 2×2 SM system can maintain the performance in a real propagation environment, especially in presence of multipath and NLOS conditions.

6.5 Summary

In this chapter, the performance of a SM system has been analyzed, for the first time, under mixed LOS/NLOS conditions with the help of an experimental framework based on NI VST modules. The software framework for the generation and the analysis of the SM signals has been presented. Moreover, an extensive analysis of the experimental setup was presented and two models of the propagation environments (controlled one and wireless one) were proposed. The case of the controlled propagation environment has the advantage of being configurable, but the multipath model is too simple. Meanwhile,

the latter tackled scenario introduces a real indoor channel environment. Since the characteristics of the real wireless channel are unknown, a channel sounding method by using the good correlation property of PN sequences has been employed in order to extract the channel coefficients. As a result, the BER performance of practical implementation for the two proposed propagation environments were analyzed and both followed well the simulation results. Specifically, the performance in terms of BER could be better in presence of multipath and NLOS propagation conditions.

CHAPTER 7

CONCLUSION AND FUTURE OUTLOOK

The final chapter summarizes the most significant results and contributions, and also suggests possible future research directions following this thesis work.

7.1 Conclusion

We can conclude this thesis by two main contributions: the research of the SM system and the research of the FDSM system.

For the SM part, the simulation framework and the practical experimentation of SM system are studied in **Chapter 3** and **Chapter 6**, respectively. **Chapter 3** discusses a SM system over a time-varying Rician fading channel. In particular, a LS-based time-varying CSI detector for channel estimation is designed instead of assuming a perfect CSI at the receiver. In addition, the antenna index and symbol are detected separately by using a low-complexity ML detection method, where the detection of antenna index is simplified as the optimization of amplitude, and the detection of symbol is simplified as the optimization of phase. The performance of the proposed SM system over a time-varying Rician fading channel is analyzed at the simulation level by the help of Keysight ADS and Matlab softwares. The co-simulation results demonstrate that the BER can be maintained at an acceptable level using the proposed CSI detector and the system has better performance with a small Rician factor, which indicates that we can detect the transmitting antenna better in presence of more multipaths.

Chapter 6 analyzes the performance of the SM system under LOS/NLOS conditions

with the help of an experimental framework based on the NI PXI chassis hardware and VST (vector signal transceivers) modules. The experimental setup is extensively analyzed and two strategies are considered in order to configure the propagation channels. The first strategy consists in constructing a controlled propagation environment. The second approach is to transmit over the air on a realistic propagation channel. In addition, a channel detection method using the good correlation property of PN sequences is applied in order to extract the channel coefficients. As a result, the BER performance of the experimental implementation in both propagation environments is analyzed, both follow well the simulation results with a slight degradation.

The contribution related to the FDSM system is discussed in **Chapter 4** and **Chapter 5**. In **Chapter 4**, a simulated framework of a 2×2 FDSM system is demonstrated. We presented in details the different modules (antenna selection, modulation and demodulation module, channel correction module, SI estimation, SIC module, etc.) to complete this simulation framework. In particular, the algorithm of the demodulation step is described in details. To analyze the performance of the proposed FDSM system, the impact of SIC accuracy on the BER performance for different INRs is highlighted. We can conclude that an acceptable BER performance requires keeping the SI estimation error within a small range. The FDSM system performs worse than the FD system when there are no errors or when there are slight errors. However, the lower sensitivity allows the FDSM system to maintain BER performance close to that of the FD system, even better than the FD system in the presence of large errors. In addition, we analyze the relationship between the BER performance and the number of symbols for detection, where INR is introduced as the ratio of self-interference signal to noise. One can remark that the number of symbols for detection has less impact on the performance when the INR is large.

In **Chapter 5**, the performance of the FDSM system with receiver nonidealities, nonlinear PA and switching imperfections is analyzed. As for the receiver nonidealities, IQ imbalance and phase noise as two main issues are highlighted. We observe that the system is more sensitive to IQ imbalance in the case of low SNR. Numerical results show that the proposed estimator can achieve an acceptable BER in presence of IQ imbalance which is in agreement with the theory. Meanwhile, the phase noise of NI PXI VST slightly influences the system BER performance and can be negligibly low. In addition, the nonlinear effects of the low-cost PA is rigorously modeled and a digital canceller is considered to suppress the SI signal impacted by the PA nonlinearities. Finally, the imperfection effect of the RF switch has also been studied, which includes the switch

response time, the insertion loss and the isolation. In particular, a solution to mitigate the switching time effect has been proposed.

7.2 Future Outlook

Some perspectives for future research are given in this section. Two of these directions are based on the existing studies, which can be considered as the short-term goals:

- **Experimental implementation of FDSM system**: The experimental evaluation of the FDSM system is ongoing when this manuscript is written. The FD operation mode is introduced into the established SM platform presented in Chapter 6. The experimental setup of a 2×2 FDSM system is presented in Figure 7.1. We assume that node A has the ability to emit SM signals while receiving the signal of interest from remote node B. Therefore, for the node A's receiver, it will be impacted by the strong SI signal. To be specific, in the indoor short-range LOS communication environment, for the receiver at node A, the signal of interest power is about -54 dBm and the SI signal strength can be up to -24 dBm, which will completely cover the signal of interest. Hence, a SIC solution is envisaged where the SI signal is firstly estimated. Once the coefficients of the SI channel are estimated, suppression of the SI signal can be implemented because the input source of the SI signal is known for the receiving end. The performance of the FDSM system is still under study, and a SI attenuation of more than 40 dB is desired in order to lower the SI power level downto the noise level (-70 dBm).

- **Low-complexity detector**: In this thesis, we have mentioned several times that for demodulation, CSI, and SI detection methods. ML is employed in the SM demodulation, although we have already proposed a low-complexity ML detection method are ignored, the system complexity may not be ideal when high-order modulation is introduced. The commonly used matched filter-based detector has the lowest complexity but also the worst BER performance. In addition, there are spherical decoders to be considered, which are based on a compromise between BER performance and complexity. We can also propose detection schemes that combine matched filtering and ML as needed. For the CSI and SI detection methods, the LS-based solutions are employed, where the increase of detection samples can improve kind of the detector performance, but also brings the increase of detection

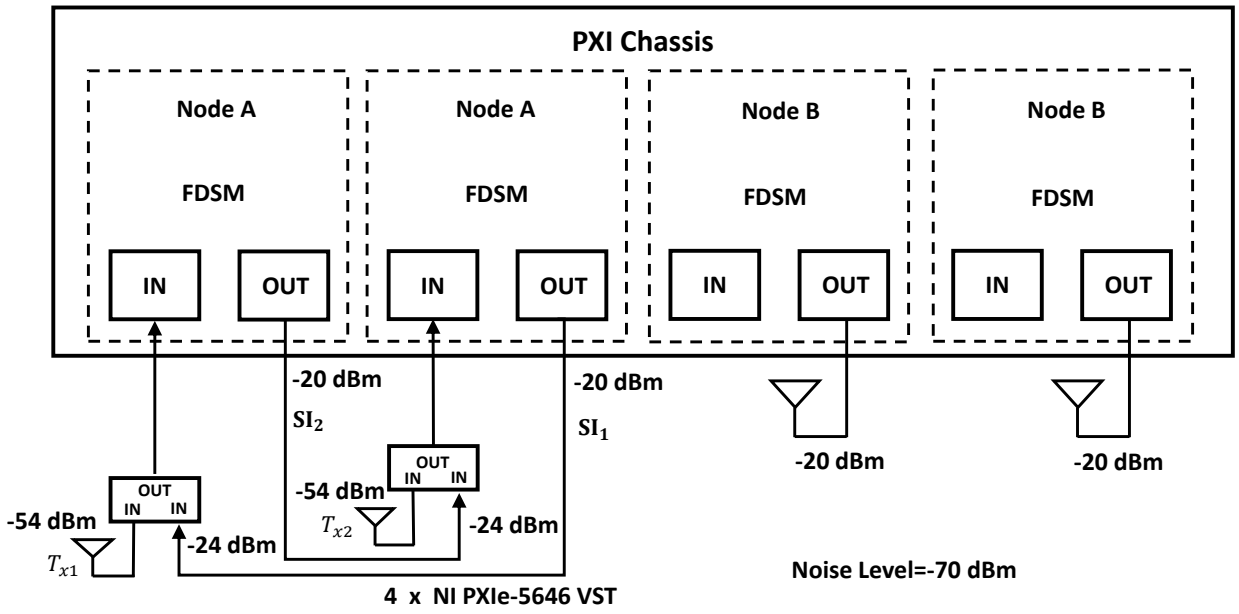

Figure 7.1: The experimental setup of a 2×2 FDSM system (For node B, only the SM part has been implemented due to limitations of hardware.)

complexity. Finding a balance between the complexity of this canceller and high reliability is a problem worthy of in-depth research.

The extension systems based on the proposed FDSM system can be potential long-term research targets, we give two possible research directions here.

- **FDSM-OFDM system**: The modulation method in this thesis is considered as a basic QPSK. If the idea of index modulation is extended from the spatial domain to the frequency domain, combining OFDM techniques with the FDSM system, the better spectral efficiency in bits/sub-carrier can be achieved. The combination with OFDM transmission is not simple given that the information is contained not only in the transmitted symbols, but also in the physical location of the antennas. That is, at each moment, for each subcarrier, only one transmitting antenna is active, while all other transmitting antennas are turned off, thus avoiding ICI at the receiving end. It should also be noted that the introduction of OFDM causes a significant increase in the complexity of the previously used ML detector.

- **Derivative techniques of SM with FD radio**: The derivative techniques of SM such as GSM, ASM, MASM and QSM have been introduced in Section 2.4.1.2. The

development of FD schemes using these modulation techniques and their performance with channel estimation errors at the receiver and in detection schemes is still an open area of research. For example, QSM is a variant of SM, where the quadrature components of the constellation symbol are separately modulated on the index of the transmit antenna, resulting in an increase in the data rate by implicitly encoding on the spatial domain. Therefore, the combination of FD and QSM will cause an increase in diversity gain and data rate in the ideal case. In summary, the combination of these techniques with FD radio can have the advantages of system capacity, BER performance or detection complexity compared with FDSM system.

- **Massive MIMO Systems with FDSM**: Large-scale MIMO systems with tens to hundreds of antennas are receiving more and more research attention, with very high spectral efficiency, high reliability, and high power efficiency. The authors in [20, 101, 105] have analyzed the application of SM and its derivative techniques for massive MIMO system, which offers the advantages of reduced RF hardware complexity, size and cost. We can suppose that the FD communication mode, once added to the researched SM massive MIMO system, will bring great application prospects because of the introduction of doubling the spectral efficiency. Of course, the significant increase in the number of antennas brings about an increase in the complexity of the transmission channel, which will significantly increase the difficulty of SIC, and this is an issue worthy of further investigation.

BIBLIOGRAPHY

[1] *BGS12SN6 Datasheet - Wideband RF SPDT Switch in ultra small package with 0.77mm2 footprint*, Infineon, (2011).

[2] *MAX2830 Datasheet - 2.4GHz to 2.5GHz 802.11g/b RF Transceiver with PA and Rx/Tx/Diversity Switch*, Maxim Integrated, (2011).

[3] *Getting started guide NI PXIe-5646R [online]*, National Instruments, (2016).

[4] *LTE; evolved universal terrestrial radio access (E-UTRA); user equipment (UE) radio transmission and reception (3GPP TS 36.101 version 14.3.0 release 14)*, ETSI, Sophia Antipolis Cedex, France, (2017).

[5] *Getting started guide NI RF Signal Analyzers [online]*, National Instruments, (2018).

[6] *Getting started guide NI RF Signal Generators [online]*, National Instruments, (2018).

[7] *TS72421K Datasheet - 10W CW GaN Broadband RF Switch SP4T*, Tagore Technology, (2018).

[8] *MM5120 Datasheet - 12GHz High Power RF SP4T Switch*, Menlo Micro, (2020).

[9] *CC2595 RF front-end transmit power amplifier for 2.4GHz ISM band systems*, (Texas Instruments Incorporated, Dallas, Texas, USA.).

[10] E. ADI, A. ANWAR, Z. BAIG, AND S. ZEADALLY, *Machine learning and data analytics for the IoT*, Neural Computing and Applications, 32 (2020), pp. 16205–16233.

[11] A. AFANA, N. ABU-ALI, AND S. IKKI, *On the joint impact of hardware and channel imperfections on cognitive spatial modulation MIMO systems: Cramer–Rao bound approach*, IEEE Systems Journal, 13 (2019), pp. 1250–1261.

[12] E. AHMED, A. M. ELTAWIL, AND A. SABHARWAL, *Rate gain region and design tradeoffs for full-duplex wireless communications*, IEEE Transactions on Wireless Communications, 12 (2013), pp. 3556–3565.

[13] M. M. ALWAKEEL, *Quadrature spatial modulation performance analysis over Rician fading channels*, J. Commun., 11 (2016), pp. 249–254.

[14] C. D. ALWIS, A. KALLA, Q.-V. PHAM, P. KUMAR, K. DEV, W.-J. HWANG, AND M. LIYANAGE, *Survey on 6G frontiers: Trends, applications, requirements, technologies and future research*, IEEE Open Journal of the Communications Society, 2 (2021), pp. 836–886.

[15] N. ANAND, E. ARYAFAR, AND E. W. KNIGHTLY, *Warplab: a flexible framework for rapid physical layer design*, in Proceedings of the 2010 ACM workshop on Wireless of the students, by the students, for the students, 2010, pp. 53–56.

[16] A. BALATSOUKAS-STIMMING, P. BELANOVIC, K. ALEXANDRIS, AND A. BURG, *On self-interference suppression methods for low-complexity full-duplex MIMO*, in 2013 Asilomar Conference on Signals, Systems and Computers, 2013, pp. 992–997.

[17] E. BASAR, *Index modulation techniques for 5G wireless networks*, IEEE Communications Magazine, 54 (2016), pp. 168–175.

[18] E. BASAR, U. AYGOLU, E. PANAYIRCI, AND H. V. POOR, *Performance of spatial modulation in the presence of channel estimation errors*, IEEE Communications Letters, 16 (2012), pp. 176–179.

[19] E. BASAR, M. WEN, R. MESLEH, M. DI RENZO, Y. XIAO, AND H. HAAS, *Index modulation techniques for next-generation wireless networks*, IEEE Access, 5 (2017), pp. 16693–16746.

[20] D. A. BASNAYAKA AND H. HAAS, *Spatial modulation for massive MIMO*, in 2015 IEEE International Conference on Communications (ICC), IEEE, 2015, pp. 1945–1950.

[21] E. BAŞAR, U. AYGÖLÜ, E. PANAYIRCI, AND H. V. POOR, *Space-time block coded spatial modulation*, IEEE Transactions on Communications, 59 (2011), pp. 823–832.

[22] D. BHARADIA AND S. KATTI, *Full duplex MIMO radios*, in 11th USENIX Symposium on Networked Systems Design and Implementation (NSDI 14), 2014, pp. 359–372.

[23] D. BHARADIA, E. MCMILIN, AND S. KATTI, *Full duplex radios*, in Proceedings of the ACM SIGCOMM 2013 conference on SIGCOMM, 2013, pp. 375–386.

[24] Z. S. BOJKOVIC, D. A. MILOVANOVIC, AND T. P. FOWDUR, *Toward green communication in 5G: New concepts and research challenges*, in 5G Multimedia communication, CRC Press, 2020, pp. 3–29.

[25] S. BORKAR AND H. PANDE, *Application of 5G next generation network to Internet of Things*, in 2016 International Conference on Internet of Things and Applications (IOTA), 2016, pp. 443–447.

[26] A. E. CANBILEN, M. M. ALSMADI, E. BASAR, S. S. IKKI, S. S. GULTEKIN, AND I. DEVELI, *Spatial modulation in the presence of I/Q imbalance: Optimal detector performance analysis*, IEEE Communications Letters, 22 (2018), pp. 1572–1575.

[27] A. E. CANBILEN, S. S. IKKI, E. BASAR, S. S. GULTEKIN, AND I. DEVELI, *Joint impact of I/Q imbalance and imperfect CSI on SM-MIMO systems over generalized beckmann fading channels: Optimal detection and cramer-rao bound*, IEEE Transactions on Wireless Communications, 19 (2020), pp. 3034–3046.

[28] CEPHELI, S. TEDIK, AND G. KARABULUT KURT, *A high data rate wireless communication system with improved secrecy: Full duplex beamforming*, IEEE Communications Letters, 18 (2014), pp. 1075–1078.

[29] F. CHEN, H. H. LEE, R. MORAWSKI, AND T. LE-NGOC, *RF/Analog self-interference canceller for 2×2 MIMO full-duplex transceiver*, in 2017 IEEE International Conference on Communications (ICC), 2017, pp. 1–6.

[30] W. CHENG, X. ZHANG, AND H. ZHANG, *Full duplex wireless communications for cognitive radio networks*, ArXiv, abs/1105.0034 (2011).

[31] J. CHOI, M. JAIN, K. SRINIVASAN, P. LEVIS, AND S. KATTI, *Achieving single channel, full duplex wireless communication*, 12 2010, pp. 1–12.

[32] J. I. CHOI, S. HONG, M. JAIN, S. KATTI, P. LEVIS, AND J. MEHLMAN, *Beyond full duplex wireless*, in 2012 Conference Record of the Forty Sixth Asilomar Conference on Signals, Systems and Computers (ASILOMAR), 2012, pp. 40–44.

[33] M. Z. CHOWDHURY, M. SHAHJALAL, S. AHMED, AND Y. M. JANG, *6G wireless communication systems: Applications, requirements, technologies, challenges, and research directions*, IEEE Open Journal of the Communications Society, 1 (2020), pp. 957–975.

[34] A. C. CIRIK, Y. RONG, AND Y. HUA, *Achievable rates of full-duplex MIMO radios in fast fading channels with imperfect channel estimation*, IEEE Transactions on Signal Processing, 62 (2014), pp. 3874–3886.

[35] B. CLERCKX, A. COSTANZO, A. GEORGIADIS, AND N. BORGES CARVALHO, *Toward 1G mobile power networks: RF, signal, and system designs to make smart objects autonomous*, IEEE Microwave Magazine, 19 (2018), pp. 69–82.

[36] M. DI RENZO AND H. HAAS, *On the performance of space shift keying MIMO systems over correlated Rician fading channels*, in 2010 International ITG Workshop on Smart Antennas (WSA), 2010, pp. 72–79.

[37] M. DI RENZO, H. HAAS, A. GHRAYEB, S. SUGIURA, AND L. HANZO, *Spatial modulation for generalized MIMO: Challenges, opportunities, and implementation*, Proceedings of the IEEE, 102 (2014), pp. 56–103.

[38] L. DING, G. T. ZHOU, D. R. MORGAN, Z. MA, J. S. KENNEY, J. KIM, AND C. R. GIARDINA, *Memory polynomial predistorter based on the indirect learning architecture*, in Global Telecommunications Conference, 2002. GLOBECOM'02. IEEE, vol. 1, IEEE, 2002, pp. 967–971.

[39] M. DUARTE, C. DICK, AND A. SABHARWAL, *Experiment-driven characterization of full-duplex wireless systems*, IEEE Transactions on Wireless Communications, 11 (2012), pp. 4296–4307.

[40] M. DUARTE AND A. SABHARWAL, *Full-duplex wireless communications using off-the-shelf radios: Feasibility and first results*, in 2010 Conference Record of the Forty Fourth Asilomar Conference on Signals, Systems and Computers, 2010, pp. 1558–1562.

[41] M. DUARTE, A. SABHARWAL, V. AGGARWAL, R. JANA, K. RAMAKRISHNAN, C. W. RICE, AND N. SHANKARANARAYANAN, *Design and characterization of a full-duplex multiantenna system for WiFi networks*, IEEE Transactions on Vehicular Technology, 63 (2013), pp. 1160–1177.

[42] O. T. ELUWOLE, N. UDOH, M. OJO, C. OKORO, AND A. J. AKINYOADE, *From 1G to 5G, what next?*, IAENG International Journal of Computer Science, 45 (2018).

[43] E. EVERETT, M. DUARTE, C. DICK, AND A. SABHARWAL, *Empowering full-duplex wireless communication by exploiting directional diversity*, in 2011 Conference Record of the Forty Fifth Asilomar Conference on Signals, Systems and Computers (ASILOMAR), 2011, pp. 2002–2006.

[44] E. EVERETT, A. SAHAI, AND A. SABHARWAL, *Passive self-interference suppression for full-duplex infrastructure nodes*, IEEE Transactions on Wireless Communications, 13 (2014), pp. 680–694.

[45] J. FU, C. HOU, W. XIANG, L. YAN, AND Y. HOU, *Generalised spatial modulation with multiple active transmit antennas*, in 2010 IEEE Globecom Workshops, 2010, pp. 839–844.

[46] F. GAO, R. ZHANG, AND Y.-C. LIANG, *Optimal channel estimation and training design for two-way relay networks*, IEEE Transactions on Communications, 57 (2009), pp. 3024–3033.

[47] D. GESBERT, M. SHAFI, D. SHAN SHIU, P. SMITH, AND A. NAGUIB, *From theory to practice: an overview of MIMO space-time coded wireless systems*, IEEE Journal on Selected Areas in Communications, 21 (2003), pp. 281–302.

[48] F. M. GHANNOUCHI AND O. HAMMI, *Behavioral modeling and predistortion*, IEEE Microwave Magazine, 10 (2009), pp. 52–64.

[49] A. GOLDSMITH, *Wireless Communications*, Cambridge University Press, 2005.

[50] B. S. GURU AND H. R. HIZIROGLU, *Electromagnetic field theory fundamentals*, Cambridge University Press, 2 ed., 2004.

[51] K. HANEDA, E. KAHRA, S. WYNE, C. ICHELN, AND P. VAINIKAINEN, *Measurement of loop-back interference channels for outdoor-to-indoor full-duplex radio relays*, Proceedings of the Fourth European Conference on Antennas and Propagation, (2010), pp. 1–5.

[52] K. HANEDA, E. KAHRA, S. WYNE, C. ICHELN, AND P. VAINIKAINEN, *Measurement of loop-back interference channels for outdoor-to-indoor full-duplex radio relays*, in Proceedings of the Fourth European Conference on Antennas and Propagation, 2010, pp. 1–5.

[53] M. HEINO, D. KORPI, T. HUUSARI, E. ANTONIO-RODRIGUEZ, S. VENKATASUBRAMANIAN, T. RIIHONEN, L. ANTTILA, C. ICHELN, K. HANEDA, R. WICHMAN, AND M. VALKAMA, *Recent advances in antenna design and interference cancellation algorithms for in-band full duplex relays*, IEEE Communications Magazine, 53 (2015), pp. 91–101.

[54] O. HIARI AND R. MESLEH, *Impact of RF–switch insertion loss on the performance of space modulation techniques*, IEEE Communications Letters, 22 (2018), pp. 958–961.

[55] M. HO, J. CIOFFI, AND J. BINGHAM, *Discrete multitone echo cancelation*, IEEE Transactions on Communications, 44 (1996), pp. 817–825.

[56] S. S. HONG, J. MEHLMAN, AND S. KATTI, *Picasso: Flexible RF and spectrum slicing*, ACM SIGCOMM Computer Communication Review, 42 (2012), pp. 37–48.

[57] H. HUI, Y. DING, Q. SHI, F. LI, Y. SONG, AND J. YAN, *5G network-based Internet of Things for demand response in smart grid: A survey on application potential*, Applied Energy, 257, p. 113972.

[58] M. JAIN, J. CHOI, T.-M. KIM, D. BHARADIA, S. SETH, K. SRINIVASAN, P. LEVIS, S. KATTI, AND P. SINHA, *Practical, real-time, full duplex wireless*, 09 2011, pp. 301–312.

[59] J. JEGANATHAN, A. GHRAYEB, AND L. SZCZECINSKI, *Generalized space shift keying modulation for MIMO channels*, in 2008 IEEE 19th International Symposium on Personal, Indoor and Mobile Radio Communications, 2008, pp. 1–5.

[60] ——, *Spatial modulation: optimal detection and performance analysis*, IEEE Communications Letters, 12 (2008), pp. 545–547.

[61] J. JEGANATHAN, A. GHRAYEB, L. SZCZECINSKI, AND A. CERON, *Space shift keying modulation for MIMO channels*, IEEE Transactions on Wireless Communications, 8 (2009), pp. 3692–3703.

[62] W. JIANG, B. HAN, M. A. HABIBI, AND H. D. SCHOTTEN, *The road towards 6G: A comprehensive survey*, IEEE Open Journal of the Communications Society, 2 (2021), pp. 334–366.

[63] B. JIAO, M. WEN, M. MA, AND H. V. POOR, *Spatial modulated full duplex*, IEEE Wireless Communications Letters, 3 (2014), pp. 641–644.

[64] S. E. JOHNSTON AND P. D. FIORE, *Full-duplex communication via adaptive nulling*, in 2013 Asilomar Conference on Signals, Systems and Computers, 2013, pp. 1628–1631.

[65] B. KAUFMAN, J. LILLEBERG, AND B. AAZHANG, *An analog baseband approach for designing full-duplex radios*, in 2013 Asilomar Conference on Signals, Systems and Computers, 2013, pp. 987–991.

[66] B. KAUFMAN, J. LILLEBERG, AND B. AAZHANG, *Analog baseband cancellation for full-duplex: An experiment driven analysis*, ArXiv, abs/1312.0522 (2013).

[67] M. H. KHADR, I. WALTER, H. ELGALA, AND S. MUHAIDAT, *Machine learning-based massive augmented spatial modulation (ASM) for IoT VLC systems*, IEEE Communications Letters, 25 (2021), pp. 494–498.

[68] A. K. KHANDANI, *Two-way (true full-duplex) wireless*, in 2013 13th Canadian Workshop on Information Theory, 2013, pp. 33–38.

[69] A. KOC, I. ALTUNBAS, AND E. BASAR, *Full-duplex spatial modulation systems under imperfect channel state information*, in 2017 24th International Conference on Telecommunications (ICT), 2017, pp. 1–5.

[70] ——, *Two-way full-duplex spatial modulation systems with wireless powered AF relaying*, IEEE Wireless Communications Letters, 7 (2018), pp. 444–447.

[71] K. KOMATSU, Y. MIYAJI, AND H. UEHARA, *Iterative nonlinear self-interference cancellation for in-band full-duplex wireless communications under mixer imbalance and amplifier nonlinearity*, IEEE Transactions on Wireless Communications, 19 (2020), pp. 4424–4438.

[72] D. KORPI, M. AGHABABAEETAFRESHI, M. PIILILA, L. ANTTILA, AND M. VALKAMA, *Advanced architectures for self-interference cancellation in full-duplex radios: Algorithms and measurements*, in 2016 50th Asilomar Conference on Signals, Systems and Computers, 2016, pp. 1553–1557.

[73] D. KORPI, L. ANTTILA, V. SYRJÄLÄ, AND M. VALKAMA, *Widely linear digital self-interference cancellation in direct-conversion full-duplex transceiver*, IEEE Journal on Selected Areas in Communications, 32 (2014), pp. 1674–1687.

[74] D. KORPI, L. ANTTILA, AND M. VALKAMA, *Nonlinear self-interference cancellation in MIMO full-duplex transceivers under crosstalk*, EURASIP Journal on Wireless Communications and Networking, 2017 (2017).

[75] D. KORPI, M. HEINO, C. ICHELN, K. HANEDA, AND M. VALKAMA, *Compact inband full-duplex relays with beyond 100 dB self-interference suppression: Enabling techniques and field measurements*, IEEE Transactions on Antennas and Propagation, 65 (2017), pp. 960–965.

[76] D. KORPI, T. HUUSARI, Y.-S. CHOI, L. ANTTILA, S. TALWAR, AND M. VALKAMA, *Digital self-interference cancellation under nonideal RF components: Advanced algorithms and measured performance*, in 2015 IEEE 16th International Workshop on Signal Processing Advances in Wireless Communications (SPAWC), 2015, pp. 286–290.

[77] D. KORPI, T. RIIHONEN, K. HANEDA, K. YAMAMOTO, AND M. VALKAMA, *Achievable transmission rates and self-interference channel estimation in hybrid full-duplex/half-duplex MIMO relaying*, in 2015 IEEE 82nd Vehicular Technology Conference (VTC2015-Fall), 2015, pp. 1–5.

[78] D. KORPI, T. RIIHONEN, V. SYRJÄLÄ, L. ANTTILA, M. VALKAMA, AND R. WICHMAN, *Full-duplex transceiver system calculations: Analysis of ADC and linearity challenges*, IEEE Transactions on Wireless Communications, 13 (2014), pp. 3821–3836.

[79] D. KORPI, J. TAMMINEN, M. TURUNEN, T. HUUSARI, Y.-S. CHOI, L. ANTTILA, S. TALWAR, AND M. VALKAMA, *Full-duplex mobile device: pushing the limits*, IEEE Communications Magazine, 54 (2016), pp. 80–87.

[80] N. LAL, S. M. TIWARI, D. KHARE, AND M. SAXENA, *Prospects for handling 5G network security: Challenges, recommendations and future directions*, Journal of Physics: Conference Series, 1714 (2021), p. 012052.

[81] J.-H. LEE, *Self-interference cancelation using phase rotation in full-duplex wireless*, IEEE Transactions on Vehicular Technology, 62 (2013), pp. 4421–4429.

[82] J. LI, M. WEN, X. CHENG, Y. YAN, S. SONG, AND M. H. LEE, *Generalized precoding-aided quadrature spatial modulation*, IEEE Transactions on Vehicular Technology, 66 (2017), pp. 1881–1886.

[83] S. LI AND R. D. MURCH, *An investigation into baseband techniques for single-channel full-duplex wireless communication systems*, IEEE Transactions on Wireless Communications, 13 (2014), pp. 4794–4806.

[84] P. LIU, M. D. RENZO, AND A. SPRINGER, *Line-of-Sight spatial modulation for indoor mmWave communication at 60 GHz*, IEEE Transactions on Wireless Communications, 15 (2016), pp. 7373 – 7389.

[85] S. LIU, L. FU, AND W. XIE, *Hidden-node problem in full-duplex enabled CSMA networks*, IEEE Transactions on Mobile Computing, 19 (2020), pp. 347–361.

[86] Y. LIU, X. QUAN, W. PAN, S. SHAO, AND Y. TANG, *Nonlinear distortion suppression for active analog self-interference cancellers in full duplex wireless communication*, 2014 IEEE Globecom Workshops (GC Wkshps), (2014), pp. 948–953.

[87] F.-L. LUO AND C. ZHANG, *Design and implementation of full-duplex transceivers*, 2016, pp. 402–428.

[88] M. LUO, *Indoor radio propagation modeling for system performance prediction*, theses, INSA de Lyon, July 2013.

[89] R. LÓPEZ-VALCARCE AND N. GONZÁLEZ-PRELCIC, *Analog beamforming for full-duplex millimeter wave communication*, in 2019 16th International Symposium on Wireless Communication Systems (ISWCS), 2019, pp. 687–691.

[90] T. MAO, Q. WANG, AND Z. WANG, *Spatial modulation for Terahertz communication systems with hardware impairments*, IEEE Transactions on Vehicular Technology, 69 (2020), pp. 4553–4557.

[91] H. MEN AND M. JIN, *A low-complexity ML detection algorithm for spatial modulation systems with MPSK constellation*, IEEE Communications Letters, 18 (2014), pp. 1375–1378.

[92] R. MESLEH, S. ALTHUNIBAT, AND A. YOUNIS, *Differential quadrature spatial modulation*, IEEE Transactions on Communications, 65 (2017), pp. 3810–3817.

[93] R. MESLEH, H. HAAS, C. W. AHN, AND S. YUN, *Spatial modulation - a new low complexity spectral efficiency enhancing technique*, in 2006 First International Conference on Communications and Networking in China, 2006, pp. 1–5.

[94] R. MESLEH, H. HAAS, C. W. AHN, AND S. YUN, *Spatial modulation-OFDM*, 2006.

[95] R. MESLEH, S. S. IKKI, AND H. M. AGGOUNE, *Quadrature spatial modulation*, IEEE Transactions on Vehicular Technology, 64 (2015), pp. 2738–2742.

[96] R. Y. MESLEH, H. HAAS, S. SINANOVIC, C. W. AHN, AND S. YUN, *Spatial modulation*, IEEE Transactions on Vehicular Technology, 57 (2008), pp. 2228–2241.

[97] K. S. MOHAMED, M. Y. ALIAS, M. ROSLEE, AND Y. M. RAJI, *Towards green communication in 5G systems: Survey on beamforming concept*, IET Communications, (2021).

[98] R. MUTAGI, *Pseudo noise sequences for engineers*, Electronics & Communication Engineering Journal, 8 (1996), pp. 79–87.

[99] S. NARAYANAN, H. AHMADI, AND M. F. FLANAGAN, *Simultaneous uplink/downlink transmission using full-duplex single-RF MIMO*, IEEE Wireless Communications Letters, 5 (2016), pp. 88–91.

[100] D. NGUYEN VIET, M. DI RENZO, V. BASAVARAJAPPA, B. BEDIA EXPOSITO, J. BASTERRECHEA, AND D. T. PHAN-HUY, *Spatial modulation based on reconfigurable antennas: performance evaluation by using the prototype of a reconfigurable antenna*, Eurasip Journal on Wireless Communications and Networking, 149 (2019).

[101] P. PATCHARAMANEEPAKORN, S. WU, C.-X. WANG, M. M. ALWAKEEL, X. GE, M. DI RENZO, ET AL., *Spectral, energy, and economic efficiency of 5G multicell massive MIMO systems with generalized spatial modulation*, IEEE Transactions on Vehicular Technology, 65 (2016), pp. 9715–9731.

[102] D. PHAN-HUY, Y. KOKAR, K. RACHEDI, P. PAJUSCO, A. MOKH, T. MAGOUNAKI, R. MASOOD, C. BUEY, P. RATAJCZAK, N. MALHOUROUX-GAFFET, J. CONRAT, J. PRÉVOTET, A. OURIR, J. DE ROSNY, AND M. D. RENZO, *Single-carrier spatial modulation for the Internet of Things: Design and performance evaluation by using real compact and reconfigurable antennas*, IEEE Access, 7 (2019), pp. 18978–18993.

[103] N. PHUNGAMNGERN, P. UTHANSAKUL, AND M. UTHANSAKUL, *Digital and RF interference cancellation for single-channel full-duplex transceiver using a single antenna*, in 2013 10^{th} International Conference on Electrical Engineering/Electronics, Computer, Telecommunications and Information Technology, 2013, pp. 1–5.

[104] J. G. PROAKIS AND S. MASOUD, *Digital communications*, McGraw-Hill, New York, 2008.

[105] W. QU, M. ZHANG, X. CHENG, AND P. JU, *Generalized spatial modulation with transmit antenna grouping for massive MIMO*, IEEE Access, 5 (2017), pp. 26798–26807.

[106] R. RAJASHEKAR, M. D. RENZO, K. HARI, AND L. HANZO, *A generalized transmit and receive diversity condition for feedback-assisted MIMO systems: Theory and applications in full-duplex spatial modulation*, IEEE Transactions on Signal Processing, 65 (2017), pp. 6505–6519.

[107] B. RAZAVI, *RF Microelectronics (2nd Edition) (Prentice Hall Communications Engineering and Emerging Technologies Series)*, Prentice Hall Press, USA, 2nd ed., 2011.

[108] G. M. REBEIZ AND J. B. MULDAVIN, *RF MEMS switches and switch circuits*, IEEE Microwave magazine, 2 (2001), pp. 59–71.

[109] M. D. RENZO, H. HAAS, AND P. M. GRANT, *Spatial modulation for multiple-antenna wireless systems: a survey*, IEEE Communications Magazine, 49 (2011), pp. 182–191.

[110] T. RIIHONEN, P. MATHECKEN, AND R. WICHMAN, *Effect of oscillator phase noise and processing delay in full-duplex OFDM repeaters*, in 2012 Conference Record of the Forty Sixth Asilomar Conference on Signals, Systems and Computers (ASILOMAR), 2012, pp. 1947–1951.

[111] M. SAAD, F. BADER, A. C. AL GHOUWAYEL, H. HIJAZI, N. BOUHEL, AND J. PALICOT, *Generalized spatial modulation for wireless terabits systems under Sub-THz channel with RF impairments*, ICASSP 2020 - 2020 IEEE International Conference on Acoustics, Speech and Signal Processing (ICASSP), (2020), pp. 5130–5134.

[112] A. SABHARWAL, P. SCHNITER, D. GUO, D. W. BLISS, S. RANGARAJAN, AND R. WICHMAN, *In-band full-duplex wireless: Challenges and opportunities*, IEEE Journal on Selected Areas in Communications, 32 (2014), pp. 1637–1652.

[113] N. SERAFIMOVSKI, A. YOUNIS, R. MESLEH, P. CHAMBERS, M. DI RENZO, C. X. WANG, P. M. GRANT, M. A. BEACH, AND H. HAAS, *Practical implementation of spatial modulation*, IEEE Transactions on Vehicular Technology, 62 (2013), pp. 4511–4523.

[114] S. SIGDEL AND W. A. KRZYMIEŃ, *Antenna and user subset selection in downlink multiuser orthogonal space-division multiplexing*, 52, p. 227.

[115] M. S. SIM, M. CHUNG, D. KIM, J. CHUNG, D. K. KIM, AND C. CHAE, *Nonlinear self-interference cancellation for full-duplex radios: From link-level and system-level performance perspectives*, IEEE Communications Magazine, 55 (2017), pp. 158–167.

[116] L. SONG, Y. LIAO, AND L. SONG, *Full-duplex WiFi networks*, Springer Singapore, Singapore, 2017, pp. 1–27.

[117] E. SOUJERI AND G. KADDOUM, *The impact of antenna switching time on spatial modulation*, IEEE Wireless Communications Letters, 5 (2016), pp. 256–259.

[118] S. SUGIURA AND L. HANZO, *Effects of channel estimation on spatial modulation*, IEEE Signal Processing Letters, 19 (2012), pp. 805–808.

[119] S. SUGIURA, T. ISHIHARA, AND M. NAKAO, *State-of-the-art design of index modulation in the space, time, and frequency domains: Benefits and fundamental limitations*, IEEE Access, 5 (2017), pp. 21774–21790.

[120] M. A. TAFRESHI, M. KOSKELA, D. KORPI, P. JÄÄSKELÄINEN, M. VALKAMA, AND J. TAKALA, *Software defined radio implementation of adaptive nonlinear digital self-interference cancellation for mobile inband full-duplex radio*, in 2016 IEEE Global Conference on Signal and Information Processing (GlobalSIP), 2016, pp. 733–737.

[121] D. TSE AND P. VISWANATH, *The wireless channel*, Cambridge University Press, 2005.

[122] G. TSOULOS, *MIMO system technology for wireless communications*, CRC press, 2018.

[123] R. VERMA, S. MAHAJAN, AND V. ROHILA, *Classification of MIMO channel models*, in 2008 16th IEEE International Conference on Networks, 2008, pp. 1–4.

[124] B. VO AND H. H. NGUYEN, *Improved quadrature spatial modulation*, in 2017 IEEE 86^{th} Vehicular Technology Conference (VTC-Fall), 2017, pp. 1–5.

[125] J. WANG, S. JIA, AND J. SONG, *Generalised spatial modulation system with multiple active transmit antennas and low complexity detection scheme*, IEEE Transactions on Wireless Communications, 11 (2012), pp. 1605–1615.

[126] N. WANG, E. HOSSAIN, AND V. K. BHARGAVA, *Joint downlink cell association and bandwidth allocation for wireless backhauling in two-tier HetNets with large-scale antenna arrays*, IEEE Transactions on Wireless Communications, 15 (2016), pp. 3251–3268.

[127] M. WEN, B. ZHENG, K. J. KIM, M. DI RENZO, T. A. TSIFTSIS, K. C. CHEN, AND N. AL-DHAHIR, *A survey on spatial modulation in emerging wireless systems: Research progresses and applications*, IEEE Journal on Selected Areas in Communications, 37 (2019), pp. 1949–1972.

[128] P. YANG, M. D. RENZO, Y. XIAO, S. LI, AND L. HANZO, *Design guidelines for spatial modulation*, IEEE Communication Surveys & Tutorials, 17 (2014), pp. 6–26.

[129] A. YOUNIS, D. A. BASNAYAKA, AND H. HAAS, *Performance analysis for generalised spatial modulation*, in European Wireless 2014; 20th European Wireless Conference, 2014, pp. 1–6.

[130] A. YOUNIS, N. SERAFIMOVSKI, R. MESLEH, AND H. HAAS, *Generalised spatial modulation*, in 2010 Conference Record of the Forty Fourth Asilomar Conference on Signals, Systems and Computers, 2010, pp. 1498–1502.

[131] A. YOUNIS, W. THOMPSON, M. DI RENZO, C. X. WANG, M. A. BEACH, H. HAAS, AND P. M. GRANT, *Performance of spatial modulation using measured real-world channels*, in 2013 IEEE 78th Vehicular Technology Conference (VTC Fall), 2013, pp. 1–5.

[132] H. YU, F. SHU, Y. YOU, J. WANG, T. LIU, X. YOU, J. LU, J. WANG, AND X. ZHU, *Compressed sensing-based time-domain channel estimator for full-duplex OFDM systems with IQ-imbalances*, Sci. China Inform. Sci, 60 (2017), p. 082303.

[133] Z. ZHAN, *On design concept for full-duplex based flexible radio transceivers*, PhD thesis, 2014. Thèse de doctorat dirigée par Gorce, Jean-Marie et Villemaud, Guillaume Télécommunications Lyon, INSA 2014.

[134] Z. ZHAN AND G. VILLEMAUD, *Combination of digital self-interference cancellation and AARFSIC for full-Duplex OFDM wireless*, in 2014 IEEE/CIC International Conference on Communications in China (ICCC), 2014, pp. 593–597.

[135] Z. ZHAN, G. VILLEMAUD, AND J.-M. GORCE, *design and evaluation of a wideband full-duplex ofdm system based on aasic*, in 2013 IEEE 24th Annual International Symposium on Personal, Indoor, and Mobile Radio Communications (PIMRC).

[136] ——, *Analysis and reduction of the impact of thermal noise on the full-duplex OFDM radio*, in 2014 IEEE Radio and Wireless Symposium (RWS), 2014, pp. 220–222.

[137] Z. ZHAN, G. VILLEMAUD, F. HUTU, AND J.-M. GORCE, *Digital estimation and compensation of I/Q imbalance for full-duplex dual-band OFDM radio*, in 2014 IEEE 25th Annual International Symposium on Personal, Indoor, and Mobile Radio Communication (PIMRC), 2014, pp. 846–850.

[138] J. ZHANG, Q. LI, K. J. KIM, Y. WANG, X. GE, AND J. ZHANG, *On the performance of full-duplex two-way relay channels with spatial modulation*, IEEE Transactions on Communications, 64 (2016), pp. 4966–4982.

[139] Z. ZHANG, Y. XIAO, Z. MA, M. XIAO, Z. DING, X. LEI, G. K. KARAGIANNIDIS, AND P. FAN, *6G wireless networks: Vision, requirements, architecture, and key technologies*, IEEE Vehicular Technology Magazine, 14 (2019), pp. 28–41.

[140] G. ZHENG, I. KRIKIDIS, J. LI, A. P. PETROPULU, AND B. OTTERSTEN, *Improving physical layer secrecy using full-duplex jamming receivers*, IEEE Transactions on Signal Processing, 61 (2013), pp. 4962–4974.

[141] Y. ZHOU, F. HUTU, AND G. VILLEMAUD, *Impact of receiver non-idealities on a full duplex spatial modulation system performance*, IEEE Wireless Communications Letters, 9 (2020), pp. 2083–2087.

[142] Y. ZHOU, Z. Z. XIANG, Y. ZHU, AND Z. XUE, *Application of full-duplex wireless technique into secure MIMO communication: Achievable secrecy rate based optimization*, IEEE Signal Processing Letters, 21 (2014), pp. 804–808.

FOLIO ADMINISTRATIF

THESE DE L'UNIVERSITE DE LYON OPEREE AU SEIN DE L'INSA LYON

NOM : ZHOU
(avec précision du nom de jeune fille, le cas échéant)

DATE de SOUTENANCE : 10/12/2021

Prénoms : Yanni

TITRE : On the Performance of Spatial Modulation and Full Duplex Radio Architectures

NATURE : Doctorat

Numéro d'ordre : 2021LYSEI094

Ecole doctorale : E.E.A.

Spécialité : Électronique, micro et nanoélectronique, optique et laser

RESUME :

Les techniques de modulation d'indice ont montré un grand potentiel pour les réseaux de communication sans fil de prochaines générations. Dans le domaine de l'indice spatial, la modulation spatiale (SM) en tant que solution à monoporteuse radiofréquence (RF), à entrées multiples et sorties multiples (MIMO), a attiré une grande attention. Le système SM n'a qu'une seule antenne d'émission activée pour chaque symbole transmis, ce qui diminue la complexité, la consommation énergétique et le coût du système, notamment côté architecture RF. Pour analyser les performances de la modulation spatiale, un simulateur système qui tient compte du réalisme des différents blocs fonctionnels de la chaine de transmission radio et qui modélise un canal à évanouissements de Rice variable dans le temps est mis en place grâce aux logiciels ADS (Keysight) et Matlab (Mathworks). Grâce à ce simulateur, les performances de la chaine de transmission à travers le critère de taux d'erreur binaire sont mises en évidence. Les résultats sont vérifiés par l'implémentation expérimentale basée sur des VST (Vector Signal Transceivers) et de l'environnement de programmation LabVIEW (National Instruments). De plus, les communications « full-duplex » (FD) ont été développées pour doubler l'efficacité spectrale de la liaison radio grâce à une communication simultanée et bidirectionnelle. Le principal challenge des systèmes FD est l'auto-interférence (SI), qui est causée par le couplage de l'antenne d'émission avec celle de réception. La combinaison de FD et SM non seulement maintiendra l'efficacité spectrale mais aussi réduira la complexité de l'annulation d'auto-interférence (SIC) grâce à la chaîne RF unique. Par conséquent, un système de modulation spatiale en full duplex (FDSM) est proposé ainsi que la méthode d'annulation de l'auto-interférence. Nous nous concentrons sur les imperfections du système FDSM, notamment le déséquilibre IQ, le bruit de phase, les non-linéarités d'amplificateur (PA) et les non-idéalités de switch RF.

MOTS-CLÉS :

Modulation spatiale, full duplex, radiofréquence, MIMO, auto-interférence, non-idéalités

Laboratoire (s) de recherche : CITI

Directeur de thèse : Guillaume VILLEMAUD, Florin-Doru HUTU

Président de jury :

Composition du jury : Christelle AUPETIT-BERTHELEMOT, Marco DI RENZO, Matthieu CRUSSIERE, Taneli RIIHONEN, Jean-Marie GORCE, Dinh-Thuy PHAN-HUY, Guillaume VILLEMAUD, Florin-Doru HUTU